TRANSPORTATION RESEARCH RECORD 949

Pavements: Designs for Heavy Vehicles, Computer Simulations and Geogrid Reinforcements

TRANSPORTATION RESEARCH BOARD

NATIONAL RESEARCH COUNCIL
NATIONAL ACADEMY OF SCIENCES
WASHINGTON, D.C. 1983

Transportation Research Record 949
Price $9.60
Edited for TRB by Jane Starkey

modes
1 highway transportation
4 air transportation

subject areas
24 pavement design and performance
40 maintenance

Library of Congress Cataloging in Publication Data
National Research Council. Transportation Research Board.
Pavements: designs for heavy vehicles, computer simulations, and geogrid reinforcements.

(Transportation research record; 949)
Reports for the Transportation Research Board's 62nd annual meeting.
1. Pavements–Design and construction–Addresses, essays, lectures. 2. Pavements–Mathematical models–Addresses, essays, lectures. 3. Pavements, Reinforced concrete–Addresses, essays, lectures. 4. Motor vehicles–Weight–Addresses, essays, lectures. I. National Research Council (U.S.). Transportation Research Board. II. Series
TE7.H5 no. 949 380.5s 84-20622 [TE251] [625.8]
ISBN 0-309-03670-4 ISSN 0361-1981

Sponsorship of the Papers in This Transportation Research Record

GROUP 2–DESIGN AND CONSTRUCTION OF TRANSPORTATION FACILITIES
Robert C. Deen, University of Kentucky, chairman

Pavement Management Section
W. Ronald Hudson, University of Texas at Austin, chairman

Committee on Flexible Pavements
R.G. Hicks, Oregon State University, chairman
James A. Sherwood, Federal Highway Administration, secretary
R.N. Doty, David C. Esch, Wade L. Gramling, Douglas I. Hanson, Newton C. Jackson, Dallas N. Little, Dennis B. Luhrs, J.W. Lyon, Jr., Joe P. Mahoney, Adrian Pelzner, William A. Phang, James A. Scherocman, James F. Shook, Eugene L. Skok, Jr., Herbert F. Southgate, William T. Stapler, Harvey J. Treybig, Harry H. Ulery, Jr., Cecil J. Van Til, Loren M. Womack, Richard J. Worch

Lawrence F. Spaine, Transportation Research Board staff

The organizational units, officers, and members are as of December 31, 1982.

Contents

Authors of the Papers in This Record

Abdel Halim, A.O., Civil Engineering Department, Carleton University, Ottawa, Ontario K1S 5B6 Canada

Barber, V.C., Department of the Army, Corps of Engineers, Waterways Experiment Station, P.O. Box 631, Vicksburg, Miss. 39180

Deen, Robert C., Kentucky Transportation Research Program, University of Kentucky, Lexington, Ky. 40506-0043

Hallin, John P., Federal Highway Administration, Portland, Oreg. 97204

Haas, Ralph, Department of Civil Engineering, University of Waterloo, Waterloo, Ontario N2L 3G1 Canada

Ladd, D.M., Department of the Army, Corps of Engineers, Waterways Experiment Station, P.O. Box 631, Vicksburg, Miss. 39180

Larsen, B. K., Institute of Roads, Transport, and Town Planning, The Technical University of Denmark, Bygning 115, DK-2800 Lyngby, Denmark

Mahoney, Joe P., Department of Civil Engineering, University of Washington, Seattle, Wash. 98195

Mayes, Jesse G., Kentucky Transportation Research Program, University of Kentucky, Lexington, Ky. 40506-0043

Phang, William A., Pavement Research Section, Ministry of Transportation and Communications, Ontario M3M 1J8 Canada

Sharma, Jatinder, Department of Civil Engineering, University of Washington, Seattle, Wash. 98195

Southgate, Herbert F., Kentucky Transportation Research Program, University of Kentucky, Lexington, Ky. 40506-0043

Terrel, Ronald L., Department of Civil Engineering, University of Washington, Seattle, Wash. 98195

Treybig, Harvey J., ARE Inc., 2600 Dellana Lane, Austin, Texas 78746

Ullidtz, P., Institute of Roads, Transport, and Town Planning, The Technical University of Denmark, Bygning 115, DK-2800 Lyngby, Denmark

Pavement Design Criteria for Heavy-Load Vehicles

V.C. BARBER AND D.M. LADD

Extensive prototype tests were conducted at the U.S. Army Engineer Waterways Experiment Station to adapt Corps of Engineers (CE) flexible pavement design criteria to pavements to be used in the MX missile program. The initial shell game concept for dispersing the MX missiles required construction of approximately 8,000 miles of roads capable of sustaining numerous passes of a missile transporter weighing about 1,500,000 lb. This research resulted in increased knowledge of the performance of pavements subjected to heavy loads. Prototype test sections of bituminous surface-treated roads and gravel-surfaced roads were designed and constructed using current CE criteria. The test sections were trafficked to the design number of operations using a trafficking rig simulating the MX missile transporter. The trafficking rig was equipped with two load tires in line, each approximately 8 ft tall by 3 ft wide, inflated to 65 psi, and having a loaded weight of 62,500 lb. Test traffic was placed on the pavement and conditions were monitored for pavement distress. Analysis of the resulting test data led to the conclusion that existing CE criteria can be modified to provide a more economical pavement than was previously expected for very heavy loads. Most distress appeared in the form of deeper consolidation caused by the very heavy loads on the unusually large tires. Other load parameters such as contact area and contact pressure were in more typical ranges and, therefore, gave more typical results.

The U.S. Air Force Regional Civil Engineer for the MX missile program (AFRCE-MX) was charged with numerous aspects of the MX Program. The principal AFRCE objective was to select design criteria and methodology for construction management of the heavy-duty, low-volume road networks that would be the heart of the MX missile deployment scheme.

The shell game concept that generated this intensive research effort and resulted in a large amount of new data consisted of 200 MX missiles, each housed in a cluster of 23 horizontal shelters for a total of 4,600 shelters. The MX system was to be deployed according to the shell game concept wherein a single missile is moved among the 23 silos of a cluster as required for deception and concealment. The horizontal silos were to have a minimum spacing of approximately 1 mile and were to be connected by roads over which the MX missile would be moved as required. Roads also connected the 200 clusters to each other and to the service and storage areas.

The MX missile was to be carried on a transporter-erector-launcher (TEL) approximately 250 ft long with a loaded gross weight of approximately 1,500,000 lb. One definition of the vehicle support system included 24 single wheels on 12 axles (6 front and 6 rear), and the anticipated wheel load was to be 62,500 lb.

The resultant road requirement consisted of approximately 8,000 miles of all-weather roads to support the TEL for approximately 430 vehicle passes during its life of 15 years. Because first cost or installation cost of the entire system was a primary consideration, the objective was to develop a satisfactory road system at the lowest possible initial construction cost. After conducting preliminary studies and considering numerous alternatives, the AFRCE selected the U.S. Army Corps of Engineers (CE) road design methods as the basis for the MX road program. The U.S. Army Engineer Waterways Experiment Station (WES) Geotechnical Laboratory (GL) Pavement Systems Division (PSD) was designated as the prime consultant to the AFRCE and the lead agency in determining a suitable design, construction, and life-cycle management technology to the AFRCE for the MX road system. In response to this requirement the WES launched an extensive support program in 1979 designated as the MX Road Design Criteria Studies (RDCS).

Although the RDCS program was discontinued in October 1981 because of the Presidential decision to use more modest basing mode concepts, extensive prototype tests were conducted that resulted in a massive volume of performance data for very heavy vehicle operations on low-volume roads with various pavement constructions. As a result of these prototype tests and the analysis conducted before program discontinuance, significant findings have been generated to date, and further analysis of the available data should significantly advance the current state of the art in heavy-load, low-volume road life-cycle management from conception to termination.

OBJECTIVE

The objective of the RDCS was twofold. The first objective was to extend the validated range of current CE design criteria to include the characteristics of the MX TEL. The second objective was to determine the most economical road type that would meet these criteria keeping in mind the 15-year life cycle. Within this framework, the specific requirements included the following:

1. Extension of existing structural criteria to provide for MX road design in terms of layer strengths and thicknesses (1).
2. Determination of surface stability requirements to minimize functional deterioration or surface loss associated with environment and traffic.
3. Evaluation of overall functional performance and minimum serviceability criteria.
4. Evaluation of the applicability of nondestructive testing procedures for increased quality control and evaluation.
5. Determination of the amount of cover required for shallow-buried drainage structures.
6. Use of the Differential Analysis System (DAS) to optimize design with respect to minimum reliability requirements (2).

SCOPE

The conduct of the RDCS included an extensive prototype test designed to satisfy the stated objectives. The prototype test section was trafficked with representative wheel loads, results were observed, and data that would be useful in a comprehensive data analysis were recorded.

Although the RDCS ended in October 1981, some preliminary analyses were accomplished that could have a significant impact on the future design of heavy-load, low-volume roads. This paper includes the preliminary results of analyses that have been conducted to date on the data accumulated from prototype tests of the test pavements.

PROTOTYPE TESTING

The test philosophy of expanding existing criteria as well as developing specialized criteria for existing field conditions of the then likely Nevada-Utah Basin range required the selection of two categories of soils. The first category was similar to soils used to develop classic criteria. The second

category was representative of field materials in the basin area and was used to make classic criteria more applicable to actual conditions. The test section consisted of three separate traffic lanes; each lane contained five test sections (referred to as items) to provide for a comprehensive spectrum of traffic-pavement-soil types.

Figure 1 shows a layout of the test section. The test items shown were designed to meet the stated objectives. Items 3, 4, and 5 in Lane 3 were designed in part to provide data for determining surface stability requirements. Although the combinations of test items, traffic lanes, and test parameters are manifold, the scope of this paper dictates that only the performance of these items be discussed to illustrate those findings of concern here. Figure 2 shows a profile view of those items used to determine surface requirements.

The test section was located at the WES, Vicksburg, Mississippi, in hangar 4. The soil in this area is a lean clay. The average water table was at a depth of approximately 9 ft. The hangar floor was leveled before excavation to facilitate uniform construction. A benchmark was used for all vertical control throughout construction and testing of the MX test section.

TESTING AND BEHAVIOR

Test Cart

Traffic tests were performed on all traffic lanes with a specially designed test vehicle (Figure 3). This vehicle was a modified prime mover built by Marathon LeTourneau, Inc. in Vicksburg, Mississippi. The vehicle was modified so that two test wheels could be installed in tandem to represent a portion of the TEL. Although the TEL experienced several design changes during the conduct of the program, one set of characteristics was used in these studies. The TEL simulated in these studies was supported on 24 tires, each having a total loaded ground weight of 62,500 lb. The total gross weight of the vehicle was expected to be approximately 1,500,000 lb and the vehicle was designed with 6 tires on each quadrant of the vehicle. The tires used had a smooth surface and were approximately 98 in. high and 39 in. wide. The tire designation was 37.5 x 39.

Operational Design

The operational scenario of the MX deployment concept called for the movement of the TEL, upon command, among 23 horizontal silos within a cluster. Because these moves were to be infrequent, a total of 430 TEL passes were anticipated during the 15-year life of the system. Because the vehicle design called for 6 wheels on each corner or 12 wheels in line on one side, the TEL-to-test vehicle trafficking ratio was 6 to 1. It would therefore require 2,600 passes of the test vehicle to represent 430 TEL passes.

All traffic was applied with the tandem-wheel configuration with a backward and forward movement along each traffic lane. The traffic was applied in a single line with no wander permitted across the traffic lane. Each pass of a wheel was defined as one coverage. Therefore one test cart pass was two coverages. Traffic was commenced and continued for 2,600 passes.

Test Items

Those test items that were monitored for purposes of evaluating surface requirements were items 3, 4, and 5 of Lane 3. A description of these items is as follows.

Item 3, Lane 3. This test item consisted of 6 ft of a blended cohesionless sand-gravel material (Blend II) considered representative of the material below the 2-ft depth in the prospective basing area. The top 6 in. of the Blend II was compacted at optimum moisture and surfaced with a double bituminous surface treatment. Surface deterioration of this item was minimal with a maximum rut depth of 1.1 in. as shown in Figure 4.

Item 4, Lane 3. This item consisted of 5 ft of Blend II material covered with 12 in. of a blended cohesionless sand-gravel material (Blend I), con-

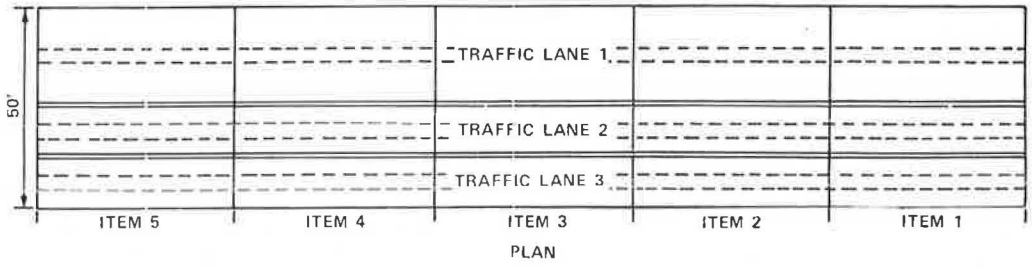

Figure 1. Plan view of test section.

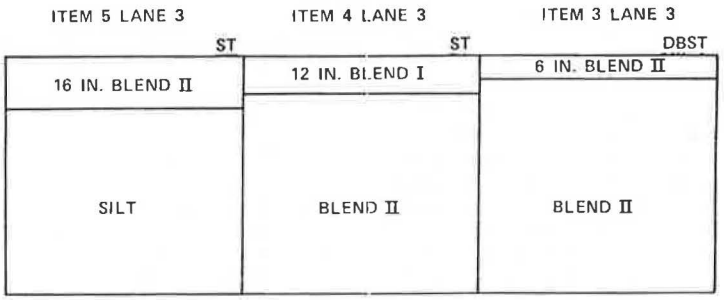

Figure 2. Profile view of Lane 3, items 3, 4, and 5.

Figure 3. Test vehicle.

sidered representative of the material in the top 2 ft of the basing area, that was compacted at optimum moisture. The item was surfaced with a single surface treatment. Deterioration of the surface of this item was also minimal with a maximum rut depth of 1.0 in. as shown in Figure 4.

Item 5, Lane 3. This item consisted of 44 in. of a silt material overlaid with 16 in. of Blend II compacted at optimum moisture and surfaced with a single surface treatment. The maximum rut depth was 0.7 in. as shown in Figure 4.

Data Collection

Data were collected before and after trafficking as well as at predetermined intervals. Cross sections, profiles, photographs, instrumentation readings, nondestructive tests, and rut-depth measurements were among the data recorded as were the physical parameters of moisture, density, and strength. Rutting in the items is the primary parameter discussed here.

ANALYSIS OF SURFACE-TREATED TEST ITEMS

Performance

Soil strengths and rut depths for the surface-treated items are shown in Table 1. Each test item was subjected to 2,600 passes of the simulated MX load cart having a loading of 125,000 lb on two tires with an inflation pressure of 65 psi. This traffic produced 1.1 in. of rutting in item 3, 1.0 in. of rutting in item 4, and 0.7 in. of rutting in item 5. Figure 4 shows the development of rutting with increased numbers of passes for each test item.

Table 1. Comparison of rut depths and CBR values for unsurfaced and surface-treated items.

Test Lane	Test Item	Top Soil Layer	Rut Depth (in.)	Rated CBR	
				Top Soil Layer	Subgrade
Unsurfaced					
1	3	Blend II	1.93	19.5	NA
	4	Blend I	4.16	36	21
	5	Silt	1.3	67	NA
Bituminous Surface Treatments					
3	3	Blend II	1.1	100+	19.5
	4	Blend I	1.0	79	21
	5	Blend II	0.7	59	24

General failure criteria for a flexible pavement is considered by the CE to be the development of rutting equal to or greater than 1.0 in. This rutting may be due to shear deformation under traffic resulting from insufficient thickness or due to densification resulting from inadequate density. Investigation of the rutting produced in these test items indicated that it was caused primarily by initial densification under traffic, because there appeared to be no shear deformation in the soil layers of the test items.

To compare the performance of the test items with current CE thickness design criteria, the allowable traffic was computed for each test item. The number of passes predicted by the CE criteria to cause failure is given in Table 2. Items 3 and 4 reached the 1.0-in. rutting failure criteria at 2,600 passes, which was significantly more than the CE criteria would predict, indicating that the CE criteria for thickness design may be conservative in

Table 2. Predicted traffic passes before failure for bituminous surface treatments.

Test Lane	Test Item	Subgrade Soil Type	Before Traffic CBR	Thickness of Cover (in.)	Predicted Passes
3	3	Blend II	15	6	<10
	4	Blend II	12	12	20
	5	Silt	22	16	>10,000

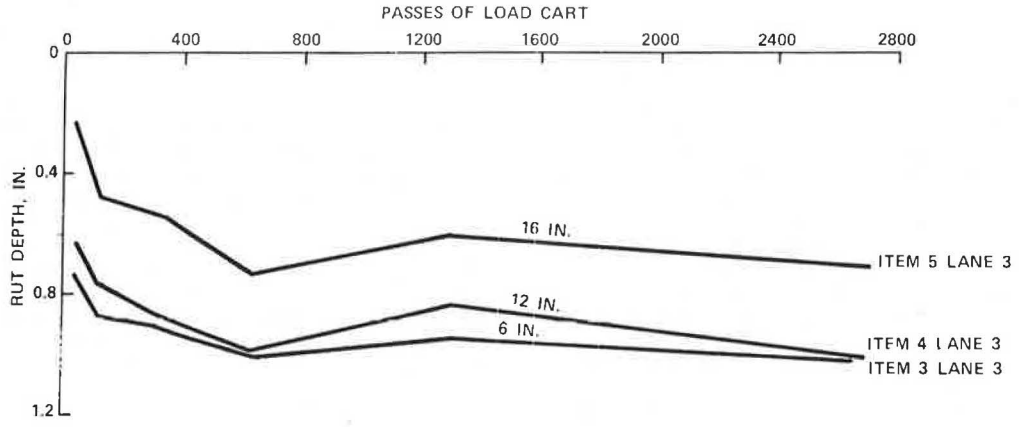

Figure 4. Rut depth measurements for surface-treated items.

the range of load, size of tire, and tire pressure tested.

Comparison

When the surface-treated items were compared to similar items having no surfacing, there was significant improvement in the performance of the surface-treated items. Data for unsurfaced items also trafficked by the simulated MX load cart are given in Table 1. As can be seen, item 3 of Lane 1 contained Blend II material at the surface and sustained 1.93 in. of rutting; whereas, item 3 in Lane 3 contained the double surface treatment on Blend II material and sustained only 1.1 in. of rutting. Also, item 4 of Lane 1 had Blend I at the surface and sustained 4.61 in. of rutting; whereas, item 4 of Lane 3 containing a single surface treatment sustained only 1.0 in. of rutting. There was also significant movement of the soil in items 3 and 4 of Lane 1 from underneath the tire to the sides of the traffic lane; this did not occur in the surface-treated items. The important implication of these results is that the application of a surface treatment on the in-place soils at the MX deployment area may be sufficient to carry the anticipated heavy loads and provide an adequately paved road.

CONCLUSIONS

The following conclusions resulted from this analysis:

1. Adequate compaction of soil layers is important to prevent densification.
2. Surface treatments performed satisfactorily under heavy loads.
3. Rutting of soil layers was reduced by the application of surface treatments.

REFERENCES

1. Planning and Design of Roads, Airbases, and Heliports in the Theater of Operations. Technical Manual 5-330, Department of the Army and Air Force, Sept. 1968.
2. V.C. Barber et al. The Deterioration and Reliability of Pavements. Technical Report S-78-8, U.S. Army Engineer Waterways Experiment Station, CE, Vicksburg, Miss., July 1978.

Development of Rigid and Flexible Pavement Load Equivalency Factors for Various Widths of Single Tires

JOHN P. HALLIN, JATINDER SHARMA, AND JOE P. MAHONEY

An analytical study to compare the effects of axles with single and dual tires on pavement performance is presented. Both rigid and flexible pavements were analyzed using currently available finite-element and elastic-layer analysis programs. The stresses and strains obtained from these programs were used in fatigue failure models to develop equivalency relationships between dual tires and various widths of single tires. Equivalent wheel-load factors were developed for various widths of single tires on both rigid and flexible pavements. These factors can be used to evaluate regulations relating to tire and axle loadings. They also permit conversion of mixed traffic having axles with single tires to equivalent 18-kip dual-tire, single-axle load applications for use in pavement design and evaluation.

An increasing number of trucks are being observed with heavy loads on axles with single tires. Concern over whether current regulations properly consider the relative effects of axles with single tires resulted following observations of serious distress on a highway in northwestern Washington State. In 1979 as the result of a railroad abandonment, transportation of limestone between a quarry and cement plant near Bellingham, Washington, shifted to trucks. The trucking contractor elected to use tandem axles with single 12-in. wide tires on double trailer trucks. This tire and axle configuration was selected to permit the maximum load on the minimum number of tires and comply with tire and axle load regulations. Washington State Department of Transportation regulations permit a maximum tire load of 550 lb/in. of width for tires less than 12 in. wide and 660 lb/in. of width for tires 12 in. wide or wider. The maximum axle loads permitted are 20,000 lb for single axles and 34,000 lb for tandem axles.

It became apparent that the use of single tires in lieu of dual tires should be examined. Thus, the objective of this study was to determine the relationship between axles with single tires and axles with dual tires and pavement performance. The results of the study can be used to answer the question: If axles with single tires are a major contributor to pavement deterioration, what changes are needed in the regulations?

Various rigid and flexible pavement sections were analyzed by using existing finite-element and elastic-layer analysis programs. The maximum calculated stresses and strains resulting from various tire loads were used to determine the fatigue life of the pavement under these loads. Equivalency factors between single and dual tires were then determined based on relative fatigue lives. Dual tires with a width of 10 in. and center to center spacing of 15 in. and single tires with widths of 10, 12, 14, 16, and 18 in. were used in the analysis. The study approach is outlined in Figure 1.

ANALYSIS OF RIGID PAVEMENTS

In the analysis of portland cement concrete pave-

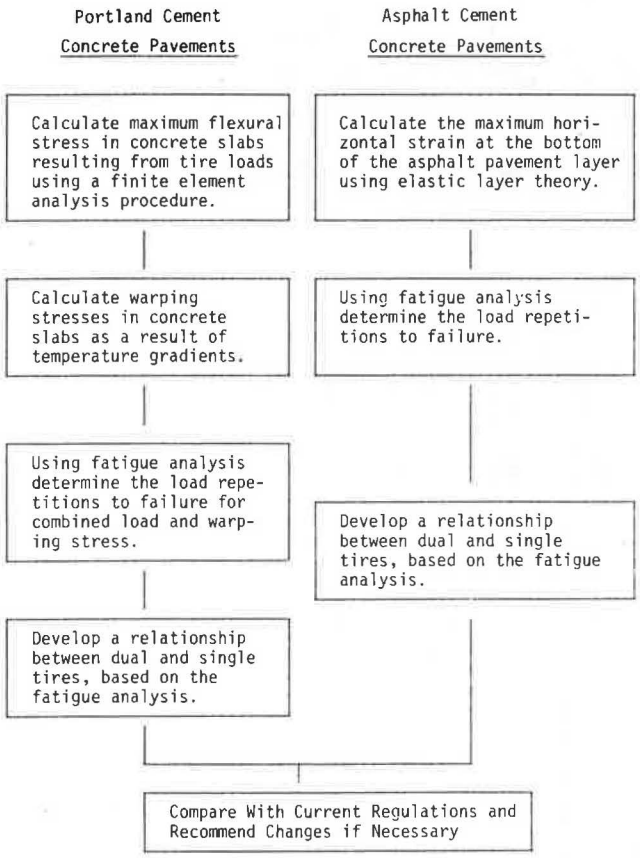

Figure 1. Study approach.

ments, the combined stresses resulting from traffic loads and temperature gradients within the pavement were considered. The magnitude of these stresses is a function of the pavement section, material properties of the concrete, joint design, and subgrade support. Most recently constructed concrete pavements in the Washington State Highway System are 9 in. thick. They are placed on a gravel or asphalt treated subbase 4 in. or more in thickness. The pavements are plain jointed concrete, and aggregate interlock provides the load transfer across the joints. Transverse joints are skewed at a ratio of 2:12 with a random spacing of 9, 10, 14, and 13 ft.

To bracket the range of conditions generally expected, plain concrete pavements with thicknesses of 7, 9, and 12 in. over a foundation with a modulus of subgrade reaction of 100 and 300 psi/in. were analyzed. Material properties of the concrete were modulus of rupture, 750 psi; modulus of elasticity, 4.5×10^6 psi; and Poisson's ratio, 0.15.

Load Stresses

Load-related stresses in concrete pavements were determined by using the ILLI-SLAB finite-element computer program (1). The program is relatively simple and inexpensive to use; and, as reported by Tabatabaie and Barenberg (2), the results agree closely with both theoretical and experimental results.

A large number of variables affect the stresses in concrete pavement. As a first step in the study, the variables that had the greatest effect on tensile stresses in the pavement slab were identified. The following are the basic parameters selected for the identification process: The maximum legal axle loads of 20,000 lb for single axles and 34,000 lb for tandem axles; and tire widths of 10 in. for dual tires, 16 in. for single tires on single axles, and 13 in. for single tires on tandem axles. These tire widths were based on the regulatory requirements for maximum tire load. Because the loaded pavement area modeled in the program is a rectangle, the transverse dimension was the tire width and the longitudinal dimension varied depending on the axle load. The tire contact pressure was 80 psi.

The initial phase of the analysis consisted of determining the magnitude of the tensile stresses in the concrete pavement for single and tandem axles at four load positions. The axle configurations examined were as follows: Case I, a single axle with dual 10-in. tires; Case II, a single axle with single 16-in. tires; Case III, tandem axles with 10-in. dual tires; and Case IV, tandem axles with single 13-in. tires. Four load positions were analyzed: (a) at the joints with the vehicle centered in the lane; (b) at the joint with the right wheel at the pavement edge; (c) at the midpoint of the slab with the right wheel at the pavement edge; and (d) at the midpoint of the slab with the right wheel 12 in. from the pavement edge. The results clearly showed that the mid-panel edge loadings caused the most stress and that maximum tensile stress was located at the bottom edge of the mid-panel slab. The mid-panel edge loadings, shown in Figure 2, were selected for use in this study.

A single axle, mid-panel edge load, 9-in. pavement, and a modulus of subgrade reaction of 100 psi/in. were selected for the analysis of the sensitivity of load-related stresses to variations in tire pressure, single tire width, and joint spacing. These were varied as follows:

1. Tire contact pressures of 70, 80, 90, and 100 psi were analyzed for both 10-in. dual tires and 16-in. single tires. The results, shown in Figure 3, indicate that the variation in edge stress is about 1 percent for tire contact pressures between 70 and 100 psi.
2. The effects of tire width were analyzed using a 20-kip single axle load with 10-, 12-, 14-, 16-, and 18-in. wide single tires. The results, shown in Figure 4, indicate a definite relationship between tire width and pavement stresses.
3. Joint spacings of 13, 15, and 20 ft were analyzed to determine the effect of joint spacing on pavement edge stress. The results, shown in Figure 5, indicate a maximum variation of less than 3 percent.

Based on the preceding a decision was made to use a tire contact pressure of 80 psi and a joint spacing of 13 ft in this analysis of pavement stresses.

Warping Stresses

Differences in temperature between the top and bottom surfaces of a concrete slab will cause the slab to warp. The weight of the slab and its contact with the subgrade restricts the movement of the slab and stresses are developed. Measurements by Teller and Southerland (3) show that the temperature differential between the pavement layers is much larger during the day than during the night. Furthermore, during the day the temperature of the upper surface of the concrete slab is higher than the temperature at the bottom of the slab placing tensile stresses at the bottom of the slab. This is important, because the maximum load-related tensile stresses also occur at the bottom of the concrete pavement slab.

To evaluate warping stresses, the temperatures at the top and bottom of the slab were computed from Weather Bureau data using a procedure developed by Barber (4). Maximum pavement temperatures were cal-

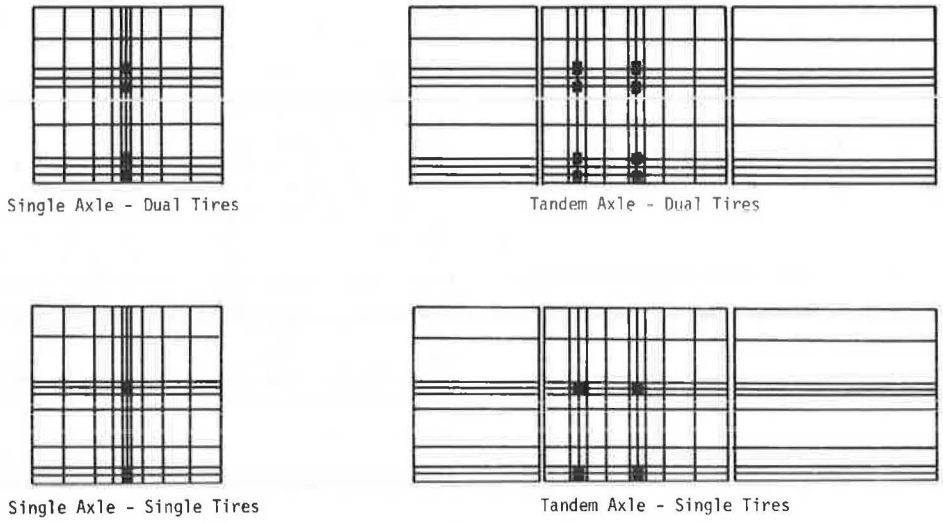

Figure 2. Loading cases used in the finite-element analysis of concrete pavement.

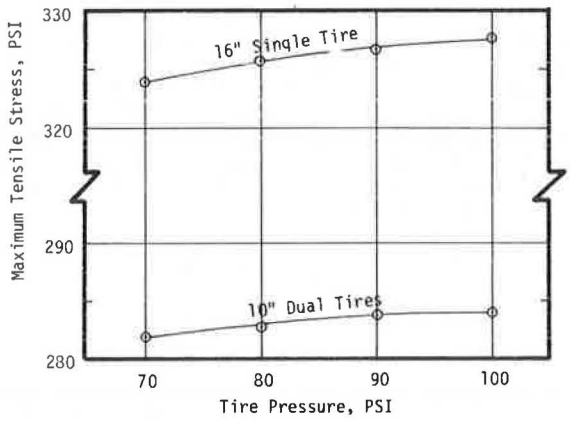

Figure 3. Effect of variations in tire pressure on edge stress.

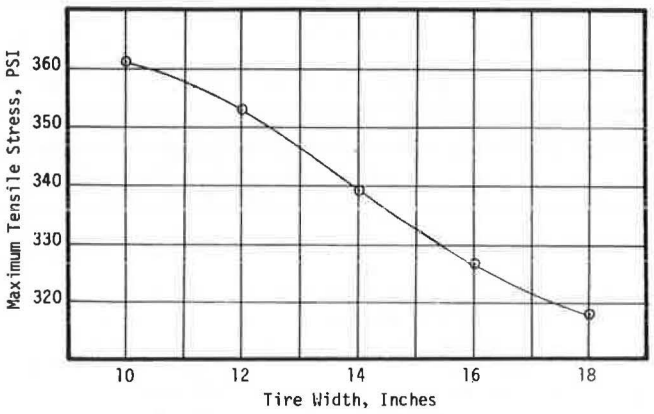

Figure 4. Effect of the width of a single tire on edge stress.

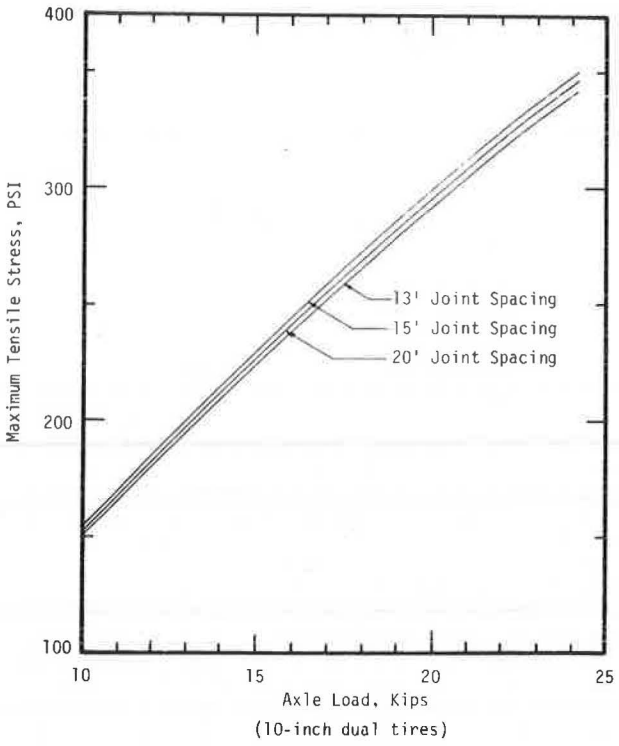

Figure 5. Effect of joint spacing on load-related edge stress.

culated for 7-, 9-, 10-, and 12-in. slabs in eastern and western Washington. Temperatures were calculated for each slab thickness, and the difference in gradients between eastern and western Washington was only about 5 percent. Therefore, to reduce the number of computations, only the western Washington pavement temperatures were used for the analysis.

To determine the maximum combined load and warping stresses, the warping stresses were calculated at the bottom center of the longitudinal pavement edge. This was where the maximum load-related edge stresses were found. Two methods for computing warping stress were considered: a procedure presented by Bradbury (5), which is based on Westergaard's work, and a set of regression equations developed by Darter (6) using data developed from a finite-element analysis.

The two methods were compared using pavement temperatures for July, which was the month with the highest temperature gradient. The following variables were used in the analysis: moduli of subgrade reaction (K) of 50, 100, 200, and 300 psi/in. and pavement thicknesses of 7, 9, and 12 in. Figure 6 shows the stresses calculated for a 9-in. pavement. For higher K-values the Bradbury analysis gave much

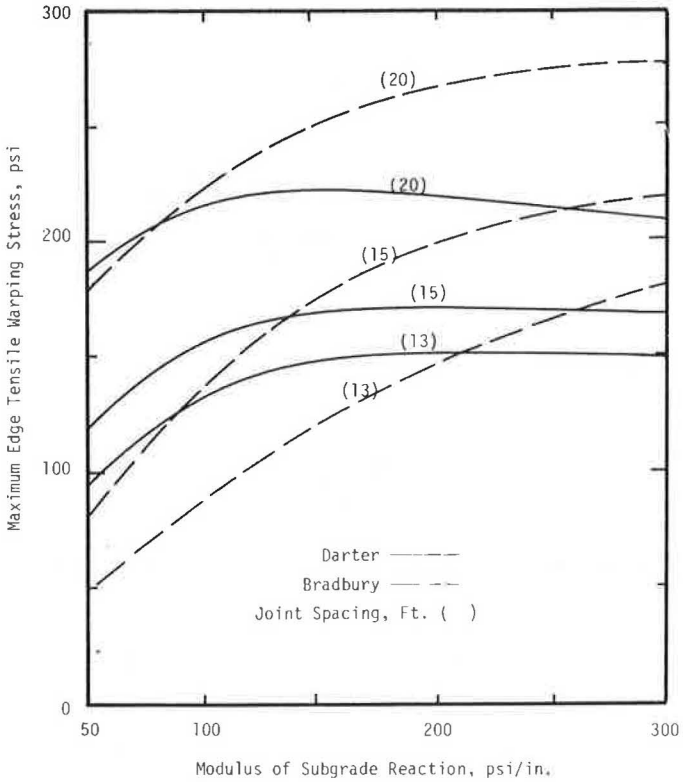

Figure 6. Warping edge stress during July for 9-in. pavements located in western Washington.

higher stresses than the Darter equations. However, the warping stresses calculated by the Bradbury procedure were generally higher than the measured stress because full restraint of the slab is assumed. Whereas, the finite-element program used by Darter allows the slab to curl in a weightless condition, then the restraining weight of the slab is added.

Based on a comparison of the two procedures and a review of previous work, the Darter equations, subject to the conditions in the following discussion, were selected to compute edge-warping stresses for this study. It was noted that above a modulus of subgrade reaction of approximately 200 psi/in. the warping stress tended to decrease. Majidzadeh, Ilves, and McComb (7) reported that when analyzing warping stresses using a coupled finite-element and elastic-multilayer subgrade program, no appreciable differences in warping stresses were noted for changes in subgrade support conditions. It was concluded that Darter's equations would be used to compute warping stresses for subgrades with K-values of 200 psi/in. and below. For K-values above 200 psi/in., the warping stress calculated for 200 psi/in. would be used. This assumed that for very weak subgrades, the subgrade yields as the slab warps. This provides uniform support over the length of the slab and reduces stress.

Fatigue Analysis

The fatigue relationship used was the one proposed by Vesic (8):

$$N_{2.5} = 225{,}000\,(MR/\sigma)^4 \quad (1)$$

where

$N_{2.5}$ = load repetitions to a serviceability index of 2.5,
MR = modulus of rupture of the concrete, psi, and
σ = tensile stress, psi.

The tensile stress was the combined load and warping stress. The fatigue analysis assumed that load repetitions were uniformly distributed over the year. The mean maximum monthly warping stress was used, which assumes that the load repetitions occurred during the day. It was felt that this assumption was adequate for comparison of tire sizes and configurations. Allowable repetitions for a specific axle load and pavement section was based on the following relationship:

$$\sum_{i=1}^{12} (n/Ni) = 1 \quad (2)$$

where

n = 1/12 of the total load repetitions, and
Ni = the allowable number of load applications for each month, based on the combined load stress and warping stress for that month.

Figure 7 shows the fatigue relationships developed for single axles on a 9-in. pavement.

Equivalency Relationships

The fatigue curves were used to determine the percent of a dual tire axle load that an axle with a specific width of single tire could carry and have an equivalent number of repetitions to a serviceability index of 2.5. It was found that each pavement depth and modulus of subgrade reaction had an individual relationship. These are shown in Figure 8.

Equivalent wheel-load factors were developed for dual tires on single axles and 10-, 12-, 14-, 16-,

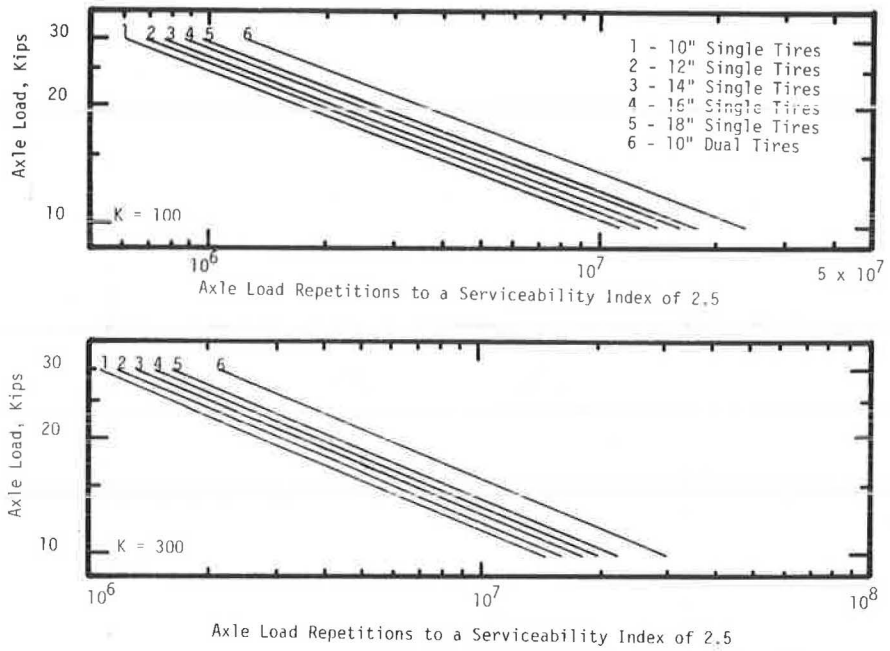

Figure 7. Axle load repetitions to a serviceability index of 2.5 for single-axle edge loading (cases I-C, II-C) on a 9-in. pavement.

and 18-in. wide single tires on single axles. The factors were developed for 7-, 9-, and 12-in. pavements with subgrade K-values of 100 and 300 psi/in. The following relationship was used to develop the equivalent wheel-load factors:

$$F_i = N_{18}/Ni \quad (3)$$

where

F_i = equivalent wheel load factor, 18-kip dual-tire, single axles;
N_{18} = repetitions to a serviceability index of 2.5 for an 18-kip dual-tire, single-axle load; and
N_i = repetitions to a serviceability index of 2.5 for the axle load being evaluated.

The equivalent wheel-load factors for single axles with single tires on a 9-in. pavement with a subgrade K-value of 100 psi/in. are given in Table 1.

ANALYSIS OF FLEXIBLE PAVEMENTS

The use of currently available analysis procedures to compare the effects of various widths of single tires with dual tires on flexible pavement performance presents an interesting problem. This is because the various elastic-layer and finite-element analysis procedures developed for flexible pavements use uniform circular loads. As a result, the width of the tire being modeled is a function of tire contact pressure and load. In a previous study, Terrel and Rimsritong (9) compared the relative damaging

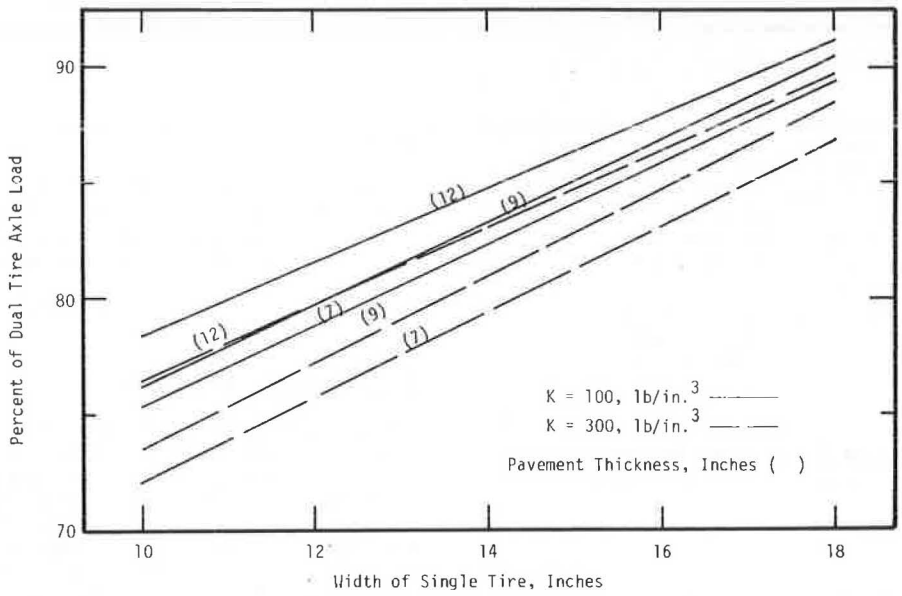

Figure 8. Percentage of dual-tire axle loads that an axle with single tires can carry for equivalent pavement life.

Table 1. Traffic equivalence factors for single axles with single tires, rigid pavement 9-in. thick, and modulus of subgrade reaction = 100.

Axle Load (kips)	Equivalent 18-kip Dual-Tire, Single-Axle Loads				
	Single Tire Width				
	10 in.	12 in.	14 in.	16 in.	18 in.
10	0.4251	0.3848	0.3407	0.2950	0.2728
12	0.6922	0.6266	0.5548	0.4803	0.4442
14	1.0453	0.9463	0.8378	0.7254	0.6709
16	1.4939	1.3524	1.1973	1.0367	0.9588
18	2.0469	1.8530	1.6405	1.4204	1.3137
20	2.7130	2.4561	2.1744	1.8827	1.7412
22	3.5005	3.1690	2.8056	2.4292	2.2466
24	4.4176	3.9992	3.5406	3.0656	2.8352
26	5.4719	4.9537	4.3857	3.7972	3.5119
28	6.6711	6.0394	5.3468	4.6294	4.2815
30	8.0227	7.2630	6.4301	5.5674	5.1490
32	9.5339	8.6310	7.6413	6.6161	6.1189
34	11.2118	10.1500	8.9861	7.7805	7.1958
36	13.0634	11.8262	10.4701	9.0653	8.3841
38	15.0954	13.6658	12.0988	10.4755	9.6882
40	17.3146	15.6748	13.8774	12.0155	11.1125

effects of various widths of single tires and dual tires. To simulate tire widths for various wheel loads, they varied the contact pressure. This resulted in contact pressures that were not representative of contact pressures encountered in the field.

The development of equivalency factors for axles with single tires in this study is an extension of the earlier study by Terrel and Rimsritong. Two additional modeling techniques were evaluated to determine if tire contact pressure or shape have a significant effect on the tensile strains at the bottom of the pavement.

Method of Analysis

The pavement sections analyzed were 3, 6, and 9.5 in. of asphalt concrete pavement on 8 in. of crushed aggregate base. The material properties used are given below.

Asphalt Concrete: The resilient modulus of asphalt concrete is a function of its temperature. Resilient modulus versus temperature relationships have been developed for Washington State University Test Track pavement (9). Assuming an average temperature of 68°F, a resilient modulus of 400,000 psi was selected. The Poisson's ratio was assumed to be 0.3.

Crushed Aggregate Base: The resilient modulus of untreated aggregates is a function of the confining stress. Repeated-load triaxial testing of crushed aggregate base on a project at the Washington State University Test Track resulted in the following relationship (9):

$$MR = 2843\theta^{0.6} \quad (4)$$

where

MR = resilient modulus, and
θ = bulk stress ($\sigma_1 + 2\sigma_3$ in the triaxial test).

This relationship and a Poisson's ratio of 0.4 were used for crushed aggregate base in the analysis for this study.

Subgrade: A wide range of modulus values for subgrade materials are encountered on highway construction in the state of Washington. Terrel and Rimsritong used a value of 6,500 psi and a Poisson's ratio of 0.45. For uniformity, these values were used in this study.

The maximum horizontal strain at the bottom of the asphalt concrete layer was calculated for various tire sizes and axle loads using the Elastic Theory Iterative Method-Dual Wheel Option (PSAD2A) computer program. This program, developed at the University of California at Berkeley, is capable of calculating stresses and strains due to dual wheel configurations. In addition, for layers with stress-dependent resilient modulus values, the modulus can be determined by an iterative process.

To compare axles with single tires to axles with dual tires, a fatigue distress model was used. Fatigue distress is assumed to be the cracking that results from repeated load applications and is a function of the horizontal strain at the bottom of the asphalt concrete layer. Fatigue analysis was used, because cracking is the principal form of asphalt pavement distress in Washington State (10). The fatigue model selected for this study was developed by Finn et al. (11). The model predicts the number of repetitions resulting in fatigue cracking equal to or less than 10 percent of the wheelpath.

$$\log N_f = 15.947 - 3.219 \log(\epsilon/10^{-6}) - 0.854 \log(E^*/10^3) \quad (5)$$

where

N_f = repetitions to failure,
ϵ = maximum tensile strain at the bottom of the asphalt bound layer, inches, and
E^* = resilient modulus, psi.

The following three techniques were used for modeling tire widths.

1. Constant Radius-Variable Pressure Method. This procedure was the method used by Terrel and Rimsritong. Three single tire widths were evaluated, 10, 15, and 18.5 in. The width of each dual tire was 10 in. The tire widths were maintained by varying the tire pressures. The maximum horizontal strains at the bottom of the asphalt pavement layer were determined and the fatigue life for various axle loads on the three pavement sections calculated. Figure 9 shows the relationship developed between axle loads and repetitions to failure for a 6 in. asphalt pavement section.

2. Double Circle-Constant Pressure Method. This method and the single circle-constant pressure method, to be discussed next, use the assumption that the axle load versus repetitions to failure curves for various single tire widths are parallel to the curve for dual tires. To determine the slope of the fatigue curves, curves were developed for dual tires using two methods: applying the wheel load through a circle with a constant radius and applying the load using a constant contact pressure of 80 psi. The slopes of the two curves were very close for the 9.5-in. asphalt pavement. However, the difference in slopes increased as the depth of the asphalt pavement section decreased.

It was concluded that the average slope would be an adequate representation of the slope of the fatigue curve. For dual tires, the average curve was fit through the intersection of the constant contact pressure and constant radium lines. An example of these curves for a 6-in. pavement section is shown in Figure 10. It is interesting to note that the intersection of these curves lies between 20- and 25-kip axle loads, which is in the load range commonly analyzed using the elastic layer programs.

To model tire width using the double circle method, two adjacent loading circles with a contact pressure of 80 psi were used. The radius of the circle was chosen so that four times the radius equalled the desired tire width. The total area, of two circles, was calculated and multiplied by the

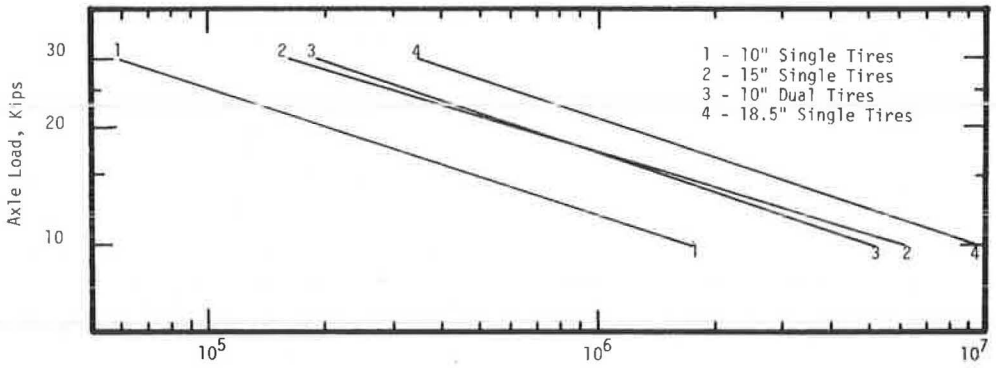

Figure 9. Axle load repetitions to failure for single axles on a 6-in. asphalt concrete pavement over an 8-in. crushed aggregate base—constant radius method.

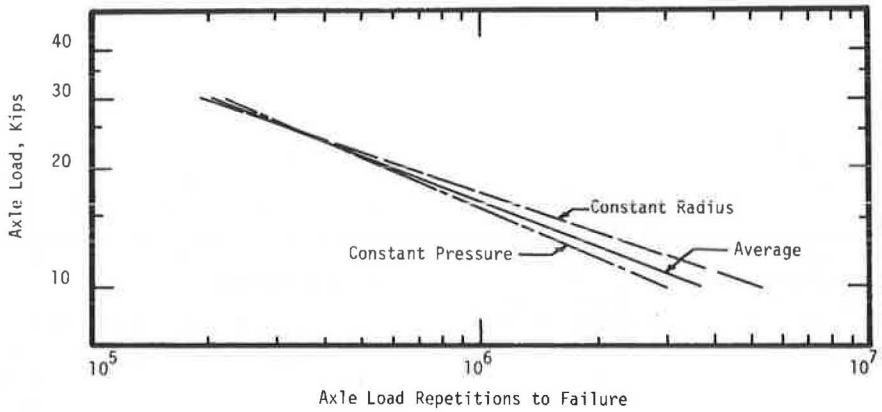

Figure 10. Fatigue relationship for single axles with dual tires (6-in. asphalt concrete pavement over 8 in. of crushed aggregate base).

contact pressure. This represented the simulated load on the single tire. The maximum horizontal strain at the bottom of the pavement layer was determined and the repetitions to failure calculated. The point representing axle load versus number of repetitions to failure was plotted and a fatigue curve fit through the point. Calculations were made for simulated tire widths of 10, 12, 14, 16, and 18 in. The resulting relationship for a 6-in. asphalt pavement section is shown in Figure 11.

3. Single Circle-Constant Pressure Method. This method is similar to the double circle method. In this case, the diameter of the circle was chosen to equal the width of the tire to be simulated. The

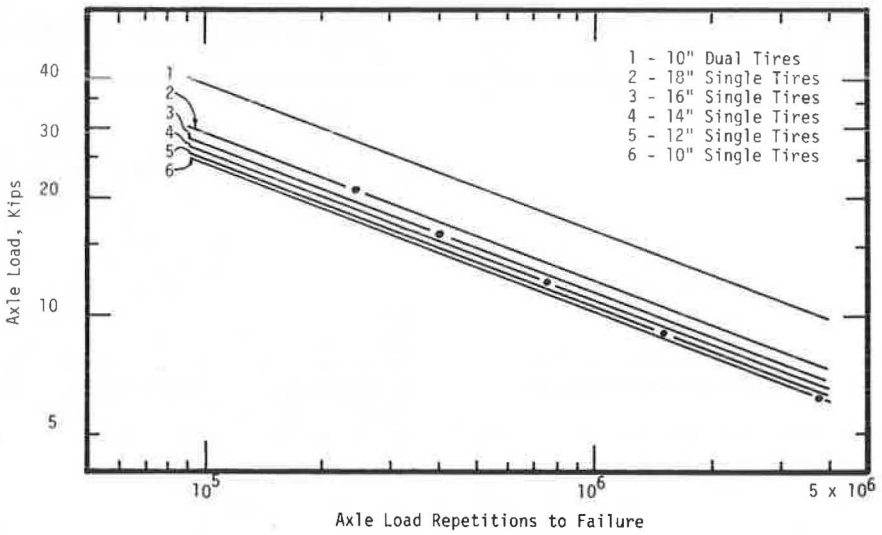

Figure 11. Axle load repetitions to failure for single axles on a 6-in. asphalt concrete pavement over an 8-in. crushed aggregate base—double circle method.

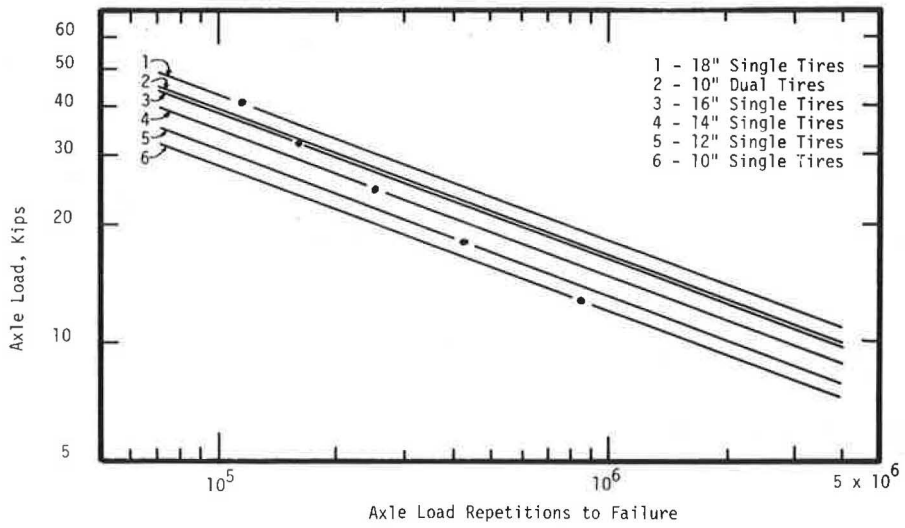

Figure 12. Axle load repetitions to failure for single axles on a 6-in. asphalt concrete pavement over an 8-in. crushed aggregate base—single circle-constant pressure method.

wheel load was equal to the area of the circle times the contact pressure, which was held constant at 80 psi. The maximum horizontal strain at the bottom of the asphalt pavement section was determined and repetitions to failure calculated. A fatigue curve was then fit through the point using the same method as in the double circle method. Fatigue curves were developed for 10-, 12-, 14-, 15-, and 18-in. wide tires. The curves for a 6-in. asphalt pavement section are shown in Figure 12.

Equivalency Relationships

For each method and pavement thickness, the percent of dual axle load that an axle with single tires could carry and have an equivalent fatigue life was determined. The equivalency relationships for a 6-in. asphalt concrete pavement are shown in Figure 13. Because of the wide range between the double-circle and the two single-circle methods, a comparison with actual field measurements was needed.

There have been only a limited number of investigations to measure the actual effects of dual tires versus single tires on pavement performance. At the AASHO Road Test an investigation was conducted to determine the performance and deflections for a number of pavement sections under loadings of several pieces of military transport equipment (12). These included the study of the use of low pressure, low silhouette (LPLS) tires on tractor and semitrailer units and the effects of the use of the GOER, a self propelled cargo or fluid transporter resembling a conventional two-axle tractor scraper. Both the LPLS and GOER tires were approximately the same width as the dual tires used for comparison.

Zube and Forsyth (13) reported on a study by the California Division of Highways in 1963 to determine the single-wheel, single-axle loading that would produce the same destructive effect as a dual-wheel, single-axle loading of 18,000 lb. The width of the single tire was approximately 12 in. At one test site they measured the horizontal strain at the bottom of the pavement section under both dual and single tire loadings.

Based on an analysis of the data from the AASHO Road Test and the California study it was concluded that an axle with a single tire equal in width to the dual tires on a 3-in. asphalt pavement section should be able to carry 120 percent of a dual tire

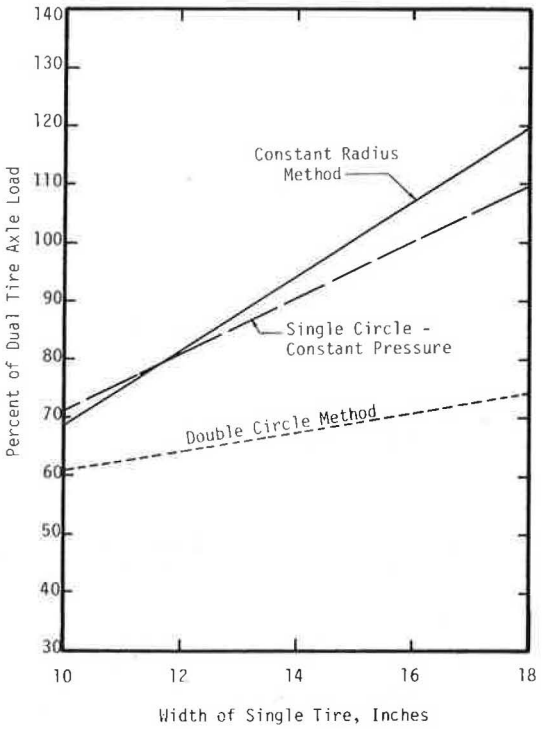

Figure 13. Percentage of dual-tire axle load that an axle with single tires can carry for equivalent fatigue life (6-in. asphalt concrete pavement).

axle load and have an equivalent destructive effect in fatigue, whereas an axle with 12-in. wide tires on a 3-in. asphalt pavement section should be able to carry 62 percent of a dual-tire axle load. Figure 14 shows these points connected with a straight line on a plot of the equivalency relationships developed for single versus dual tires on a 3-in. pavement. The line appeared to fall midway between the single and double circle lines. Therefore, an average relationship was developed between the single methods and the double-circle method.

The results shown in Figure 15 indicate that the average single-tire to dual-tire equivalency is close to the equivalency developed using available

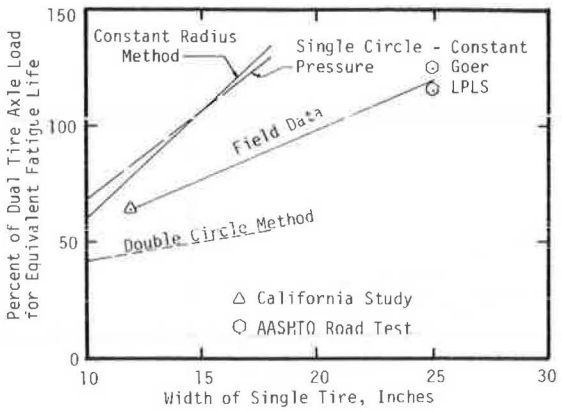

Figure 14. Comparison of methods for computing the equivalency of single tires to dual tires with field data for a 3-in. asphalt concrete pavement.

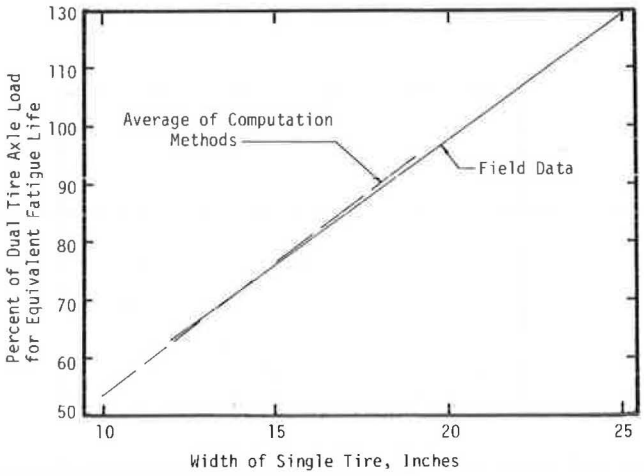

Figure 15. Comparison of the average between the single-circle and double-circle computation methods and available field data for 3-in. asphalt concrete pavement.

field data. For this reason, it was decided to use an average between the single-circle and double-circle equivalencies for all three pavement sections. These are shown in Figure 16. Admittedly, there is little data to support the use of the average relationship; and field studies will be undertaken to improve this relationship. These studies will include measurements of deflections under axles with single and dual tires using extensometers installed in the pavement structure.

The fatigue curves for dual tires and the equivalency relationships in Figure 16 were used to develop equivalent wheel-load factors for 10-, 12-, 14-, 16-, and 18-in. wide tires on flexible asphalt concrete pavement (ACP) sections with approximate AASHTO structural numbers of 2, 4, and 6. The equivalency factors were calculated using the relationship in Equation 3. The equivalency factors for a pavement section with an SN of 4 are given in Table 2.

CONCLUSIONS

Load equivalency relationships have been developed that can be used to determine the effects of axle loads, with various widths of single tires, on both rigid and flexible pavements. These relationships can be used to evaluate regulations relating to tire

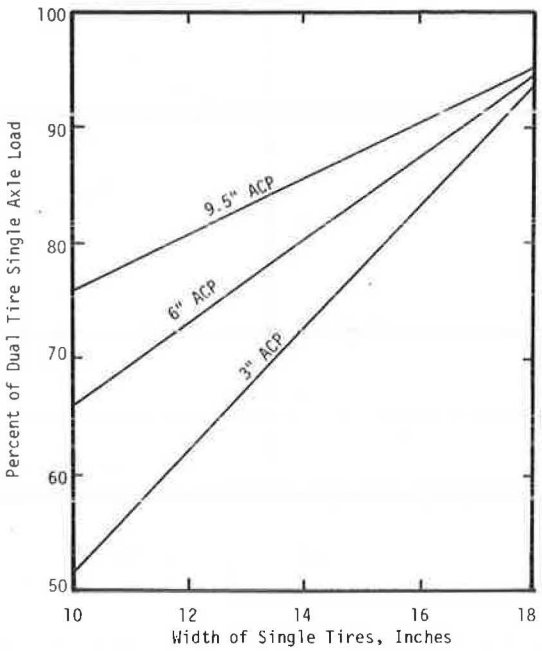

Figure 16. Average equivalency of single axles with single tires to single axles with dual tires for 9.5-, 6-, and 3-in. asphalt concrete pavements.

Table 2. Traffic equivalence factors for single axles with single tires, asphalt concrete pavement, and SN = 4.

Axle Load (kips)	Equivalent 18-kip Dual-Tire, Single-Axle Loads				
	Single Tire Width				
	10 in.	12 in.	14 in.	16 in.	18 in.
10	0.6309	0.4790	0.3731	0.2969	0.24050
12	1.0286	0.7809	0.6082	0.4840	0.39210
14	1.5549	1.1805	0.9195	0.7317	0.59277
16	2.2243	1.6887	1.3153	1.0466	0.84793
18	3.0502	2.3157	1.8038	1.4353	1.16279
20	4.0458	3.0715	2.3925	1.9038	1.54232
22	5.2237	3.9658	3.0891	2.4580	1.99136
24	6.5962	5.0077	3.9007	3.1038	2.51455
26	8.1750	6.2064	4.8343	3.8468	3.11643
28	9.9718	7.5705	5.8969	4.6923	3.80141
30	11.9979	9.1087	7.0951	5.6457	4.57379
32	14.2643	10.8293	8.4353	6.7121	5.43778
34	16.7818	12.7406	9.9241	7.8968	6.39749
36	19.5610	14.8505	11.5675	9.2045	7.45695
38	22.6123	17.1670	13.3719	10.6403	8.62014
40	25.9458	19.6978	15.3432	12.2089	9.89093

Note: SN = 4 represents 5 to 8 in. of ACP over aggregate base.

width and axle loading configurations. They also permit conversion of mixed traffic, including axles with single tires, to equivalent 18-kip dual-tire, single-axle load applications for use in pavement design and evaluation.

A summary of size and weight limits published by the American Trucking Associations (14) indicate that at least 24 states have regulations that control maximum tire loads. Ten additional states have regulations that limit the load on axles with single tires. Of the states having regulations limiting the maximum tire load, 19 permit tire loads in excess of 550 lb/in. of tire width. This includes six states that permit tire loads of 800 lb/in. of width. The relative effects of single versus dual tires on pavement performance were compared with the regulations for maximum tire loads.

This comparison for a 20,000 lb dual-tire axle load is shown in Figure 17. The comparison supports the requirement of 550 lb/in. of tire width. However, tire loads above 550 lb/in. of tire width are not supported. For example an axle with 14-in. single tires on a 9-in. concrete pavement with a subgrade K = 100 can carry approximately 82 percent of a dual-tire axle load or a maximum of 16,400 lb for an equivalent fatigue life, whereas regulations permitting 660 lb/in. of tire width would allow an axle load of 18,400 lb and regulations permitting 800 lb/in. of tire width would allow the maximum 20,000 lb axle load.

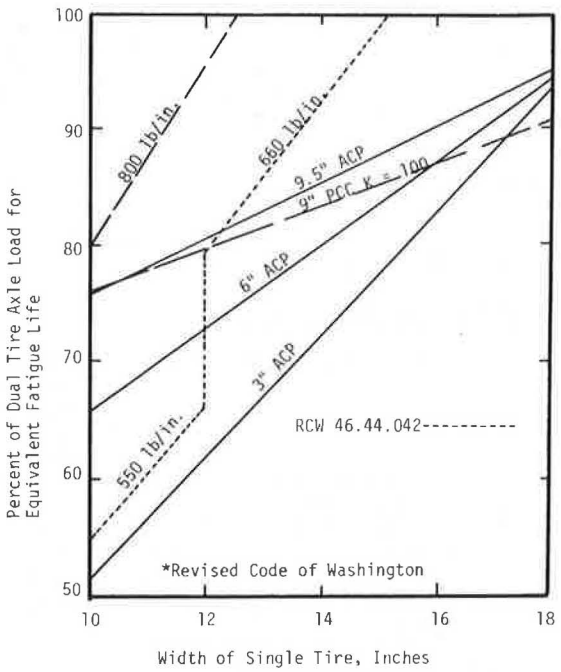

Figure 17. Comparison of the regulatory requirements for maximum tire loads with the dual and single tire relationships for equivalent fatigue life where the dual tire axle load equals 20,000 lb.

ACKNOWLEDGMENT

This work was sponsored by the Washington Department of Transportation in cooperation with FHWA.

REFERENCES

1. A.M. Tabatabaie and E.J. Barenberg. Longitudinal Joint Systems in Slip-Formed Rigid Pavements, Vol. 3, User's Manual. Rept. FAA-RD-79-4-III, Federal Aviation Administration, 1979.
2. A.M. Tabatabaie and E.J. Barenberg. Finite-Element Analysis of Jointed or Cracked Concrete Pavements. TRB, Transportation Research Record 671, 1978.
3. L.W. Teller and E.C. Southerland. The Structural Design of Concrete Pavements, Part 2: Observed Effects of Variations in Temperature and Moisture on the Size, Shape and Stress Resistance of Concrete Pavement Slabs. Public Roads, Vol. 16, No. 9, 1935.
4. E.S. Barber. Calculation of Maximum Pavement Temperature from Weather Reports. HRB, Bull. 168, 1957.
5. R.D. Bradbury. Reinforced Concrete Pavements. Wire Reinforcement Institute, Washington, D.C., 1938.
6. M.I. Darter. Design of Zero Maintenance Plain Jointed Concrete Pavement, Vol. 1, Development of Design Procedures. Rept. FHWA-RD-77-111, FHWA, 1977.
7. K. Majidzadeh, G.J. Ilves, and R. McComb. Mechanistic Design of Rigid Pavements. Proc., 2nd International Conference on Concrete Pavement Design, Purdue University, West Lafayette, Ind., April 1981.
8. A.S. Vesic and S.K. Saxena. Analysis of Structural Behavior of AASHO Road Test Rigid Pavements. HRB, NCHRP Rept. 97, 1970.
9. R.L. Terrel and S. Rimsritong. Pavement and Response Equivalencies for Various Truck Axle Tire Configurations. Research Rept. 17.1, Washington State Highway Commission, Olympia, Wash., 1974.
10. Washington State Department of Transportation. 1979 Final Pavement Condition. Olympia, Wash., 1979.
11. F. Finn, C. Saraf, R. Kulkarni, K. Nair, W. Smith, and A. Abdullah. The Use of Distress Prediction Subsystems for the Design of Pavement Structures. 4th International Conference on Structural Design of Asphalt Pavements, Univ. of Michigan, 1977.
12. The AASHTO Road Test, Report 6: Special Studies. HRB, Special Report 61F, 1962.
13. E. Zube and R. Forsyth. An Investigation of the Destructive Effect of Flotation Tires on Flexible Pavement. HRB, Highway Research Record 71, 1965.
14. American Trucking Associations. Summary of Size and Weight Limits. Washington, D.C., 1981.

Strain Energy Analysis of Pavement Designs for Heavy Trucks

HERBERT F. SOUTHGATE, ROBERT C. DEEN, AND JESSE G. MAYES

Classical concepts of work, or strain energy, as applied to the analysis of stresses, strains, and deflections under various vehicular load configurations on pavement systems are summarized and controlling equations for strain energy density are presented. When considering strain energy density, strain energy, or work, all components of stresses or strains must be taken into account so that total internal behavior can be evaluated. Previously, pavement thickness design systems have been developed using only one component of strain, typically at the bottom of the asphaltic concrete layer or at the top of the subgrade. Strain energy concepts permit modifications to thickness design systems to account for the net effect of all components of strains or stresses. Effects of loads and distribution of loads on vehicles are summarized. One startling result shows the large increase in fatigue rate due to unequal distribution of loads between the two axles of a tandem group relative to the fatigue rate caused by an equal load distribution. Damage factors and pavement thickness designs for heavily loaded trucks exceeding legal load limits are also discussed. The effects of those vehicles on Interstate pavements are compared to the effects of more normally loaded vehicles.

The work done by a force when its point of application is displaced is the product of that force (parallel to the direction of movement) and the displacement. When work is done on some systems, the internal geometry is altered in such a way that there is a potential to give back work when the force is removed, and the system returns to its original configuration. This stored energy is defined as strain energy. Strain energy per unit volume at a given point in the body is the strain energy density at that point.

STRAIN ENERGY

Strain energy density is a function of Young's modulus of elasticity and Poisson's ratio of the material and the nine strain (or stress) components; however, it is independent of the coordinate system. Stress and strain components, referenced to a local cylindrical coordinate system, for each load are calculated by the Chevron program (1). The classical equation for strain energy density derived by Sokolnikoff (2) is as follows:

$$W = \Sigma\ \Sigma\ [(1/2)\lambda\nu\,\epsilon_{ii} + G\,\epsilon_{ij}\epsilon_{ij}]$$

$$-(1/2)\lambda\nu^2 + G(\epsilon^2_{11} + \epsilon^2_{22} + \epsilon^2_{33} + 2\epsilon_{12} + 2\epsilon^2_{23} + 2\epsilon^2_{13}) \quad (1)$$

where

W = strain energy density (or energy of deformation per unit volume);
ϵ_{ij} = i,jth component of the strain tensor;
G = $E/[2(1 + \mu)]$, the modulus of rigidity (or the shear modulus);
E = Young's modulus;
μ = Poisson's ratio;
λ = $E\mu/[(1 + \mu)(1 - 2\mu)]$; and
ν = $\epsilon_{11} + \epsilon_{22} + 33$.

Strain energy density may be calculated using stress components by the equation

$$W = -\mu\Theta^2/2E + [(1+\mu)/2E](\sigma^2_{11} + \sigma^2_{22} + \sigma^2_{33}) +$$

$$[(1+\mu)/E](\sigma^2_{12} + \sigma^2_{23} + \sigma^2_{31}) \quad (2)$$

where

$\Theta = \sigma_{11} + \sigma_{22} + \sigma_{33}$ and
σ_{ij} = i,jth component of the stress tensor.

Inspection of Equation 1 shows that the term $E/[2(1 + \mu)]$ is contained by means of the terms λ and G. Also, it is noted that the strain components are squared. Having calculated strain energy density, work strain (3) may be obtained from

$$\epsilon_w = (2\,W/E)^{0.5} \quad (3)$$

where ϵ_w is work strain. The associated work stress is given by $E\epsilon_w$.

Interpretations of Work Strain

Admittedly, work strain is not a true strain because Poisson's ratio has not been eliminated before taking the square root; however, it is of the same order of magnitude as any of the strain components. Calculating the work strain is a minor effort because all terms of the equations are either required input to, or calculated output of, the Chevron N-layer (1,4) program. Work strain is also the composite, or net effect, of all strain components and thus is an indicator of the total strain behavior. Figure 1 shows that there is a direct correlation between a strain component and work strain.

Uses for Work Strain

Some thickness design systems for flexible pavements are based partly on tensile strain criteria at the bottom of the asphaltic concrete layer. Kentucky's

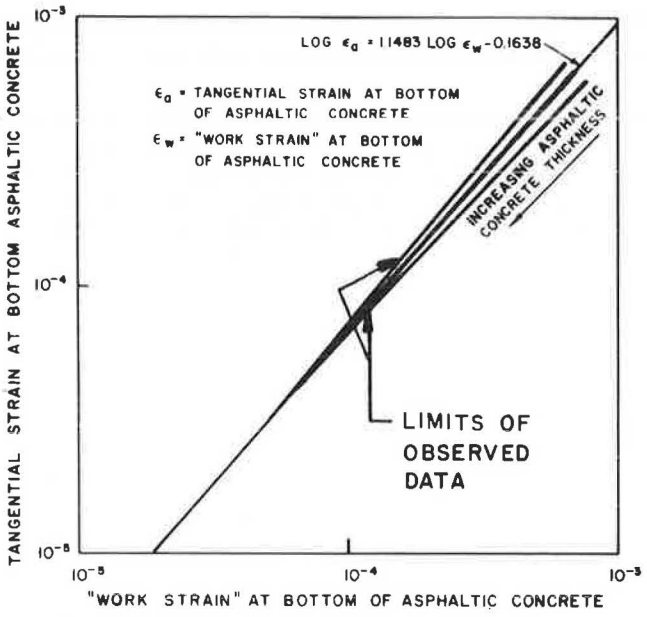

Figure 1. Tensile strain versus work strain.

proposed system (5-7) is based in part on the tangential strain component. The tangential component is generally the largest in magnitude, but the radial component often is nearly as large. Only the tangential component has been used because laboratory test data yield one component of tensile strain. The net effect of all components of strain (work strain) can be correlated with any component of strain. Thus, design systems based on one component of strain may be converted to a design system that uses the net effect of all component strains. The load-damage factor relationships presented in this paper are based on work strain. All comments concerning component strains also apply to component stresses.

Fatigue Concepts

The equivalent axle load (or EAL) approach converts all axle load weights that pass over a pavement during its design life to some reference axle load. The reference axle load weight selected in Kentucky was 80 kN (18,000 lb). Any axle load could have been selected, and the change from one axle load reference to another should not change the results of a design system. The 80-kN (18,000-lb) axle load was probably selected because it represented, at the time the EAL concept was developed, the typical legal axle load limit recognized in many states. The 80-kN (18,000-lb) axle load was also the reference used at the AASHO Road Test in the early 1960s.

The passage of one 80-kN (18,000-lb) axle load results in the application of one EAL. An 89-kN (20,000-lb) axle load is equivalent to applying 1.7 EALs; the 89-kN (20,000-lb) axle load would cause 1.7 times the damage to the pavement as would one 80-kN (18,000-lb) axle load. The EAL for a given group of axles, thus, represents the damage factor (load equivalency) for that particular group.

Figure 2 illustrates how the damage factor for selected axle groups varies with increasing loads on those groups. The load-damage factor relationships shown in Figure 2 were developed from analyses using the Chevron N-layer computer program, which is based on elastic theory. Pavements analyzed were the hundred possible combinations of thicknesses, of which 67 were built and tested, at the AASHO Road Test. The tire loads and axle spacings were those used on the test vehicles at the AASHO Road Test. The load-damage factor relationship is expressed by

$$DF = 10^{[a + b(\log Load) + c(\log Load)^2]} \quad (4)$$

where

DF = damage factor and
a,b,c = coefficients by regression analyses.

Table 1 gives the numerical values for the coefficients in Equation 4 for each axle configuration. The coefficients have been published previously (8) for the two- and four-tired single axle and eight-tired tandem axle groups.

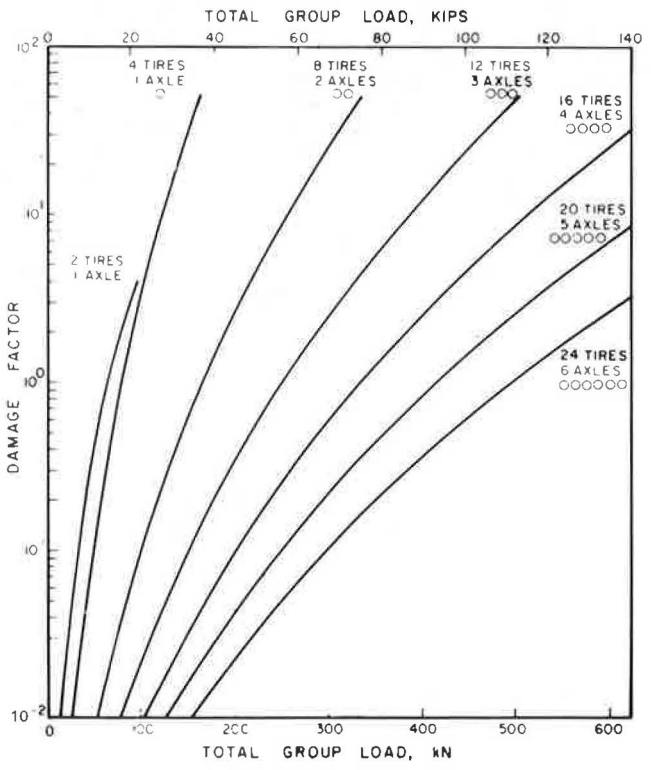

Figure 2. Variation of damage factor for selected axle groups as load on axle group is changed.

Table 1. Regression coefficients to calculate damage factors for various axle configurations.

Log (Damage Factor) = a + b (Log Load) + c [Log Load]^2

AXLE CONFIGURATION	COEFFICIENTS a	b	c
Two-Tired Single Front Axle	-3.540112	2.728860	0.289133
Four-Tired Single Rear Axle	-3.439501	0.423747	1.846657
Eight-Tired Tandem Axle	-2.979479	-1.265144	2.007989
Twelve-Tired Tridem Axle	-2.740987	-1.973428	1.964442
Sixteen-Tired Quad Axle	-2.589482	-2.224981	1.923512
Twenty-Tired Quint Axle	-2.264324	-2.666882	1.937472
Twenty-Four Tired Sextet Axle	-2.084883	-2.900445	1.913994

Figure 3 shows how the damage factor increases due to an increasing difference of load distribution between the axles of a tandom group. The significance of unevenly distributed loads between the two axles of a tandem is indicated by an examination of individual axle loads for 335 vehicles of the 3S2 (five-axle semitrailer) configuration listed in the 1976 W6 tables for Kentucky. Appropriate damage factors were applied to those individual axle loads. Figure 4 shows the large difference between uniform and nonuniform load distributions using factors from Figure 2 and those adjusted by Figure 3 for nonuniform load distributions. AASHTO (9) damage factors also were applied to the same vehicle loads. Figure 4 shows that there is very little difference in the summation of EALs based on AASHTO damage factors and the energy-based factors adjusted for nonuniform loading.

For example, it has been found that only about 10 percent of the tandem axle groups observed in Kentucky have loads uniformly distributed between the two axles. Analyses indicate that the nonuniform distribution between the axles in a tandem group can account for as much as a 40-percent increase in the damage to a pavement. The difference between the

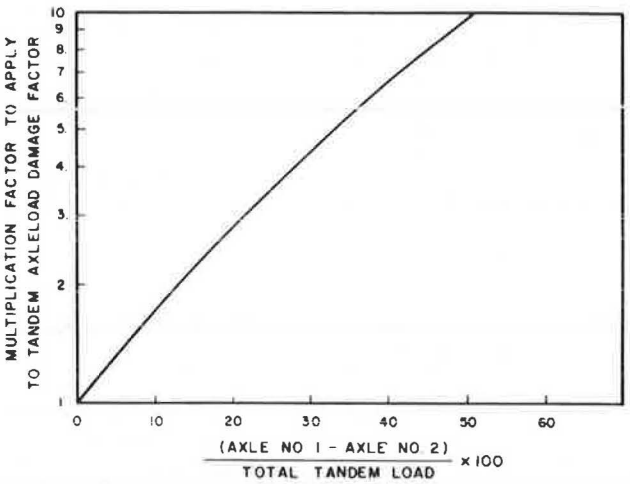

Figure 3. Multiplying factors increasing damage factors due to nonuniform load distribution between axles of a tandem.

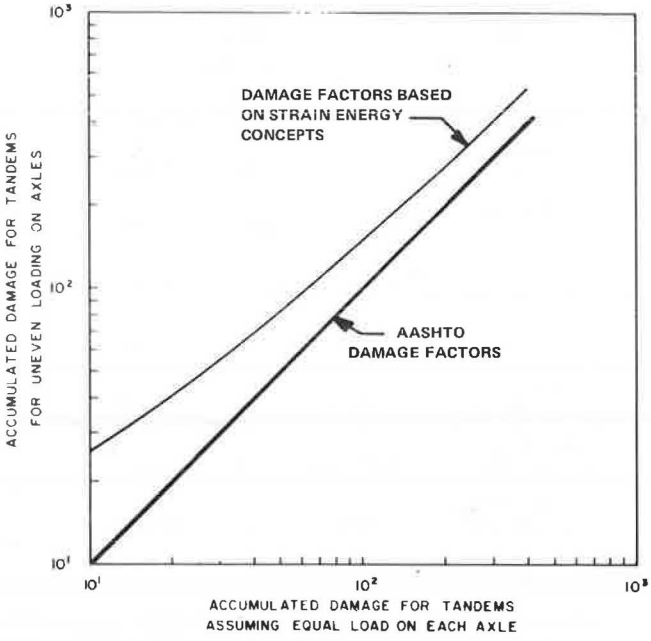

Figure 4. Accumulated fatigue of 335 vehicles from 1976 W6 tables for Kentucky.

axles exceeded 8.9 kN (2,000 lb) for three of 10 tandems on semitrailers and two of 10 tandems on tractors. The use of floating axles also may be undesirable unless a means is found to ensure that the floating axle carries its proper share of the load. It has been observed that loads carried by floating third axles may vary from a low portion of the total load, providing little benefit from the additional axle and shifting the additional load to the two remaining axles in the group, to an unduly large percentage of the load. Both conditions increase the damage significantly over the situation where the load is distributed uniformly among all axles.

Experience indicates that the elastic theory and work concept used in Kentucky predict reliably the number of EALs a given pavement system can support in its lifetime. Conversely, it is possible to design a pavement that will adequately resist the damage of a specified number of EALs. However, the problem of predicting the rate at which EALs will accumulate remains. This involves estimating the numbers and types of vehicles that will use a section of highway as much as 30 years in advance. To illustrate the problem, a section of KY 15 was designed to carry a given number of EALs. The pavement, however, failed after only 8 months. Analyses showed that the pavement did carry the EALs for which it was designed. Unfortunately, the opening of a coal producing operation that created a high-volume of heavy traffic was not foreseen, and the rate of accumulating EALs was underestimated.

HEAVY LOAD DESIGN

In almost any state, some commodity is transported on overloaded trucks. Coal and limestone are two such commodities in Kentucky. In other states, industries that generate overloaded trucks might be logging, pulp wood, minerals, ores, grains, or other agricultural products. Many county roads in Illinois, for example, lead to a grain elevator and have only one paved lane. Typical gross loads are given in Table 2 for three truck configurations in Kentucky coal fields. Table 2 also gives the corresponding damage factors obtained from Figure 2. Classification counts in 1981 on one of the main coal-haul non-Interstate routes were used to obtain the percentages of the three configurations. Note that the 3S3 can carry 111 kN (25,000 lb) more than the 3S2, yet the 3S3 produces slightly less total damage per trip.

Table 3 gives only the design EALs for the three truck configurations of Table 2. Two of the thickness design charts contained in the proposed Ken-

Table 2. Damage factors for typical heavily loaded truck configurations.

CONFIGURATION	GROSS LOAD (kips)	FRONT AXLE LOAD (kips)	FRONT AXLE DAMAGE FACTOR	TANDEM LOAD (kips)	TANDEM DAMAGE FACTOR	TRIDEM LOAD (kips)	TRIDEM DAMAGE FACTOR	TOTAL DAMAGE PER TRIP	NUMBER OF TRUCKS PER 100 TRUCKS	TOTAL DAMAGE PER 100 TRUCKS
Single Unit Three-Axle Dump	96	20	3.2	76	57.0			60.2	25	1,505
Five-Axle Semi-Trailer 3S2	115	15	1.15	2@ 50	2@ 4.65			10.5	70	732
Six-Axle Semi-Trailer 3S3	140	15	1.15	50	4.65	7.5	4.50	10.3	5	51
Total EALs										2,288

Table 3. Pavement thickness designs for heavily loaded trucks.

NUMBER OF TRUCKS PER DAY	DESIGN YEARS	DESIGN EALs $P_t = 3.5$	DESIGN THICKNESS (in.) 50% AC[a]	100% AC[b]
100	1	617,760	-	-
	5	3,088,800	18.2	11.8
	10	6,177,600	20.1	13.1
	20	12,355,200	22.1	14.5
200	1	1,235,520	-	-
	5	6,177,600	20.1	13.1
	10	12,355,200	22.1	14.5
	20	24,710,400	24.2	15.8

Assumptions:
Sundays = 52
Holidays = 8
Bad Weather = 5

Total Non-work = 65
Working days per year = 365 - 65 = 300

[a]50 percent - half of pavement thickness is asphaltic concrete, half is unbound granular base
[b]100 percent - full-depth asphaltic concrete

tucky thickness design system (6) are shown in Figures 5 and 6. Assuming a design CBR of 5.2, which is typical for many Kentucky soils and is the same soil used at the AASHO Road Test, the required thicknesses are given in Table 3 for the various combinations of truck volumes and design periods. Kentucky assigns a terminal serviceability of 3.5 for pavements expected to support 4 million or more 80-kN (18,000-lb) EALs in the design life.

Comparison with Interstate Traffic

Interstate traffic is a mixture of loaded and empty trucks, as reflected by loadometer studies. Average damage factors (5,6) were calculated and applied to eight classification counts made in 1981 at two locations. The volume of truck traffic was 28.3 percent on I-65 and 39.0 percent on I-71. However, the number of trucks was nearly the same on each route and almost identical regardless of which quarter of the year the count was made. Thus, truck traffic was fairly constant. Table 4 shows that the daily and annual EALs for these two routes were nearly the same. The data in Table 3 indicate that approximately 200 heavily loaded trucks per day can cause the same fatigue as all trucks using I-65 or I-71.

A second comparison was made on the basis of net tonnage and the associated accumulation or fatigue. Table 5 gives the tare weight for typical vehicles for both the heavily loaded trucks and those normally found on Interstates and other routes. This permits a theoretical comparison of net tonnage hauled by the two groups of vehicles. The following assumptions were made:

1. The number of trucks was taken from I-65 data in Table 4 for the corresponding classifications in Table 2. This represents typical use on Interstates.
2. The remainder of the traffic stream would be constant for both comparisons and therefore are not included in this example problem.

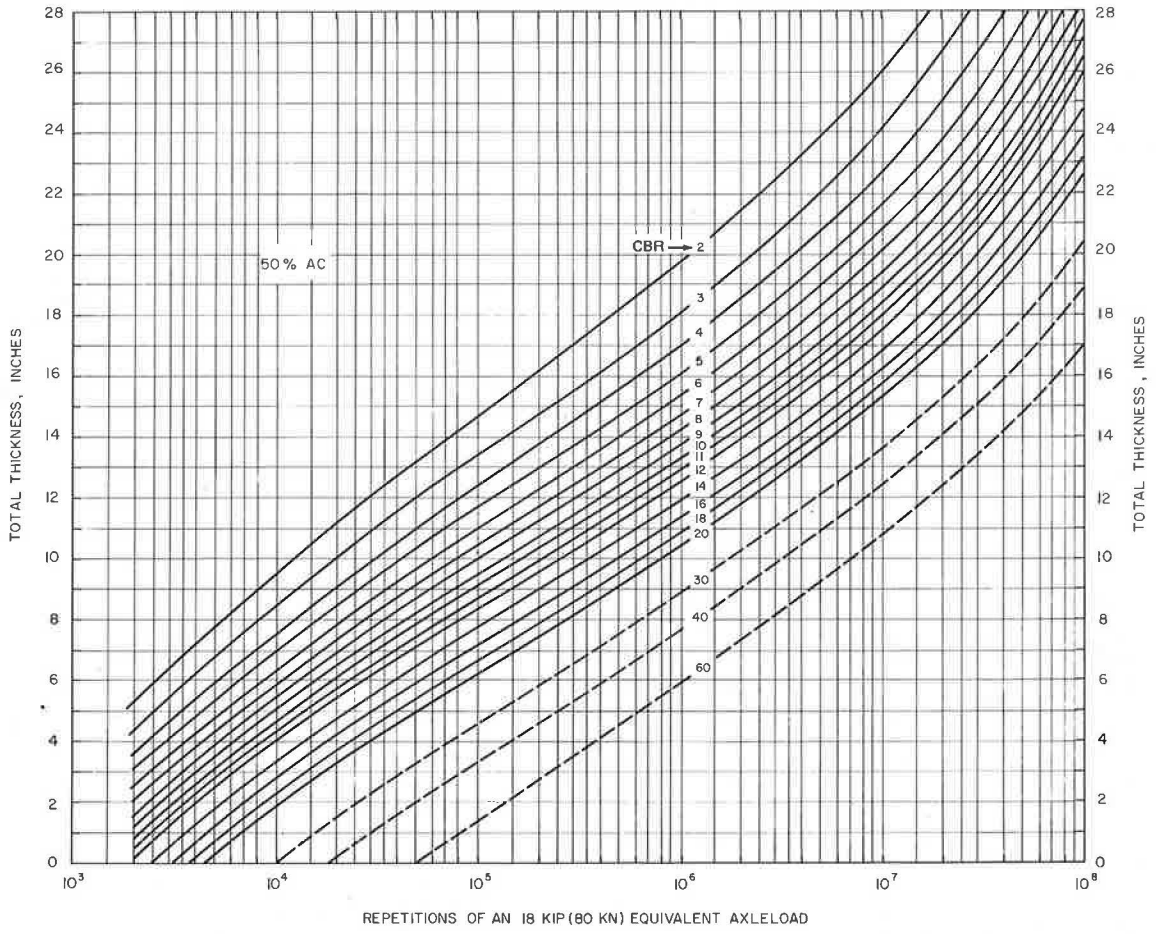

Figure 5. Thickness design curves for pavement structures where 50 percent of the total pavement thickness is asphaltic concrete.

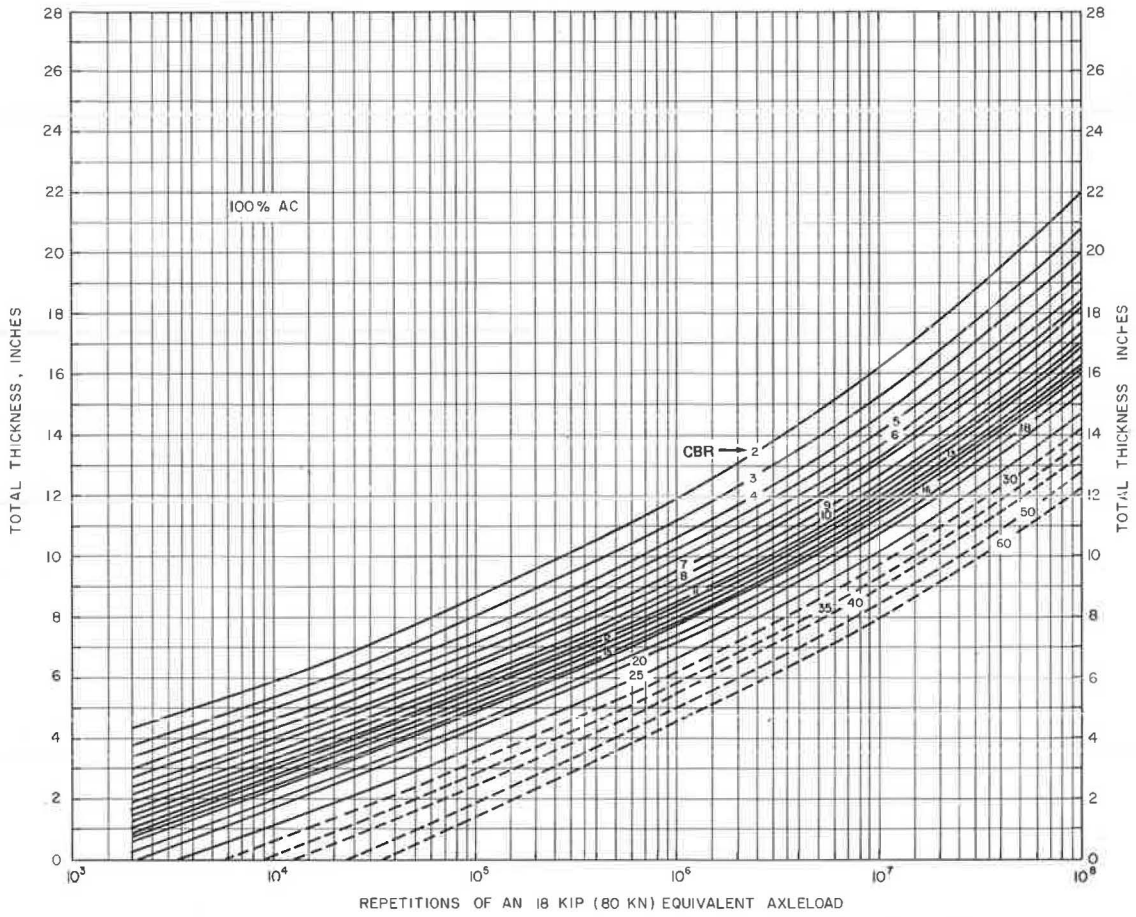

Figure 6. Thickness design curves for pavement structures where 100 percent of the total pavement thickness is asphaltic concrete.

3. Each axle group is loaded to the legal maximum.
4. For an Interstate, 365 days are assumed for EAL calculations because truck traffic does not appear to vary significantly on any given day. However, for coal or similar commodities, there are market slumps and bad-weather days that reduce the total number of working days to approximately 300.

The following methodology was used to calculate the net loads:

1. Legally loaded trucks for the three classifications reported for I-65 were used to calculate the fatigue for 1 year. The fatigue for 1 year for 100 heavily loaded trucks also was calculated. The ratio of the two fatigue calculations multiplied by the original 100 heavily loaded trucks produces the total number of heavily loaded trucks required to produce the same fatigue as the trucks reported on I-65.
2. For each classification of legally loaded trucks, the number of trucks per day were multiplied

Table 4. Vehicle classification counts and corresponding EAL for two sites on Kentucky Interstates.

		SINGLE UNIT TRUCKS				SEMI-TRAILER TRUCKS				
AVERAGE DAMAGE FACTOR	AUTOS & PICKUPS 0.0501	TWO AXLES FOUR TIRES 0.0605	TWO AXLES SIX TIRES 0.2953	THREE AXLES 0.6386	FOUR AXLES 0.6386	THREE AXLES 0.6353	FOUR AXLES 0.7514	FIVE AXLES 0.6267	SIX AXLES 0.6000	TOTAL
VOLUME: TOTAL OF FOUR DAILY COUNTS										
I-65	51,026	52	2,435	272	15	266	1,442	15,319	67	70,894
I-71	32,392	356	2,015	426	137	372	945	15,889	150	52,682
EALs										
I-65	2,556.4	3.1	719.1	173.1	9.6	169.0	1,083.5	9,600.4	40.2	14,355.0
Average										3,588.8[a]
I-71	1,622.8	21.5	595.0	272.0	87.5	236.3	710.0	9,957.6	99.6	13,602.6
Average										3,400.6[b]

[a]Annual EAL for I-65 = 365 x 3,588.8 = 1,309,895.
[b]Annual EAL for I-71 = 365 x 3,400.6 = 1,241,235.

Table 5. Gross, empty, and net weights of selected vehicle configurations.

CLASSIFICATION	NORMAL TRUCKS				HEAVILY LOADED TRUCKS			
	EMPTY WEIGHT (kips)	GROSS WEIGHT (kips)	NET WEIGHT (kips)	DAMAGE FACTOR PER TRIP	EMPTY WEIGHT (kips)	GROSS WEIGHT (kips)	NET WEIGHT (kips)	DAMAGE FACTOR PER TRIP
Three- Axle Single-Unit	20	46	26	1.18	30[a]	96	66	60.2
Five-Axle Semi-Trailer	30	80	50	1.80	30	115	85	10.45
Six-Axle Semi-Trailer	32	96	64	1.74	34	140	106	10.30

[a]Different from empty weight of normally loaded trucks.

by the net load and accumulated. The product of the number of heavily loaded trucks and their net loads was also calculated.

3. The total net load per day for the legally loaded trucks was divided by the total net load for the heavily loaded trucks.

For the same fatigue, calculations shown in Figure 7 indicate that the number of heavily loaded trucks is approximately 10 percent of the number of legally loaded trucks. Furthermore legally loaded trucks would transport approximately 7.7 times more payload than would the heavily loaded trucks with only about one-fourth (1/3.72 from Figure 7) of the fatigue damage.

Classification	Number of Trucks	Net Weight[a] (kips)	Total Net Weight (kips)	Average Damage Factor[a]	Total EAL
Normally Loaded Trucks[b] (per day for 365 days per year)					
Three-axle single unit	68	26	1,768	1.18	80.24
Five-axle semitrailer	3,830	50	191,500	1.80	6,894
Six-axle semitrailer	17	64	1,088	1.74	29.58
Total	3,915		194,356		7,003.82
					x 356
				EAL per year	2,556,394
Heavily loaded trucks (per day for 300 days per year)					
Three-axle single-unit	25	66	–	60.2	1,505
Five-axle semitrailer	70	85	–	10.45	731.5
Six-axle semitrailer	5	106	–	10.30	51.5
Total	100				2,288.0
					x 300
				EAL per year	686,400

Ratio of EAL = $\frac{\text{normal trucks}}{\text{heavy trucks}} = \frac{2,556,394}{686,400} = 3.72$ for equivalent fatigue damage

Number of heavy trucks			
3.72 x 25 =	93.1	66	6,145
3.72 x 70 =	260.7	85	22,159
3.72 x 5 =	20.7	106	2,194
Total	374.5		30,498

Ratio of net load = $\frac{\text{legally loaded}}{\text{heavily loaded}} = \frac{194,356 \times 365}{30,498 \times 300} = 7.7$

[a]From Table 5. [b]Daily volume: one-fourth of volumes in Table 4.

Figure 7. Sample calculation sheet to compare fatigue and payloads.

Deterioration of Pavements

Many Kentucky pavements have been subjected to heavily loaded vehicles. Some observations of the effect on pavements are given in the following paragraphs.

Pavements designed for light to medium traffic will deteriorate rapidly under heavy loads, and the paved surface of a rural secondary road may be broken up and even disappear in 1 to 2 years. During construction of 11 km (7 miles) of KY 15, two unanticipated strip mine operations were opened. Eight months later, a 102-mm (4-in.) asphaltic concrete overlay was placed to eliminate severe rutting and some cracking. The overlay was required and laid before the official opening of the new construction to traffic.

On an experimental full-depth asphaltic concrete pavement with cross sections ranging from 254 to 457 mm (10 to 18 in.), cold weather temperature cracking was observed in the passing lane. Those transverse cracks were 1.2 to 1.8 m (4 to 6 ft) apart in some areas. The cracks were evident in the outer lane only at the outer and centerline paint stripes. Evidently, the heavily loaded trucks kneaded the pavement surface together. It is not known whether the cracks extend below the surface layer.

On a 432-mm (17-in.) full-depth asphaltic concrete pavement on the Daniel Boone Parkway, there is a long steep grade that shows progressively deeper rutting as the top of the hill is approached. The change in rutting was pronounced and occurred over a fairly short length where drivers downshift into a lower gear. The amount of rutting then remained relatively constant over a considerable distance. When the driver shifted to an even lower gear, another significant increase in rutting occurred and remained constant over a considerable length. The lengths of constant rutting decreased as the truck approached the top of the hill. Rutting varied from 6.4 mm (0.25 in.) at the bottom of the grade to 76 mm (3 in.) at the top of the hill. Two experiments were conducted to help understand the cause of the rutting.

First, a full-depth trench was excavated across the climbing lane containing the severe rutting. Inspection of the cross section showed that rutting occurred only in the top 152 mm (6 in.) and all construction interfaces below the 152-mm (6-in.) depth were parallel and straight. Above 152 mm (6 in.) construction interfaces were undulating and layer thicknesses varied due to differential densification under traffic. Also in the upper layers, the normally random orientation of aggregate particles was totally reoriented so that the particles were parallel to each other.

The second experiment consisted of making two shallow saw cuts across the lane. One was perpendicular to the centerline, and the other was on a 45 degree angle with the lower end of the cut at the shoulder. Both cuts were filled with small-diameter glass beads used in highway paint stripping. Four weeks later these cuts were inspected. Both cuts in both wheel track areas had been displaced downgrade

by 16 mm (0.6 in.). Thus, the high torque at the tire pavement interface caused a downward flow of the surface mix. The lack of stability of the bituminous mixture was determined to be caused primarily by a soft grade of asphaltic cement. An overlay with a stiffer grade of asphaltic cement was placed.

SUMMARY

Pavements can be designed for heavily loaded trucks, but the rate of accumulating fatigue is greatly accelerated. The accumulation of fatigue for heavy trucks is highly disproportionate to the amount of payload transported. For the same fatigue and assumed proportions of trucks, the number of trucks loaded to the legal maximum axle loads is approximately 10 times the number of heavily loaded trucks. For the same fatigue, legally loaded trucks can transport approximately 8.2 times more payload than can heavily loaded trucks.

Pavements designed for normally loaded trucks may deteriorate rapidly and severely when subjected to heavily loaded trucks. Observed deterioration varies from accelerated rutting, both in depth and time, to severe breakup of the paved surface.

ACKNOWLEDGMENT

This study was conducted at the University of Kentucky Transportation Research Program and in part was sponsored cooperatively by the Kentucky Transportation Cabinet and the Federal Highway Administration.

REFERENCES

1. J. Michelow. Analysis of Stresses and Displacements in an N-Layered Elastic System under a Load Uniformly Distributed on a Circular Area. Chevron Research Corporation, Richmond, Calif., 1963.
2. I.S. Sokolnikoff. Mathematical Theory of Elasticity, Second Edition. McGraw-Hill, New York, 1956.
3. R.C. Deen, H.F. Southgate, and J.G. Mayes. The Effect of Truck Design on Pavement Performance. Proc., Association of Asphalt Paving Technologists, Minneapolis, Minn., Feb. 1980.
4. H. Warren and W.L. Dieckmann. Numerical Computation of Stresses and Strains in a Multiple-Layered Asphalt Pavement System. Chevron Research Corporation, Richmond, Calif., 1963.
5. H.F. Southgate, R.C. Deen, J.H. Havens, and W.B. Drake. Kentucky Research: A Flexible Pavement Design and Management System. Proc., 4th International Conference, Structural Design of Asphalt Pavements, University of Michigan, Ann Arbor, 1977.
6. J.H. Havens, R.C. Deen, and H.F. Southgate. Design Guide for Bituminous Concrete Pavement Structures. Kentucky Transportation Research Program, College of Engineering, University of Kentucky, Rept. KTRP-81-17, Lexington, Aug. 1981.
7. H.F. Southgate, R.C. Deen, and J.H. Havens. Development of a Thickness Design System for Bituminous Concrete Pavements. Kentucky Transportation Research Program, College of Engineering, University of Kentucky, Rept. KTRP-81-20, Lexington, Nov. 1981.
8. Traffic Factors Used in Flexible Pavement Design. TRB, Research Circular No. 240, April 1982.
9. Interim Guide for Design of Pavement Structures. AASHTO, Washington, D.C., 1972.

Pavement Analysis for Heavy Hauls in Washington State

RONALD L. TERREL AND JOE P. MAHONEY

An evaluation of the haul routes associated with moving heavy nuclear power plant components over existing state and county roads is described. These routes were associated with the planned construction of the power plants at Satsop (southwestern Washington state) and Sedro Wooley (northwestern Washington state). The procedures for evaluating the proposed moves are provided and include descriptions of the field and laboratory tests and analytical techniques. Ultimately, the haul routes analyzed were not used.

In recent years construction of nuclear power plants instigated analyses of the feasibility of using existing highways for hauling very large and heavy machinery. These hauls require special tractors and trailers to accommodate the machinery as well as to spread the load to minimize damage to pavements and bridges.

A special permit is required by those who perform the heavy hauling. For modestly oversize or overweight vehicles, obtaining a permit is somewhat routine as long as local requirements of wheel load and spacing are met, and the fee is usually nominal. Very heavy loads, however, require considerably more analysis to assess potential damage to the existing facilities, and the fee is commensurate with the expected cost to repair the damage.

Plans for constructing two nuclear power plants in Washington State instigated pavement analysis for the purpose of obtaining permits. Each plant had a different owner, and each owner was required to back up the application with an analysis of the significant damage that would be incurred, if any. For one project, Skagit, the supplier of the reactor equipment was required by the plant owner to deliver the equipment to the job site, so the supplier arranged for a consultant to evaluate the proposed route. The consultant's report was, in turn, presented to the Washington State Department of Transportation (WSDOT). For the other project, Satsop, the plant owner requested that the pavement evaluation be made by WSDOT, but be paid for by the plant.

The proposed routes were evaluated to determine expected immediate damage (during hauling) as well as reduced service life. In addition the alternatives of improving the roadway before hauling or making repairs after hauling were considered.

Each project is treated as a separate case history. Figure 1 shows the general location of the projects. In each case the projected route covered local (county) and state highways. The primary analysis was for the main highway. Unsurfaced local roads or new access roads were considered separately and were treated as expected reconstructions to meet load and geometry requirements.

Figure 1. Site map for nuclear power plant component haul locations.

Ultimately, the proposed haul routes were not used. An alternate route was constructed for the Satsop plant because of right-of-way acquisition problems and the other project was cancelled.

CASE 1, SATSOP NUCLEAR POWER PLANT

The Satsop plant is located near Elma, Washington, west of Olympia on US-12. The route to be investigated was about 12 miles along US-12. The data and other information used in evaluating US-12 for the planned heavy hauls were from two primary sources.

The first source was field studies conducted by WSDOT and included the following:

1. Benkelman beam deflection survey;
2. Soil borings, samples of granular materials, and cores of asphalt concrete pavement (ACP) and cement treated base (CTB) pavement; and
3. Plate bearing tests.

Test samples including soil borings, granular base and fill samples, and ACP and CTB cores were obtained during January 1979. The Benkelman beam deflection survey data were used in selecting test sampling locations. Plate bearing tests performed during April 1979 completed the WSDOT field studies. Additionally, during May 1979 a falling weight deflectometer (FWD) was used at selected stations to obtain deflection information and estimate modulus relationships for the pavement layers. Possible pavement distress caused by a slope stability failure along the proposed haul route was also analyzed by WSDOT personnel.

The second source of data was developed at the University of Washington (UW) Department of Civil Engineering pavement materials laboratory in Seattle. The overall goal of the laboratory program was to develop strength parameters for the primary structural materials contained in the US-12 cross sections and specifically to develop the required elastic parameters to enable modeling of the pavement structure as a layered-elastic system.

Field Testing

First, a Benkelman beam deflection survey was performed early in the study so that locations could be selected for soil boring, disturbed granular samples, and ACP and CTB coring. The primary reason for selecting these test sample locations was high pavement surface deflections. It is significant that almost all the Benkelman beam recorded surface deflections were low (preferable condition). A pavement condition survey, which indicated that little surface distress was present, also preceded the selection of the final boring and coring locations.

Twenty-four soil bore samples were obtained by using a hollow stem auger; the average depth was about 22 ft. These borings were used to identify the soil types underlying this portion of US-12 as well as to obtain standard penetration blow counts and undisturbed and disturbed soil samples. Figure 2 shows the soil types encountered as determined from the soil bore samples and the locations where core samples were obtained.

WSDOT personnel obtained plate bearing test data at selected US-12 locations using both the 12-in. and 24-in. diameter steel plates. Table 1 gives the maximum measured deflection for each of the two plates and the corresponding maximum load. Deflections range from a low of 0.005 in. to a maximum of 0.1 in. The lower deflections occurred at stations 584-00 and 602+00. These stations contain 6-in. thick CTB layers overlaid by 3 in. of ACP. Because of the stiffness of the CTB layer, deflections were low when compared to the other locations (stations 173+25 to 453+60). The principal structural layer for these other stations is 9-in. of ACP. The variability of these data is indicated by some of the significant differences that occurred between the measured deflections at the same station for the outer wheel path (OWP) and the between wheel path (BWP) test locations (a transverse distance of approximately 3 ft).

Laboratory Testing

Samples from the field exploration phase of the study were tested by the WSDOT Materials Division and the UW Department of Civil Engineering pavement materials laboratory. Most of the tests performed can be categorized for three material groups: ACP cores, CTB cores, and granular materials. A few undisturbed subgrade soil bore samples were also provided but these samples were not incorporated into the laboratory testing program because of the complex nature of the soil profile and the stress sensitivity of the resilient modulus for these materials.

The following sections describe the kinds of tests and results for the three material groups studied.

ACP Cores

Figure 3 shows the testing sequence for selected ACP cores. The two primary material characterization tests were resilient modulus and Marshall stability and flow. Typical results are shown in Figure 4 and Table 2.

CTB Cores

Only two CTB samples were obtained and both of these

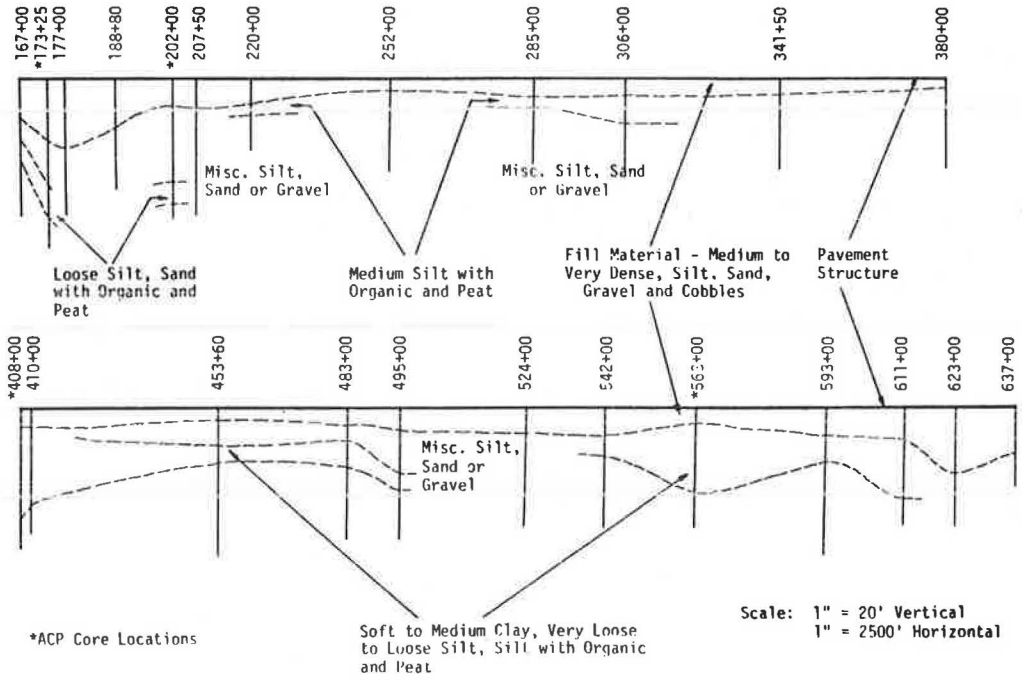

Figure 2. Generalized soil profile of proposed US-12 haul route.

Table 1. Summary of plate bearing tests for US-12.

Station[a]	12-in. Dia. Plate			24-in. Dia. Plate		
	Max. Deflection (in.)	Max. Load (lbs.)	Pavement Temperature (°F)	Max. Deflection (in.)	Max. Load (lbs.)	Pavement Temperature (°F)
173+25 (OWP)[b]	0.033	19,600	62	0.048	27,400	63
173+25 (BWP)[c]	0.077	19,600	69	0.044	27,400	68
202+00 (OWP)	0.032	19,600	64	0.016	27,400	64
202+00 (BWP)	0.044	19,600	72	0.047	27,400	69
341+50 (OWP)	0.080	19,600	80	0.035	27,400	83
341+50 (BWP)	0.054	19,600	85	0.036	27,400	87
408+00 (OWP)	-	-	-	0.026	39,000	62
408+00 (BWP)	0.051	19,600	64	-	-	-
453+60 (OWP)	0.084	19,600	74	-	-	-
453+60 (BWP)	-	-	-	0.100	35,200	75
584+00 (OWP)	0.006	19,600	59	0.005	41,000	58
584+00 (BWP)	0.012	41,000	57	0.006	37,200	56
602+50 (OWP)	0.006	19,600	62	0.010	37,200	65
602+50 (BWP)	0.012	19,600	63	0.006	37,200	60

Note: Data provided by WSDOT.

[a]All measurements made in eastbound outside lane.

[b]Outside wheel path.

[c]Between wheel paths.

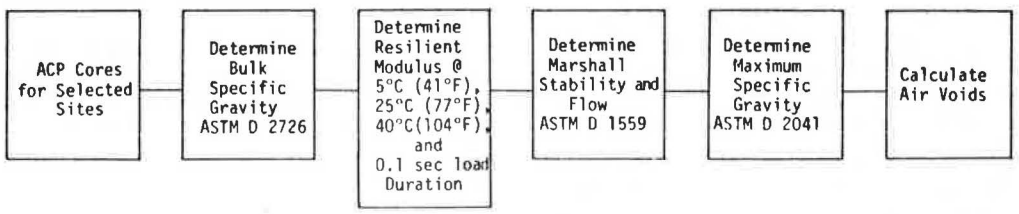

Figure 3. Test sequence for ACP cores from US-12.

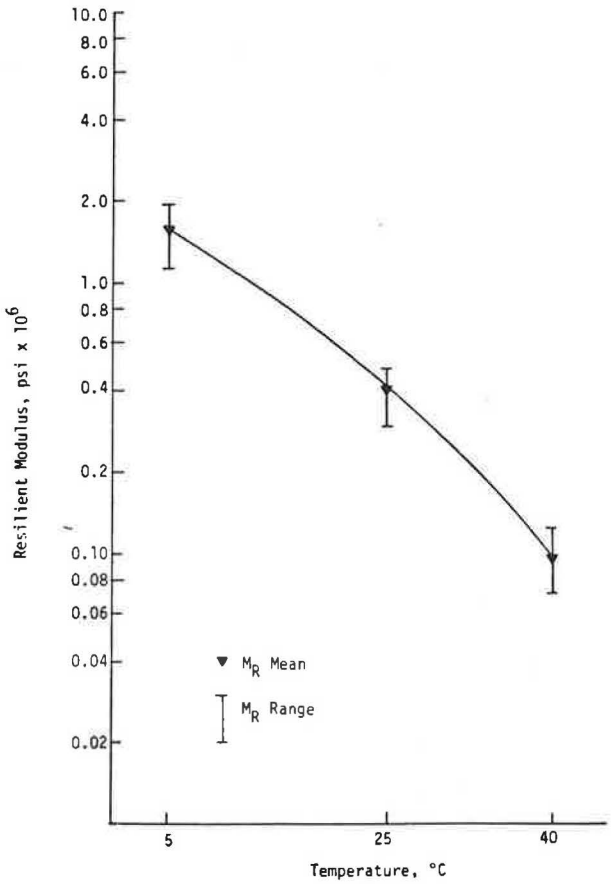

Figure 4. Typical resilient modulus (M_R) of US-12 ACP cores as a function of temperature—station 173+25.

were from station 563+00. The tests conducted on these specimens were resilient modulus and indirect tensile strength. The tensile strength ranged from 320 to 410 psi.

Granular Materials

The granular, disturbed materials sampled by WSDOT were obtained from the shoulder area of US-12 that underlies the relatively thin ACP shoulder surfacing. The samples were placed in canvas bags for delivery to the UW laboratory. Two kinds of granular samples were obtained: crushed surfacing, top-course material and gravel fill material that underlies much of the US-12 haul route. This gravel fill material contained some cobbles with sizes in excess of 2 in. Figure 5 shows the laboratory sequence used to evaluate the granular materials and a partial list of CBR results is given in Table 3.

Evaluation

The overall goal of the field and laboratory investigations of the materials was to obtain by testing, or to be able to otherwise estimate, the elastic parameters required to model US-12 pavement structures as a layered-elastic system. This evaluation uses the calculated stresses, strains, and deflections obtained from the layered-elastic modeling and applies appropriate limiting values or failure criteria to them. Thus, the potential pavement failure or reduction in pavement life attributable to the planned hauls can be estimated.

Modeling the response of the pavement structures consists of the following steps:

1. Select appropriate layered-elastic computer program (Chevron N-Layer and BISAR).
2. Select pavement structures (cross sections) to be evaluated and required material inputs (Figure 6 shows a typical example).
3. Determine load configurations (dimensions and weights, see Figures 7 and 8).
4. Select appropriate limiting values or failure criteria for the predicted pavement stresses, strains, or deflections.
5. Predict stresses, strains, and deflections by using the layered-elastic computer program (step 1) and applying to these results the appropriate limiting value or failure criteria (step 4).

Load Configurations

Two types of heavy haul loads are considered in this analysis: (a) the two trailers used to carry steam generators and the nuclear reactor vessel and (b) the prime mover vehicle. Both the trailer and the prime mover have unique numbers of wheels and wheel loads. To input these loads into a layered-elastic computer program, the analysts had to first find the critical location and then determine the number of wheels needed to distribute the load (see Figures 7 and 8).

The loading conditions used in the analysis included the following:

1. Trailer
   a. 5,675-lb wheel load, ACP temperature of 77°F,
   b. 5,675-lb wheel load, ACP temperature of 90°F,

Table 2. Summary of Marshall test results for US-12 ACP cores.

Sample No.	Bulk Specific Gravity	Air Void Content (%)	Marshall Stability (lbs)	Marshall Flow (0.01 in)
173-1-1	2.47	4.9	1250	18
173-1-3	2.42	7.0	1025	20
173-3-2	2.45	5.7	1273	22
173-3-4	2.43	6.6	1102	16
202-1-1	2.43	8.6	1763	19
202-1-3	2.41	9.5	855	22
202-3-2	2.45	7.8	631	20
202-3-4	2.45	7.8	1144	21
408-1-1	2.51	3.6	1440	25
408-1-3	2.50	4.0	1675	16
408-3-2	2.51	3.6	1904	22
403-3-4	2.53	2.8	1716	18
563-2-1	2.34	3.8	1945	20

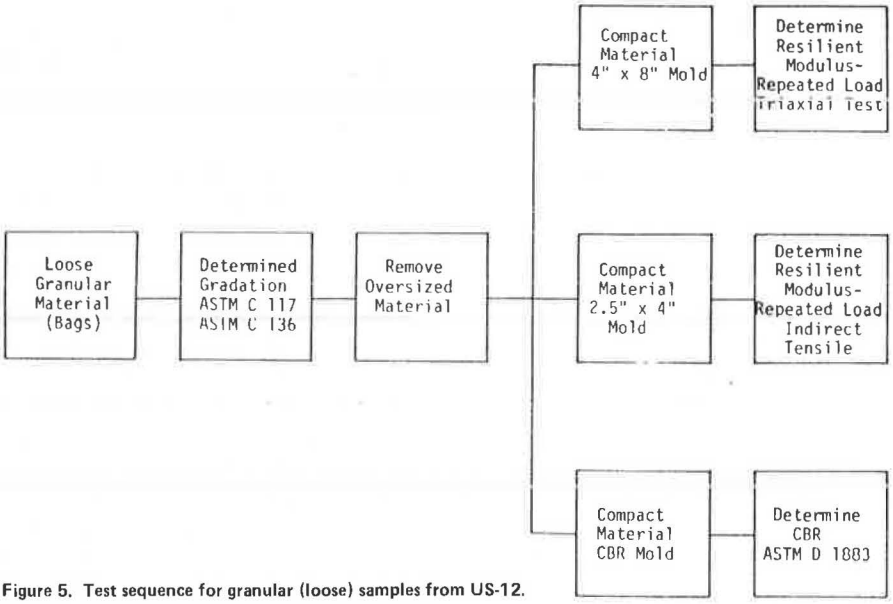

Figure 5. Test sequence for granular (loose) samples from US-12.

Table 3. Summary of CBR results for granular materials—US-12.

Sample No.	Density (lb/ft³)		Moisture Content (%)		Swell (%)	CBR
	In situ	As Molded	In situ	As Molded		
4 (Sta. 202+00)	146.3	151.2	7.9	7.8	0	24
6 (Sta. 341+50)	146.3	152.6	7.3	7.1	0	100+
7 (Sta. 408+00)	139.0	146.0	5.4	5.6	0	100+
9 (Sta. 408+00)	151.3	153.7	6.8	7.2	0	100+
11 (Sta. 453+60)	145.2	148.8	7.0	7.3	0	100+
12 (Sta. 593+00)	143.5	149.1	6.4	5.7	0	100+

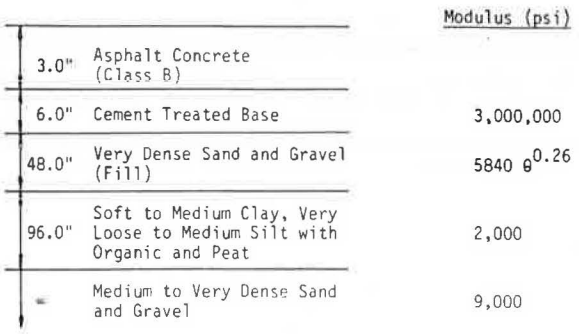

Figure 6. Cross section for station 602+50.

c. 7,000-lb wheel load, ACP temperatures of 77°F, and
d. 8,000-lb wheel load, ACP temperature of 77°F.

2. Prime Mover
   a. 84 tons total and
   b. 42 tons total.
3. Standard Axle
   a. 18,000-lb dual-tired single axle, ACP temperature of 77°F.

Limiting Values and Failure Criteria

The results obtained from modeling the US-12 pavement structures to determine the stresses, strains, and deflections for various loading configurations is of little value unless some limiting criteria is applied. Such criteria include limiting tensile strains for the ACP, vertical compressive strains in the subgrade layers, and tensile stresses and strains in the CTB. (Various, and often significantly different, values or relationships have been developed and reported by others.)

The limiting values and failure criteria used in this analysis fall into the following groups:

1. Fatigue (Figure 9): tensile strain at the bottom of the ACP layer,
2. Rutting (Figure 10): vertical compressive strain at the top of the subgrade layers, and
3. Strength: tensile strength of CTB layer.

A limiting value of strength was applied to the CTB layers evaluated. Because CTB is a brittle material, excessive stress induced by heavy hauls could result in cracking and ultimately accelerate deterioration of the overall pavement structure. When calculated stress exceeds the CTB indirect tensile strength, modifications to the applied load or pavement structure may be appropriate.

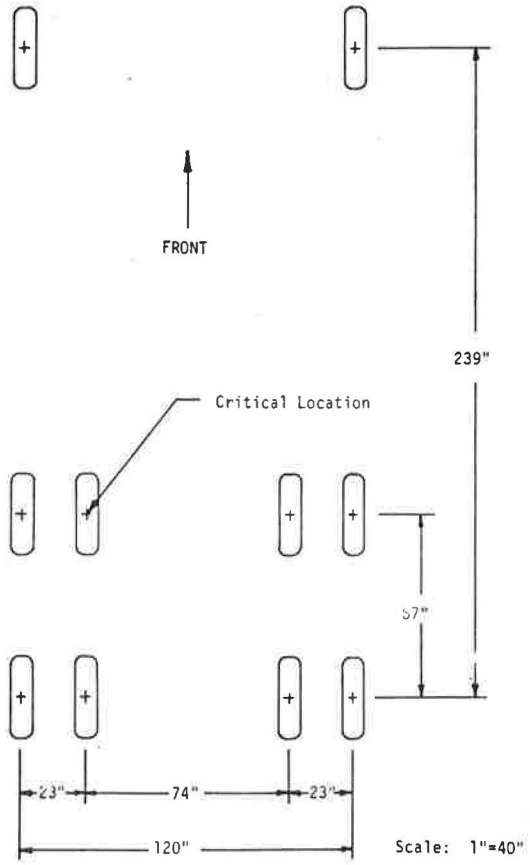

Figure 7. Plan view of prime mover wheel configuration.

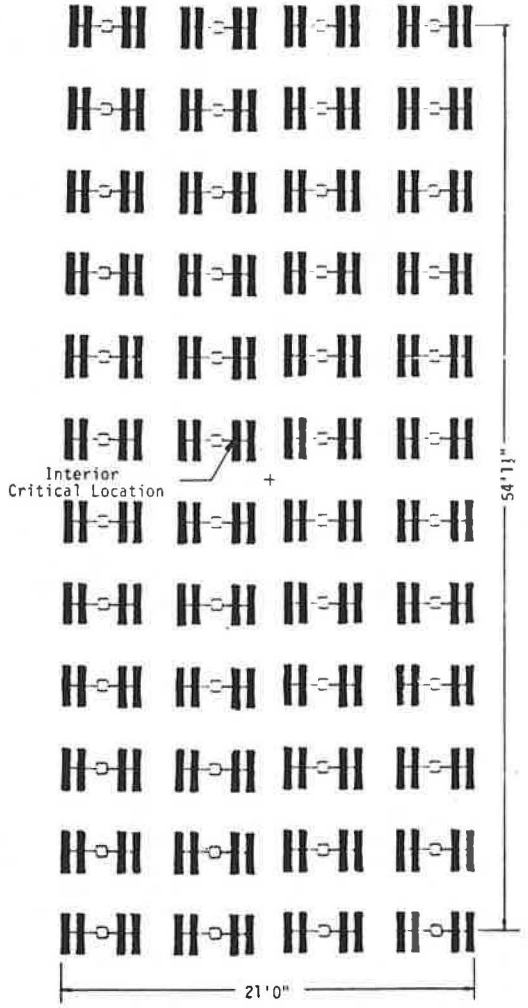

Figure 8. Plan view of one trailer unit (192 wheels).

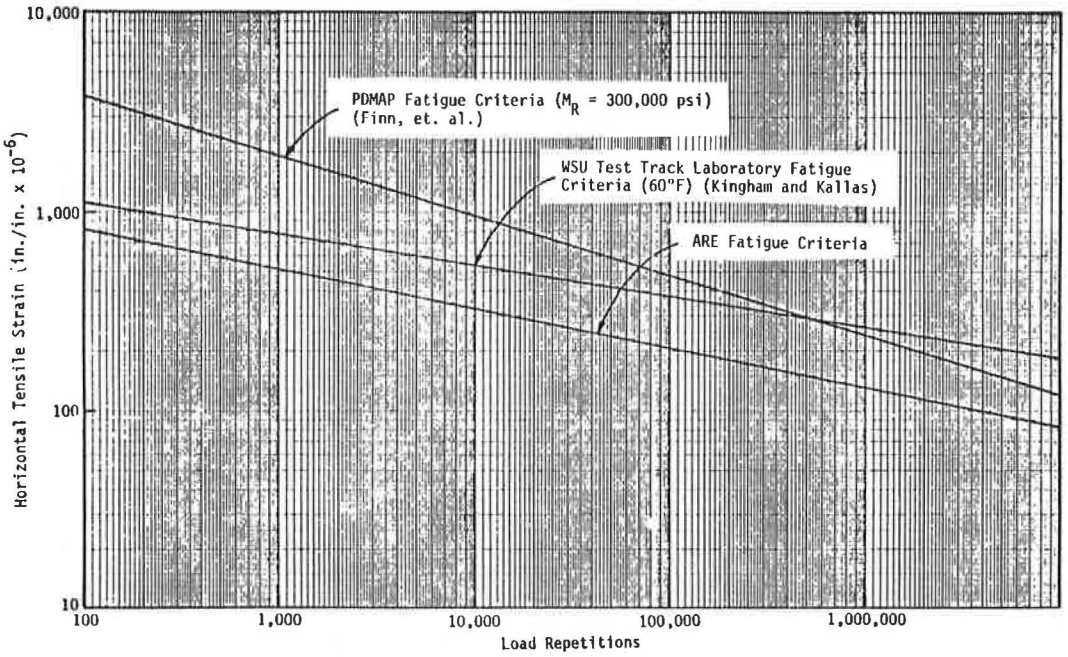

Figure 9. Fatigue criteria for horizontal tensile strain at the bottom of the ACP layer.

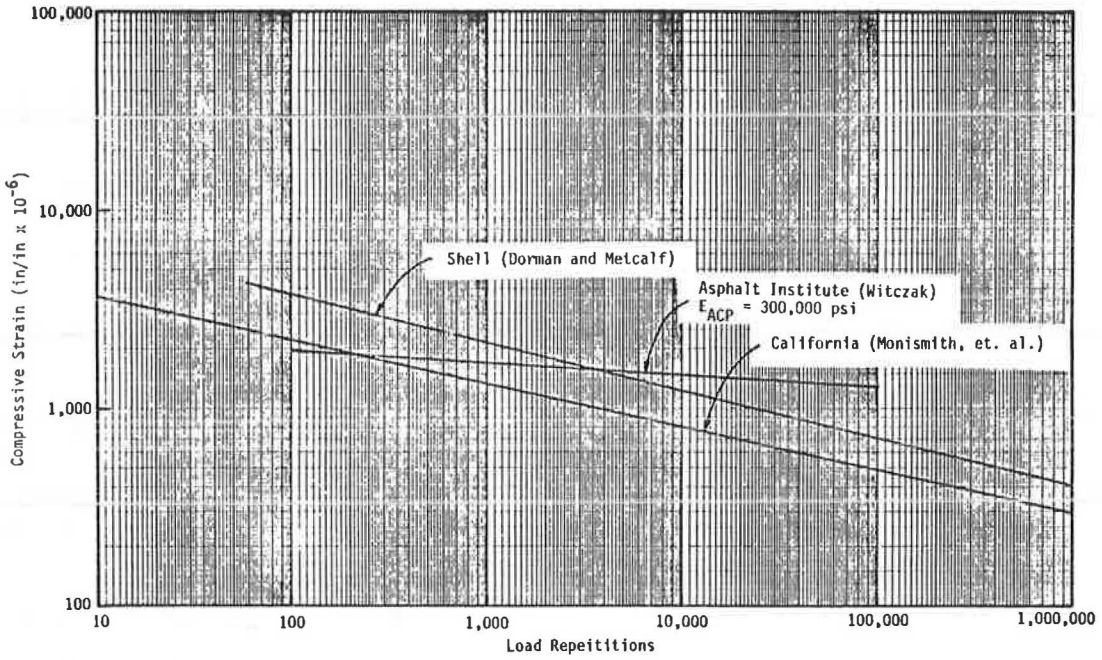

Figure 10. Criteria for vertical compressive subgrade strain to minimize rutting.

Evaluation Results

The preceding data were used to estimate potential damage to the US-12 pavement structures by the originally planned heavy hauls. The modeled pavement cross sections and haul loads were input to the BISAR computer program; then the resulting response data were compared with appropriate failure criteria to estimate pavement damage. Results obtained from the BISAR program were summarized for all pavement sections, and an example is given in Table 4.

An examination of estimated repetitions to failure in Table 5 shows the large differences between the fatigue criteria listed. The fatigue criteria developed by Kingham and Kallas from the Washington State University (WSU) test track are felt to represent best the US-12 ACP (1). The rutting criteria developed for California conditions (Table 6) were felt to represent best the US-12 subgrade soil conditions.

The maximum expected number of wheel load applications at any point along the proposed US-12 haul route would be 144 repetitions for the two trailer units (six separate moves and 24 axles for each move) and 24 repetitions for the prime movers. By dividing the maximum expected repetitions by the allowable repetitions for a specific loading configuration, an approximate estimate was made of the pavement life consumed.

Because a wide range in the fatigue criteria was observed, pavement life reductions were calculated for all three. The most probable category was assigned to the Kingham and Kallas criteria (1), the optimistic category to the Finn et al. criteria (2), and pessimistic to the ARE, Inc. criteria (3). Small percentage reductions in the pavement life are estimated for the load configurations considered for the most probable and optimistic categories (Table 7). Somewhat larger values are reported for the pessimistic category, however, the largest reduction (for the 8,000-lb wheel load on the trailer) is less than 10 percent.

Conclusions: Case 1

1. Subgrade soils along the proposed haul route were highly variable in composition and strength.
2. The existing US-12 pavement structure was well constructed and was in good structural condition. The asphalt concrete and cement treated base materials were of good-to-high quality and strength.

Table 4. Calculated stresses, strains, and surface deflections for trailer with 8,000-lb wheel load and ACP temperature of 77°F—station 408+00.

Layer No.	Layer Thickness (in.)[a]	Top or Bottom of Layer	Stress (psi)		Strain (in./in. x 10^{-6})	
			Vertical Stress	Maximum Horizontal Stress	Maximum Horizontal Strain	Vertical Strain
1	9.0	Top	-100	-237	-485	113
		Bottom	-12	190	462	-348
2	1.8	Top	-12	-4	462	-1,114
3	3.6	--	--	--	--	--
4	24.0	Top	-10	-3	464	-1,020
5	204.0	Top	-6	-1	647	-1,430
6	∞	--	--	--	--	--

Note: Tension (+); Compression (-).

[a]Pavement Surface Deflection = 0.192 in.

Table 5. Estimated repetitions to failure for various load configurations and fatigue criteria—station 408+00 (1-3).

Load Configuration	Maximum Horizontal Strain (in/in x 10^{-6})	Estimated Repetitions to Failure		
		ARE Fatigue Criteria[a]	PDMAP Fatigue Criteria[b] (Finn et al.)	WSU Test Track[c] Laboratory Fatigue (Kingham and Kallas)
Trailer(each wheel):				
5675-lb (ACP 77°F)	341	7730	312,610	146,010
5675-lb (ACP 90°F)	443	2000	132,130	31,370
7000-lb (ACP 77°F)	413	2880	166,420	47,370
8000-lb (ACP 77°F)	462	1610	115,070	24,510
Prime Mover(total wt.)				
84-ton (ACP 77°F)	532	800	72,330	10,700
42-ton (ACP 77°F)	309	12,860	432,370	260,550
Standard Axle:				
18,000-lb (ACP 77°F)	225	66,130	1,228,210	1,681,080

[a]Equation: $W_{18} = 9.7255 \times 10^{-5}(\frac{1}{\varepsilon})^{5.1627}$.

[b]Equation: $\log N_f(\leq 10\%) = 15.947 - 3.291 \log(\frac{\varepsilon}{10^{-6}}) - 0.854 \log(\frac{E}{10^{-3}})$.

[c]Equation: $\log N_f = -17.2278 + 5.87687 \log(\frac{1}{\varepsilon}) + 0.033594(\text{Temp})$.

Table 6. Estimated repetitions to failure for various load configurations and rutting criteria—station 408+00 (4-5).

Load Configuration	Maximum Vertical Subgrade Strain (in/in x 10^{-6})	Estimated Repetitions to Failure		
		Shell (Dorman and Metcalf)	California (Monismith et al.)	Asphalt Institute (Witczak)
Trailer(each wheel):				
5675-lb (ACP 77°F)	-1017	100,000	25,000	>10,000,000
5675-lb (ACP 90°F)	-1067	80,000	18,000	>10,000,000
7000-lb (ACP 77°F)	-1258	31,000	7,000	>10,000,000
8000-lb (ACP 77°F)	-1430	16,000	3,000	100,000
Prime Mover(total wt.):				
84-ton (ACP 77°F)	-	-	-	-
42-ton (ACP 77°F)	-592	1,700,000	400,000	>10,000,000
Standard Axle:				
18,000-lb (ACP 77°F)	-406	10,000,000	2.300,000	>10,000,000

Table 7. Pavement life used by heavy hauls—station 408+00.

Load Configuration	Pavement Life Consumed (%)					
	Most Probable[a]		Optimistic[b]		Pessimistic[c]	
	Fatigue	Rutting	Fatigue	Rutting	Fatigue	Rutting
Trailer (each wheel):						
5675-lb (ACP 77°F)	0.099	0.576	0.046	-	1.863	-
5675-lb (ACP 90°F)	0.459	0.800	0.109	-	7.200	-
7000-lb (ACP 77°F)	0.304	2.057	0.087	-	5.000	-
8000-lb (ACP 77°F)	0.588	4.800	0.125	-	8.944	-
Prime Mover (total wt.):						
84-ton (ACP 77°F)	0.224	-	0.033	-	3.000	-
42-ton (ACP 77°F)	0.009	0.006	0.006	-	0.187	-
Standard Axle:						
18,000-lb(ACP 77°F)	-	-	-	-	-	-

[a]Kingham and Kallas (1).

[b]Finn et al (2).

[c]ARE, Inc. (3).

3. The most probable damage to the noncement-treated base pavement sections (fatigue and rutting caused by the 5,675-lb trailer wheel loads and the 42-ton prime mover) is expected to be small--less than 1 to 2 percent of available pavement life. Increasing the trailer wheel loads to 8,000 lb would use approximately 5 to 10 percent of the available pavement life. An increase in both the wheel loads and pavement temperature would produce greater losses in pavement life. To illustrate this point, an increase of pavement temperature of only 13°F (from 77°F to 90°F) for the 5,675-lb trailer wheel load indicates that the loss in pavement life can increase by a factor of one to almost four depending on the failure criterion used.
4. Based on limited data, tensile stresses in the CTB layer due to the 5,675-lb trailer wheel loads may exceed tensile strength. The possibility therefore exists that cracking of the layer may occur. Such cracking would accelerate pavement deterioration and ultimate failure.

CASE 2, SKAGIT NUCLEAR PLANT

This proposed project, which has since been abandoned, is located in the northwestern part of Washington State (Figure 1). Many of the features of this analysis are similar to those for Satsop, although the projects were owned by different agencies and the hauling was to be done by different companies. The plant was to have been near the town of Sedro Woolley, and the nuclear reactor vessel and other large components would be transported by barge up the Skagit River then off-loaded from a barge and transferred to a special vehicle consisting of a transporter-tractor and two trailer units. This heavy hauling unit and the reactor together would weigh approximately 3,000,000 lb.

Specifically, the original objectives of the study were

1. To examine whether heavy hauling on the two pavement structures, Fruitdale Road (gravel surfaced) and US-20 (ACP surfaced), would cause pavement failure,
2. To determine relative damage to the pavements due to heavy hauling, and
3. To recommend procedures and necessary precautionary measures or construction either before hauling or afterward.

The approach used was similar to that for the Satsop project; therefore, much of the basic material data will not be presented. Two different types of roadways were included in the route: a country road (Fruitdale) and a state highway (US-20).

Field Investigation

The field study included the following:

1. Benkelman beam deflection survey,
2. Soil borings,
3. Plate bearing test, and
4. Falling weight deflectometer study.

The Benkelman beam deflection survey was performed as a first step early in the study so that soil borings, disturbed soil samples, and asphalt concrete coring locations could be selected. It was significant that almost all recorded surface deflections were high. Also, preceding the selection of the final boring and coring locations, a pavement condition survey was made which indicated that the two roads, US-20 and especially Fruitdale Road, had severe surface distress.

Soil samples at various depths and asphalt pavement cores were obtained at selected sites and were used to identify the soil type underlying the two roads as well as to obtain standard penetration blow counts and material samples. Examination of these data revealed a soil profile that was relatively uniform with respect to the kind and strength of the various soil layers encountered. Most of the materials in various layers of Fruitdale Road and US-20 are sand with varying amounts of gravel and silt.

All the asphalt core samples obtained were on US-20 because Fruitdale Road had only a surface treatment layer. All the materials below the AC layer obtained were loose, disturbed samples. Water content and in-place density were also determined for materials about 1 to 2 ft below the surface.

Plate bearing tests were conducted at the locations that appeared to be critical. The plate bearing test included the use of 8-, 18-, 24-, and 30-in. diameter steel plates. Most, if not all, deflection values at maximum plate loads were between 0.2 to 0.3 in., which indicated the two roads were relatively weak.

Additionally, FWD tests were made at selected sites along the Fruitdale Road and US-20 haul route to obtain deflection information and estimate moduli for the pavement layers.

Laboratory Testing

The granular base and subbase for both US-20 and Fruitdale Road are similar. In many areas, the subbase material is almost the same as the subgrade, extending to considerable depth. Disturbed or grab samples were received in the laboratory for testing. Both the California Bearing Ratio (CBR) and resilient modulus (M_R) were measured on laboratory compacted specimens.

These materials were generally uniform throughout and consisted primarily of sand with varying amounts of gravel and silt. In-place density and water content were determined.

Pavement Analysis

The field and laboratory material investigations were used in the pavement analysis performed for both US-20 and Fruitdale Road. The data resulting from these investigations were used to estimate the elastic parameters required to enable modeling of both highways as layered elastic structures.

By applying appropriate limiting values or failure criteria to the calculated stresses, strains, or deflection resulting from the layered elastic modeling, potential pavement failure, or reduction in pavement life was estimated for various loading conditions.

The modeling of the response of the US-20 and Fruitdale Road pavement structures required several steps and was similar to that done for the Satsop project. A typical result of the overall pavement characterization effort is shown in Figure 11.

Load Configurations

Two types of heavy haul loads are considered in this analysis: (a) the two trailers used to carry the steam generators and nuclear reactor vessel and (b) the prime mover vehicle.

Trailer

The trailer system was composed of 12 axle sets of 16 wheels (192 wheels total). Alternatively, one-half of the trailer system could be composed of 14 axle sets of 16 wheels each (for a total of 224

Station 149+58

		Modulus (psi)
4"	Asphalt Concrete	E = 280,000 psi
17"	Dry, dense sand with well-graded, rounded gravel	E = 25,000 psi
33"	Moist, moderate firm silt with trace sand	E = 3,000 psi
∞	Moist, medium dense sand with some silt and organics	E = 3,500 psi

Station 156+86

		Modulus (psi)
	Asphalt Concrete	E = 220,000 psi
14.5"	Moist, dense, gravelly sand with considerable silt	E = 12,000 psi
90"	Moist, medium dense, silty sand with some gravel and organics	E = 4,500 psi
78"	Saturated, medium dense sand with some silt and organics	E = 3,000 psi
∞	Moist, very soft silt with some sand	E = 3,000 psi

Station 190+68

		Modulus (psi)
2"	Asphalt Concrete	E = 140,000 psi
19"	Moist, dense sand with some gravel	E = 20,000 psi
∞	Moist, hard silt with some sand and gravel	E = 19,000 psi

Figure 11. Typical cross sections and material parameters of various stations on SR-20.

wheels). The configuration was similar to that shown in Figure 8.

To enter these loads into the layered-elastic computer program, first the critical location was found. Based on previous work, the number of wheels selected for the trailer system was 15 clustered around the critical point. Other wheel loads further from the critical point than these 15 did not contribute significantly to the cumulative stress or strain conditions. In fact, some of these wheels tend to reduce the net stress and strain at the critical point for some loading conditions.

The expected wheel load for each wheel on the trailers is 7,750 lb for 12 axles and 6,642 lb for 14 axles. The expected total weight of a steam generator move including the trailer weight is approximately 2,976,000 lb.

Prime Mover

It was understood that two prime movers would be used for each haul, one to pull and one to push. These vehicles are heavily ballasted to increase tire contact friction with the pavement. The total prime mover load can range from 84 tons to 42 tons distributed on 10 wheels. Hence, three gross weights were studied for this vehicle: (a) 42 tons, (b) 63 tons, and (c) 84 tons. A plan view of the prime mover wheel configuration was shown in Figure 7.

Based on the above discussion, the following wheel loads were used for further pavement analysis.

1. Trailer
   a. 7,750-lb wheel load
   b. 6,642-lb wheel load
2. Prime Mover
   a. 84 tons total - 16,800-lb wheel load
   b. 63 tons total - 12,600-lb wheel load
   c. 42 tons total - 8,400-lb wheel load

Evaluation of Pavement Analysis Results

The results of the computer analysis of heavy hauls for three pavement structures (stations 49+11, 149+50, and 209+28) are summarized in Table 8. At station 49+11, the pavement structure has no significant bituminous surface layer. Thus, only the vertical strains and stresses were computed.

An examination of Table 8 shows that for station 49+11, the critical vehicle load is the prime mover at 84 tons because the surface deflection is the highest for that wheel load. Maximum vertical strains for all loads appeared to be about the same for this station.

For station 149+58 if the maximum vertical strain is used as the failure criterion, the prime mover load of 84 tons appears to be the critical load. On the other hand the horizontal strain at the bottom of the AC layer is highest for the trailer load of 7,750 lb per wheel even though the radial stress is lower than for the prime mover at 84 tons. The critical load for station 209+28 is similar to station 149+58.

Using the failure criteria previously selected, the estimated allowable repetitions of various vehicle loads for the three stations were determined and summarized in Table 9. For station 49+11, all the vertical strains due to various loads including the standard axle load of 18,000 lb are similar. The allowable number of repetitions for those magnitudes of strain are less than available rutting criteria can be used to predict.

Table 10 is a summary of the reduction in pavement life due to heavy hauls assuming that three hauls are made on each road. Using that as a base, the number of repetitions for the prime mover would be equal to 2 (prime movers) x 3 (number of axles) x 3 (hauls) or 18 repetitions. For the trailer, the number of repetitions for 7,750 lb/wheel would be equal to 2 (trailers) x 14 (axles) x 3 (hauls) or 84. By dividing the expected repetitions by the allowable repetitions for a specific loading configuration, an approximate estimate of the pavement life reduction was made.

Overlay Designs

Station 49+11 on Fruitdale Road and 209+28 on US-20 were selected for overlay designs because they were the critical sections. For trailer loads of 7,750 lb/wheel, to keep the reduction in pavement life within 10 percent, the gravel overlay for Fruitdale Road was estimated to be about 10 in. On US-20, the asphalt concrete should be about 7.5 in. For a trailer load of 6,642 lb/wheel, the gravel overlay on station 49+11 should be about 8 in. and the asphalt concrete on US-20 about 5 in. to keep pavement life within reasonable limits.

Conclusions and Recommendations: Case 2

Overall, the most critical situation was for US-20. The heavy haul exceeded criteria normally used to prevent rutting and cracking. However, the pavement was currently at or exceeding (in some areas) these criteria and it was probably unfair to apply the criteria directly as one would for a newly con-

Table 8. Summary of heavy haul responses.

Location		Vehicle Type	Load	Maximum Surface Deflection, ξ, in.	Maximum Tensile Stress, σ_R, psi	Maximum Tensile Strain, ϵ_{R1} 1X10^{-6}	Maximum Vertical Strain, ϵ_{V1} 1X10^{-6}
Fruitdale Road	49+11	Trailer	7750 lb./Wh	0.3172	-	-	5,664
			6642 lb./Wh	0.2755	-	-	5,699
		Prime Mover	42 tons	0.1920	-	-	6,060
			63 tons	0.2710	-	-	5,890
			84 tons	0.3460	-	-	5,610
		Standard Axle Load	18,000 lb.	0.0902	-	-	5,680
SR 20	149+58	Trailer	7750 lb./Wh	0.2284	180	582	2,095
			6642 lb./Wh	0.1960	169	521	1,798
		Prime Mover	42 tons	0.1190	169	456	1,300
			63 tons	0.1770	190	525	1,620
			84 tons	0.2330	201	567	2,130
		Standard Axle Load	18,000 lb.	0.0394	-	411	1,000
	209+28	Trailer	7750 lb./Wh	0.3201	330	1,061	3,153
			6642 lb./Wh	0.2756	316	1,002	2,926
		Prime Mover	42 tons	0.1760	326	902	3,190
			63 tons	0.2580	345	975	3,720
			84 tons	0.3390	344	995	4,040
		Standard Axle Load	18,000 lb.	0.0647	-	848	2,460

Table 9. Summary of allowable repetitions of various heavy haul loads (1-3).

Location		Vehicle Type	Load	Tensile Strain, ϵ_R, 1X10^{-6}	Allowable Repetition, N	Vertical Strain, ϵ_V, 1X10^{-6}	Allowable Repetition, N
Fruitdale Road	49+11	Trailer	7750 lb./Wh	-	-	5,664	-[a]
			6642 lb./Wh	-	-	5,699	-[a]
		Prime Mover	42 tons	-	-	6,060	-[a]
			63 tons	-	-	5,870	-[a]
			84 tons	-	-	5,610	-[a]
		Standard Axle Load	18,000 lb.	-	-	5,680	-[a]
SR 20	149+58	Trailer	7750 lb./Wh	582	6,000	2,095	310
			6642 lb./Wh	521	11,000	1,798	720
		Prime Mover	42 tons	456	30,000	1,300	5,000
			63 tons	525	10,500	1,620	1,400
			84 tons	567	7,200	2,130	270
		Standard Axle Load	18,000 lb.	411	54,000	1,000	25,000
	209+28	Trailer	7750 lb./Wh	1,061	140	3,153	-[a]
			6642 lb./Wh	1,002	200	2,926	-[a]
		Prime Mover	42 tons	902	380	3,190	-[a]
			63 tons	975	250	3,720	-[a]
			84 tons	995	210	4,040	-[a]
		Standard Axle Load	18,000 lb.	848	580	2,460	110

[a]Allowable repetitions are low because strains exceed reasonable failure criteria.

structed pavement. In other words, some of US-20 pavement had already failed.

Even though the findings of this analysis were not implemented, the results were used to determine the improvements necessary to upgrade the two roads for heavy loads. The following improvements were recommended.

1. Reduce the loading for both the trailer and prime mover to 42 tons maximum load and place two additional lines of axles on each trailer. This would increase the total wheels to 224 per trailer and reduce each wheel load to 6,642 lb.

2. Fruitdale Road. Widen the shoulders to accommodate the wide load and add an overlay of 8 in. of compacted crushed aggregate over the entire roadway. A bituminous surface treatment before hauling should keep the surface from raveling and provide a smoother haul. A repeat of the surface treatment after hauling may be required.

Table 10. Pavement life reduction due to heavy hauls (3-6).

Location		Vehicle Type	Load	Pavement Life Reduction (%)	
				Based on ε_c	Based on ε_r
Fruitdale	49+11	Trailer	7750 lb./Wh	-	-[a]
			6642 lb./Wh	-	-[a]
		Prime Mover	42 tons	-	-[a]
			63 tons	-	-[a]
			84 tons	-	-[a]
SR 20	149+58	Trailer	7750 lb./Wh	1	23
			6642 lb./Wh	< 1	12
		Prime Mover	42 tons	0	< 1
			63 tons	0	1
			84 tons	0	7
	209+28	Trailer	7750 lb./Wh	51	-[a]
			6642 lb./Wh	42	-[a]
		Prime Mover	42 tons	5	-[a]
			63 tons	7	-[a]
			84 tons	9	-[a]

[a]Strains exceed failure criteria.

3. US-20. If the actual hauling will not take place for at least 2 years, make final surface condition and roughness surveys on US-20 just prior to the hauling operation. Following the hauling, repeat the surveys and assess the actual pavement damage due to the heavy loads. Also, an overlay of asphalt concrete will probably be required on US-20 within 2 or 3 years because of current heavy truck traffic. The heavy hauls will cause additional damage but the extent of the damage is a function of the WSDOT maintenance or rehabilitation performed to US-20 to accommodate traffic conditions.

ACKNOWLEDGMENT

The authors acknowledge the Washington State Department of Transportation (WSDOT) for the funding associated with the proposed Satsop haul route, specifically, the efforts of the personnel of the WSDOT Materials Laboratory who were crucial in the successful completion of that portion of the report work. Also, the authors acknowledge the support for the Skagit project provided by the American-Marks Company.

REFERENCES

1. R.I. Kingham and B.F. Kallas. Laboratory Fatigue and its Relationship to Pavement Performance. Res. Rept. 72-3, The Asphalt Institute, College Park, Md., April 1972.
2. F. Finn et al. The Use of Distress Prediction Subsystems for the Design of Pavement Structures. Proc., 4th International Conference on the Structural Design of Asphalt Pavements, Univ. of Minn., Minneapolis, Minn., 1977, pp. 3-38.
3. Austin Research Engineers. Asphalt Concrete Overlays of Flexible Pavements--Vol. I. Development of New Design Criteria. Rept. FHWA-RD-75-75, Federal Highway Administration, U.S. Department of Transportation, Wash., D.C., June 1975.
4. G.M. Dorman and C.T. Metcalf. Design Curves for Flexible Pavements Based on Layered System Theory. HRB, Highway Research Record 71, 1964, pp. 69-84.
5. N.W. Witczak. Design of Full-Depth Asphalt Airfield Pavements. Proc., 3rd International Conference on the Structural Design of Asphalt Pavements, Univ. of Mich., Ann Arbor, 1972, pp. 550-567.
6. C.L. Monismith, N. Ogawa, and C.R. Freeme. Permanent Deformation Characteristics of Subgrade Soils Due to Repeated Loading. TRB, Transportation Research Record 537, 1975, pp. 1-17.

Equivalency Factor Development for Multiple Axle Configurations

HARVEY J. TREYBIG

Through the analysis of AASHO pavements a fundamental relationship is developed between subgrade compressive strain and equivalency factor. Other elements such as tensile strain in the surface and deflection were examined, but the best relationship evolved when the subgrade compressive strain was used. Once the basic relation of equivalency factor and strain is developed, the equivalency factors for axle configurations other than single and tandem can be computed over a wide range of loads. The elastic-layered theory was used for computing strain. The computed results were compared to extrapolations of the AASHO equations used to compute equivalency factors. These comparisons were good in some instances; in others, they were not. The equivalency-factor concept can be extended to new size and weight configurations of highway vehicles. Thus it will be possible to include these new loads in both new and rehabilitative pavement design procedures that use the concept of equivalent loadings.

The equivalency factor concept for considering traffic mixes in a simplified way was developed in the pavement research studies at the AASHO Road Test. The load equivalencies have received widespread use, but unless a rational basis is established for extending this concept to new vehicles of changing configuration and increased loads, many pavement design procedures will be obsolete. As loads become heavier and axle configurations change, as reported by Peterson (1), Graves (2), and Chu et al. (3), a problem arises when the AASHO equivalency factors are extrapolated outside the range for which they were developed.

One result of the AASHO Road Test was to develop equivalency factors to estimate how many applications of a load being considered would cause the same amount of damage as one application of a standard load. The results are given for two standard axle configurations: single and tandem axles with loads less than 40 to 48 kips (178 to 214 kN), respectively. Equivalency factors for heavier loads and different axle configurations are extrapolated from the AASHO equivalency factors and are outside the boundaries for which they were developed. Therefore, a more fundamental relationship must be found to facilitate the extrapolation to other axle configurations such as triple axles with heavier loads.

EXISTING METHODS

Field performance data do not exist to determine equivalency factors for non-AASHO Road Test axle configurations (single tires, tridems, etc.). As axle configurations change, it becomes necessary to estimate the damage based on assumptions not supported by either theoretical considerations or field observations. For example, the damage caused by tridem axles has been estimated to be the same as that caused by the combination of a single and tandem axles. This estimate is based on equivalency factors for axle configurations that were not used at the AASHO Road Test. The basic assumption is that the load equivalency factor concept is a valid procedure for describing the effects of mixed loading configurations on pavement performance.

Based on the hypothesis that pavement distress is related to the state of stress, strain, or deflection induced by traffic loads, equivalency factors can be developed from computations of these pavement response parameters. Various approaches have been used to derive load equivalency factors. The results for each approach are highly dependent on the parameters, environmental conditions, and methods used to define pavement failure.

A review of different methods for computing or extrapolating equivalency factors for flexible pavements is given by Yoder and Witczak (4) and graphically summarized in Figure 1. Asphalt pavement design methods, such as the Asphalt Institute thickness design procedure (5), account for varying axle loads by using a linear relationship between axle load and the logarithm of equivalency factor derived from the AASHO Road Test data, assuming a terminal serviceability index of 2.5. Southgate et al. (6) reported a similar axle load-damage factor relationship based on experience in Kentucky (Figure 2).

Deacon (7, 8,), Witczak (9), and Terrel (10) used calculated asphaltic tensile strain to evaluate the effect of increased axle weight and different tire configurations on flexible pavements. Damage equivalencies were established based on a flexural fatigue distress. The results showed that single tires produce considerably more pavement damage at the same total load than dual tires, which illustrates the significance of tire configuration. Also, the results showed substantial reductions in pavement life when axle loads were increased.

Layton et al. (11) used the AASHO design method equations and elastic-layered analysis to evaluate the effect of increased vehicle weight. Jung and Phang (12) determined load equivalency factors from theoretically determined subgrade deflections correlated with AASHO Road Test data. Ramsamooj et al. (13) proposed a method of deriving load equivalency factors from longitudinal stress intensity factor profiles obtained from theoretical fracture mechanics concepts. These authors propose to calculate the tandem, axle-load equivalency factors as the ratio of the sum of the fourth power of the peak. Then calculate the peak-to-trough value of the stress intensity factor produced by the tandem axle load to the fourth power of the peak value produced by the standard axle load as shown in Figure 3.

Although various procedures have been used to compute equivalencies, most are based on a failure criterion of either rutting or fatigue cracking. The procedures for determining equivalencies based on performance are not readily applicable to axle configurations other than single and tandem load axles [see Figure 4 (14)].

RESPONSE VARIABLE

To develop a theoretical evaluation procedure, the response variables must be related to future performance of the pavement; and the location in the pavement structure where this response will be critical must be known. Pavement failure is assumed to be a function of the response to vehicle loadings. The damage produced by an application of an axle load may be calculated from a mathematical equation established from the results of laboratory tests and theoretical considerations and verified by field observation.

Pavement surface deflection has often been ac-

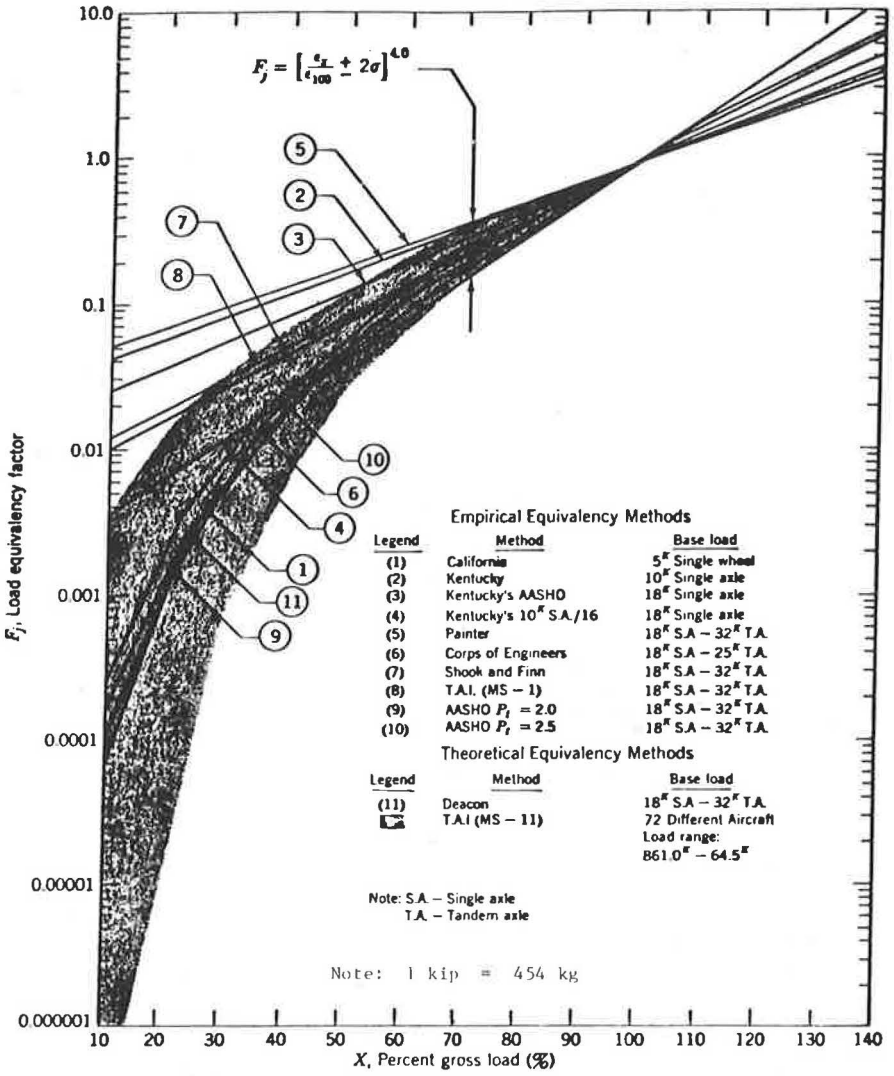

Figure 1. Comparison of various load equivalency methods as a function of percent of gross load (4).

cepted as a good indicator of changes in pavement behavior [Kingham (15), (16)], but surface deflection alone is only a fair indicator of the structural strength of a pavement. High values for surface deflection have been used as limiting criteria for pavement design (Figure 4), as reported by Jung et al. (17); however, maximum surface deflection may not be readily related to performance over a wide range of loading conditions.

Of the various observable distress mechanisms for flexible pavement, fatigue and rutting can be directly related to critical strains in the pavement structure. The horizontal tensile strain at the bottom of the asphaltic concrete can be related to fatigue, whereas vertical compressive strain at the top of the subgrade can be related to rutting. Models that relate pavement failure to repeated applications of vehicle loadings are summarized by Barker et al. (18) and Rauhut et al. (19).

For rigid pavements, horizontal tensile stress has generally been accepted as the response variable providing the best relationship to the pavement distress of cracking. The Vesic equation (20) and the stress ratio used by the Portland Cement Association (21) are most commonly used to predict failure, although many failure-prediction equations exist as stated by Treybig et al. (22).

SINGLE AND DUAL TIRES

An equivalent single wheel load (ESWL) has commonly been used in various design or evaluation procedures to aggregate the effects of different wheel configurations, as described by Van Buren (23). Normally, either equal contact area (U.S. Army Corps of Engineers) or pressure is used to represent the dual tire load for determining ESWL.

The greatest difficulty in applying the ESWL concept is that the failure mechanism in a given pavement structure may vary for different loadings. Thus, the critical parameters do not remain constant for the same pavement structure with a change in axle load. Deacon (24) reported that axles with single tires are three times more damaging than dual tires with the same load, whereas Terrel et al. (10) and Christison et al. (25) reported them as 7 to 10 times more damaging.

Considering the previously mentioned information, it can be concluded that a single tire of the same contact area as a dual tire cannot be used to accurately represent a dual tire configuration; and hence, the single-tire axles should be identified and treated separately in equivalency studies.

Because of the data collection techniques at the AASHO Road Test, the present AASHO equivalency

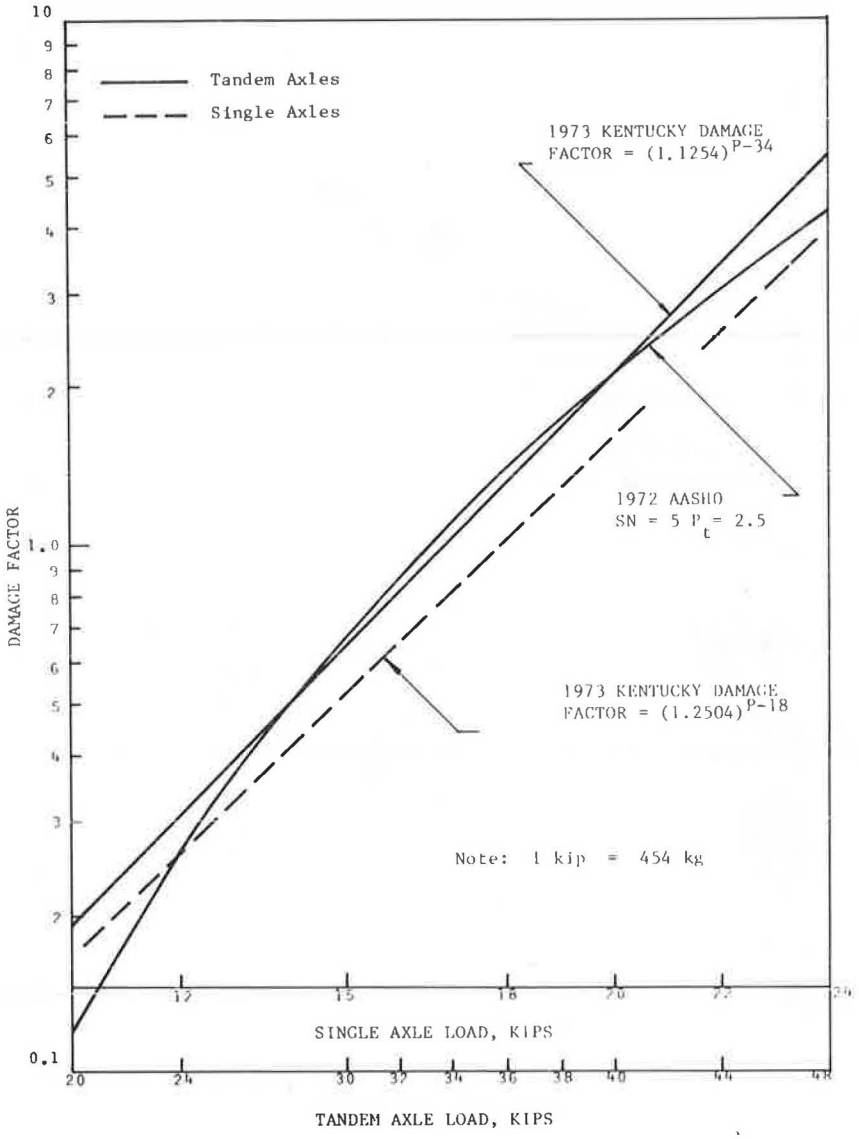

Figure 2. Damage factor versus tandem and single axle load based on experience in Kentucky.

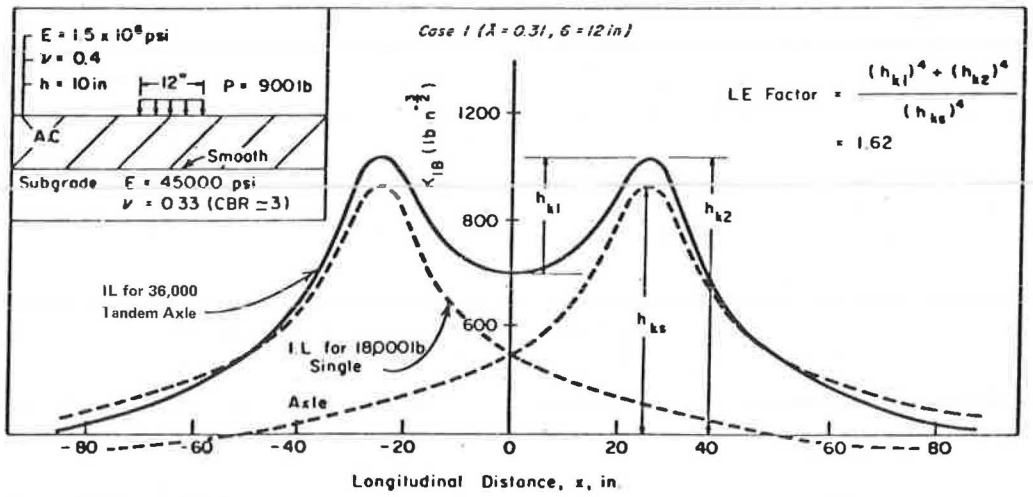

Note: 1 lb = 454 kg
1 in = 2.54 cm

Figure 3. Load equivalency factor for 36-kip tandem axle (13).

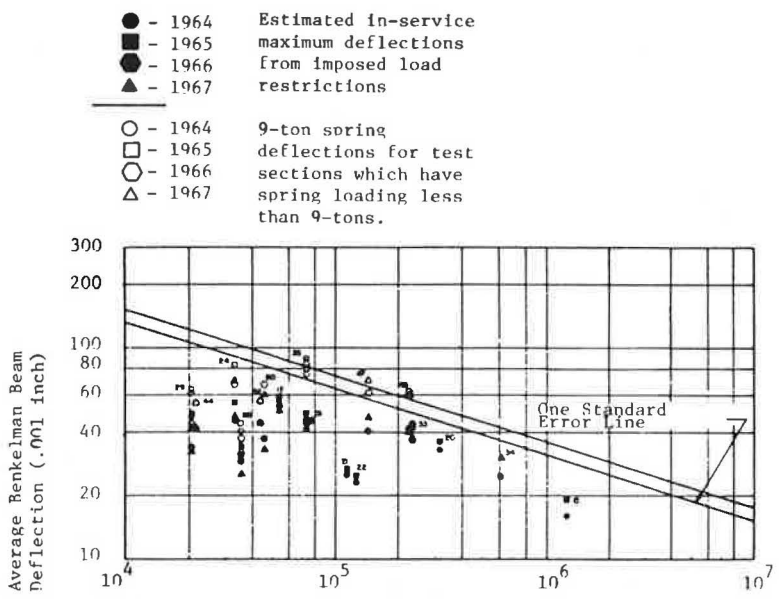

Figure 4. Variation of measured spring deflections with total equivalent 18-kip axle load through 1966 (14).

factors combine the damage caused by a single-tire, steering-axle loading with damage caused by the trailing axles (26). It is possible to determine equivalencies for these single tires by separating the damage caused by single and dual tires at the AASHO Road Test. The equations for calculating this separation of damage are developed and explained in FHWA Report No. RD-79-73 (27). Table 1 gives the resulting new equivalency factors for the specific AASHO conditions for the flexible pavements. As shown, there is little difference between the equivalency factors reported by AASHO and those developed for the load axles after steering axle damage was separated out. As also shown, the single tire loadings produce significantly more damage than does a comparable loading of dual tires as was shown in Deacon's theoretical studies (7) and Christison's theoretical and field studies (25).

The same analysis was used to develop the rigid pavement load equivalency factors in an attempt to separate the damage resulting from dual and single tires. The results of this procedure produced less damage for tire loads on rigid pavements, whereas more damage was computed for single tire loads on flexible pavements than that produced during the AASHO Road Test. Therefore, it was concluded that

Table 1. Comparison of equivalency factors with and without the effect of steering axles based on performance criteria for SN = 4.0, P_t = 2.0, and a flexible pavement.

	Steering Axle Load		Tandem Axle Load		
Total Axle Load (kips)	Predicted Without Single Tires	AASHO With Single Tires	Predicted Without Single Tires	AASHO With Single Tires	Steering Axle
2	.00009	.002	--	--	--
4	.002	.002	--	--	.009
6	.009	.01	--	--	.05
8	.08	.08	.006	.01	.25[a]
10	.08	.08	.006	.01	
12	.18	.18	.01	.01	.46
14	.34	.35	.02	.03	--
16	.61	.61	.04	.05	--
18	1.00	1.00	.07	.08	--
20	1.56	1.55	.11	.12	--
22	2.34	2.31	.16	.17	--
24	3.39	3.33	.23	.25	--
26	4.77	4.68	.33	.35	--
28	6.53	6.42	.45	.48	--
30	8.75	8.65	.61	.64	--
32	11.51	11.46	.80	.84	--
34	14.89	14.97	1.03	1.08	--
36	18.98	19.28	1.32	1.38	--
38	23.87	24.55	1.66	1.72	--
40	29.68	30.92	2.06	2.13	--
42	--	--	2.53	2.62	--
44	--	--	3.09	3.18	--
46	--	--	3.73	3.83	--
48	--	--	4.47	4.58	--

Note: 1 kip = 454 kg.

[a]Equivalency factor for the 9-kip steering axle load.

the damage produced by single tire loads could not be separated from the total damage included in the rigid equivalency factors by the techniques used and information available.

DYNAMIC EFFECTS

As repeated applications of loads pass over pavements, forces are imposed that are a combination of vehicle static weight and induced dynamic forces. These dynamic forces result from the motions imparted to the vehicle by road surface irregularities, and their magnitude depends on vehicle characteristics, vehicle speed, and the nature of the road surface irregularities as explained by Whittmore et al. (28). Dynamic forces have an influence on the life expectancy of pavements, but the actual amount has not been fully determined or explained. The variable nature of the dynamic response of vehicles severely complicates the problem of predicting load equivalency factors for pavement performance. Because the AASHO equivalency factors were developed from in service data, some amount of dynamic force influence is built into the factors.

It may be assumed that the increase or decrease in the response variable caused by the dynamic forces produced by the base load is proportionate to the increase or decrease in the response caused by some other axle load or configuration. This assumption should result in the same ratio of response variable for the dynamic and static conditions for a specific pavement structure, but there is no conclusive evidence to support this assumption. Hence, for simplicity, the equivalency factors determined from the analytical techniques given below are assumed to be constant for the static and dynamic loading conditions.

MODELS

Two computer models were used extensively to calculate response variables for predicting equivalency factors.

1. Elastic-layered analysis (ELSYM 5, 29).
2. Discrete element analysis (SLAB 49, 30).

Currently, elastic-layered theory is the most promising approach for evaluating pavement response to varying loads because it is simple and inexpensive. These procedures have been used by various authors including Jung et al. (12) and Deacon (7). The limiting factor in this procedure is the inability to estimate the modulus of elasticity and Poisson's ratio for each material in the pavement structure. A discrete element analysis model was used to analyze rigid pavements. This model (SLAB 49) permits analysis of interior, edge, and corner loading conditions and provides output that can be used to evaluate their effect on rigid equivalency factors.

MECHANISTIC APPROACH

For purposes of these analyses, it was assumed that a relationship could be developed between a component of strain, stress, or deflection in the pavement and AASHO performance-based equivalency factors. A relationship was first formulated for single loads on AASHO pavement cross sections (Figure 5) and then used to predict AASHO equivalency factors for tandem loads. If these tandem equivalency factors were comparable to the AASHO performance equivalencies, the response variable, equivalency relationship could be extended to other load configurations. These relationships could then be compared with pavement flexural fatique and rutting criteria used to define pavement failure and would provide support for the concepts and methodology used in other studies for deriving equivalency factors for various loading conditions.

FLEXIBLE PAVEMENTS

Results of computations for surface deflections and interfacial strains in the asphaltic concrete and the subgrade were used to obtain quantitative assessments of the relative damaging effects caused by different loading configurations on flexible pavements. Because equivalency factors based on performance are a function of load and structural number (31), computations were performed for both single and tandem axle loads over a range in the structural number (SN). The use of Equation 1 produced estimates of equivalence factors that corresponded closely to those based on AASHO performance. Equation 1 will be referred to, hereafter, as the Curvature Method.

$$F(x_n) = [\epsilon_1(x_n)/\epsilon(18_s)]^B + \sum_{i=1}^{n} \left\{[\epsilon_{i+1}(x_n)] - [\epsilon_{i-i+1}(x_n)]/\epsilon(18_s)\right\}^B \quad (1)$$

where

$$B = \text{Log } F(x_s)/\text{Log } [\epsilon(x_s)/\epsilon(18_s)] \quad (1a)$$

$F_i(x_n)$ = predicted equivalency factor for axle configuration n of load x.
$\epsilon(18_s)$ = maximum asphalt tensile strain or subgrade vertical strain for the 18-kip (80 kN) equivalent single axle load (ESAL), in./in.
$\epsilon_1(x_n)$ = maximum asphalt tensile strain or subgrade vertical strain under the leading axle or axle configuration n of load x, in./in.
$\epsilon_{i+1}(x_n)$ = maximum asphalt tensile strain or subgrade vertical strain under axle i+1 of axle configuration n of load x, in./in.
$\epsilon_{i-i+1}(x_n)$ = asphalt tensile strain or subgrade vertical strain, in critical direction, between axles i and i+1 of axle configuration n of load x, in./in.
$F(x_s)$ = AASHO performance equivalency factor for an x-kip single axle load.
$\epsilon(x_s)$ = maximum asphalt tensile strain or subgrade vertical strain for an x-kip single axle load, in./in.

Tensile Strain

ELSYM 5 was used to compute maximum tensile strain at the bottom of the asphalt concrete as a function of axle load for different structural numbers. These computations were completed for the pavement cross section and material properties given in Figure 5. Material properties selected to represent AASHO Road Test conditions were taken from References (22) and (26), and AASHO structural coefficients must be used in computing structural numbers for the analysis. The relationship between AASHO equivalency factor and maximum tensile strain is illustrated in Figure 6.

Using Equation 1a and asphalt tensile strain, the B value was computed to be 5.06 for a structural number of 3.75 and a terminal serviceability of 2.0. Results of numerous reported laboratory fatigue tests indicate that the exponent B is primarily dependent on mix composition. Numerous studies have yielded values ranging from 3.0 to 5.0 as reported by Monismith and Salam (32). [Finn et al. (33), Rauhut et al. (19), and Treybig et al. (34).]

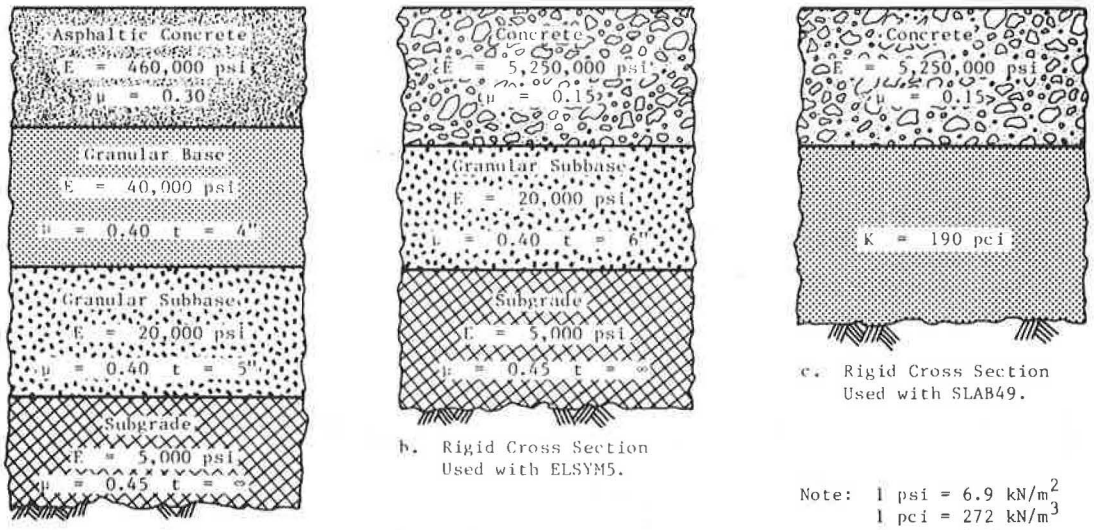

a. Flexible Cross Section Used with ELSYM5.

b. Rigid Cross Section Used with ELSYM5.

c. Rigid Cross Section Used with SLAB49.

Figure 5. Pavement material properties used to develop an initial relationship to predict the AASHO tandem equivalency factors.

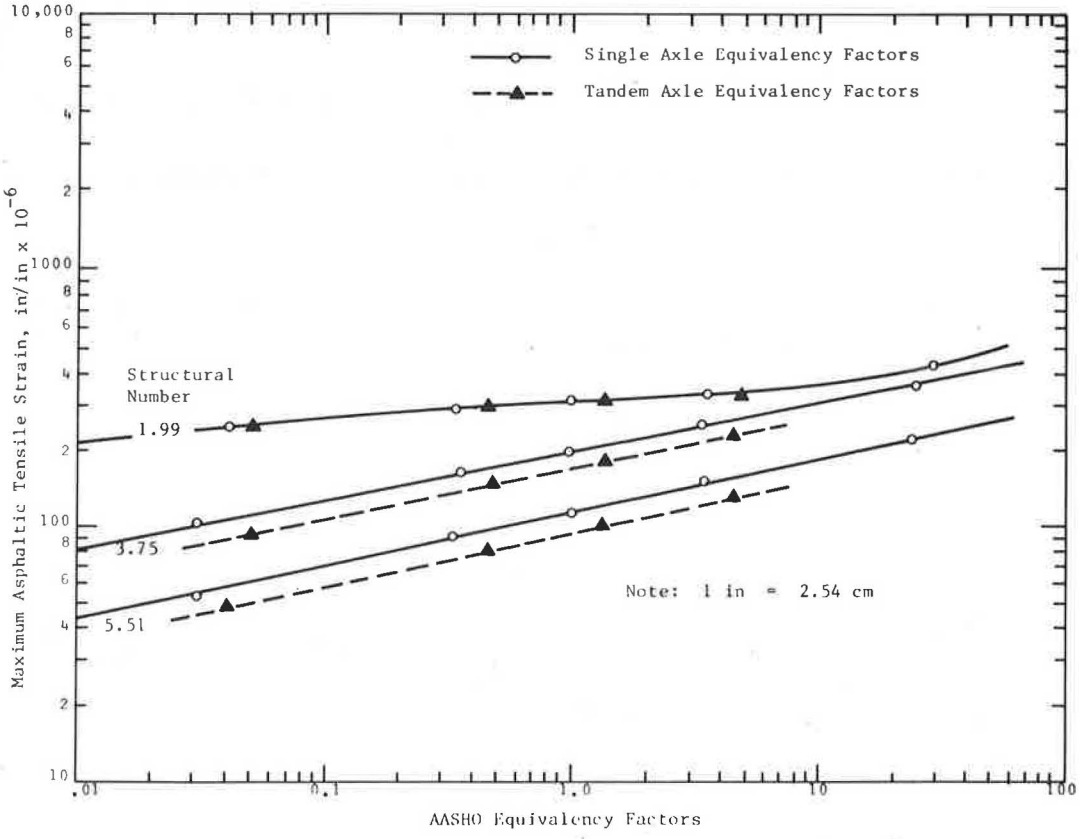

Figure 6. Comparison of AASHO equivalencies with maximum asphaltic concrete tensile strain, computed with ELSYM 5.

Equivalency factors predicted by Equation 1 are shown in Figures 7 and 8. In Equation 1, zero strain should be used in computing the difference in strain values between and under axles if the asphalt tensile strain between the axles is compressive. Equivalency factors were predicted using this procedure for numerous axle loads and configurations and are published in FHWA Report No. RD-79-73 (27).

Subgrade Strain

ELSYM 5 was also used to calculate maximum compressive strain at the top of the subgrade as a function of axle load for different structural numbers. These calculations were completed for the pavement cross section and material properties given in Figure 5. The relationship between AASHO equivalency

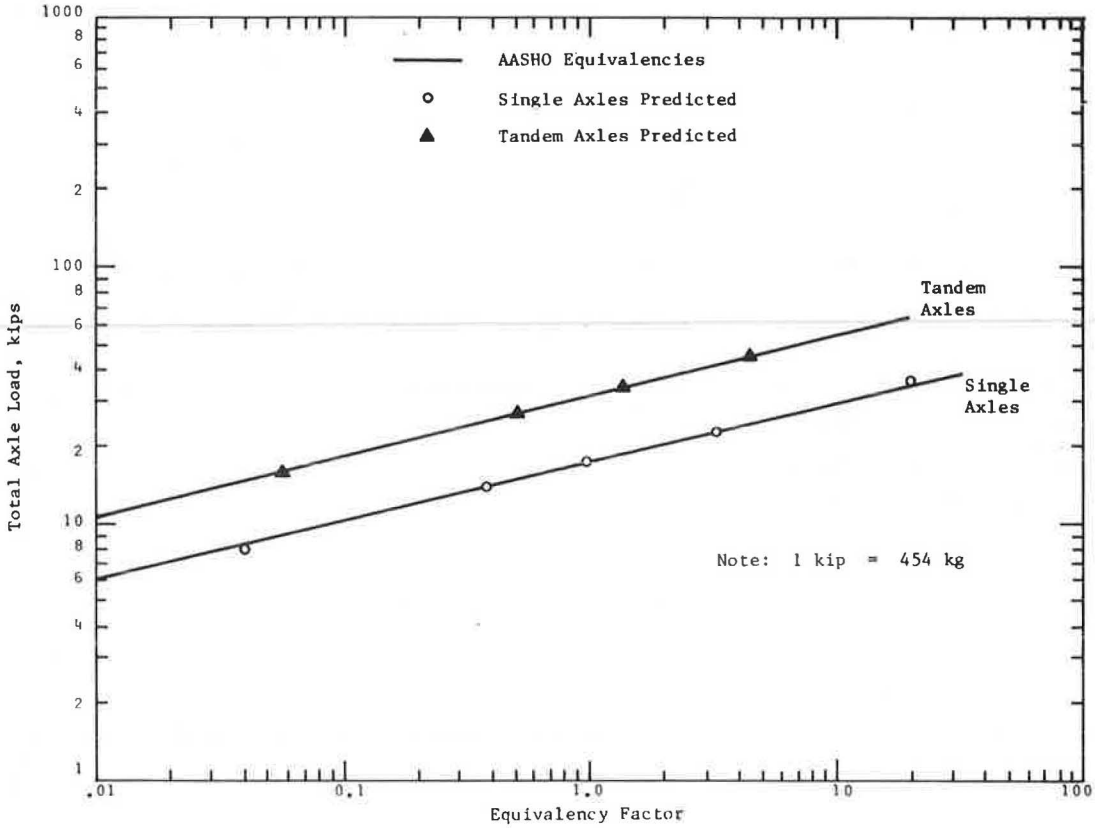

Figure 7. Development of equivalency factors based on asphalt concrete tensile strain using the Curvature Method—SN = 3.75.

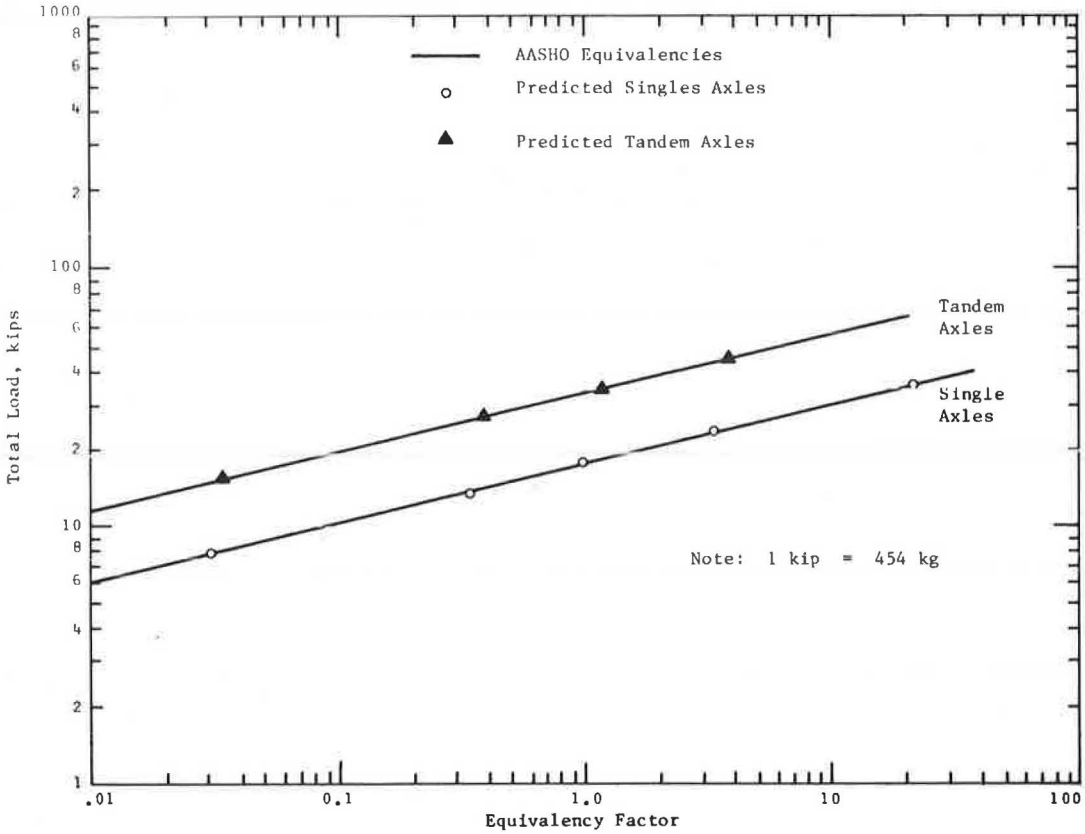

Figure 8. Development of equivalency factors based on asphalt tensile strain using Curvature Method—SN = 5.51.

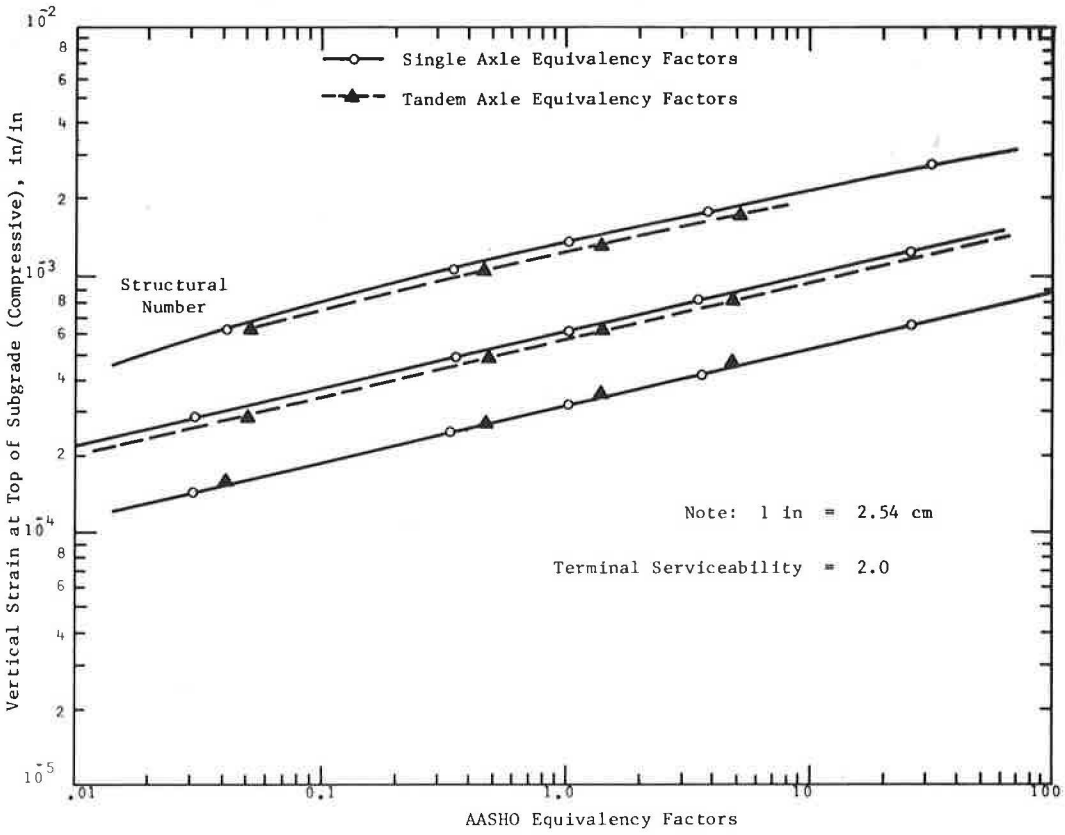

Figure 9. Comparison of AASHO equivalencies with subgrade compressive strain at the top of the subgrade computed with ELSYM 5.

factor and maximum compressive strain is presented in Figure 9.

The B value calculated for this condition was 4.49 for a structural number of 3.75 and a terminal serviceability of 2.0. Similar values have been reported by Shell (35) and Santucci (36). The results using the Curvature Method of Equation 1 are given in Figures 10-12. If the subgrade vertical strain between the axles is tensile, then zero strain should be used in computing the difference in strain values between and under axles. Equivalency factors were predicted for numerous axle loads and configurations using this procedure and are published in FHWA Report No. RD-79-73 (27).

RIGID PAVEMENTS

Computations of concrete tensile stresses and surface deflections caused by various loading configurations on a rigid pavement were used to obtain quantitative assessments of the relative damage effects on pavements. Based on AASHO performance, equivalency factors are a function of load and concrete thickness. Therefore, both single and tandem axle loads were used along with a range of thicknesses in predicting the AASHO equivalency factors. Both ELSYM 5 and SLAB 49 were used to calculate the response variables for predicting the equivalencies. The pavement cross section and material properties used by each model in calculating the critical response variables are given in Figure 5.

The same type of relationship described in Equation 1 was used in predicting rigid equivalency factors. By using the response variables of deflection and stress computed with the various models, the predicted equivalency factors were not within reasonable accuracy for the AASHO material properties and general cross sections. The predicted equivalency factors were different from those developed at the AASHO Road Test by a factor of two or greater. Some examples of predicted versus AASHO equivalency factors are shown in Figures 13-15. Equivalency factors were shown to depend to some degree on the model and loading conditions used to simulate field conditions. The following interrelated explanations are given as to why the AASHO equivalency factors were not predictable using the given analytical techniques.

1. Loss of Support. The analytical models cannot be used to simulate the effect of pumping with time. Because the tandem axle loads have a much larger deflection basin than the single axle loads, the effect of pumping on pavement performance may be more severe for tandem axle loads than single axle loads.
2. Load Transfer. The loss of load transfer at joints could increase at a greater rate for applications of tandem axles than single axles resulting in higher tensile stresses for tandem axles.
3. Dynamic Loads. The effect of dynamic loads at joints may be much greater for tandem axles than for single axles. Also, this dynamic effect at joints (corner loading) could have a larger influence on pavement performance than the dynamic effect based on interior loading conditions, which is normally simulated for asphalt pavements. Hence, the assumption of equal relative effect for the static, as well as the dynamic load effect, could be in error for jointed concrete pavements.
4. Slab Curling. When considering the movement of a tandem axle across a joint as opposed to a single axle, curling stresses could cause the tandem axles to be more damaging.

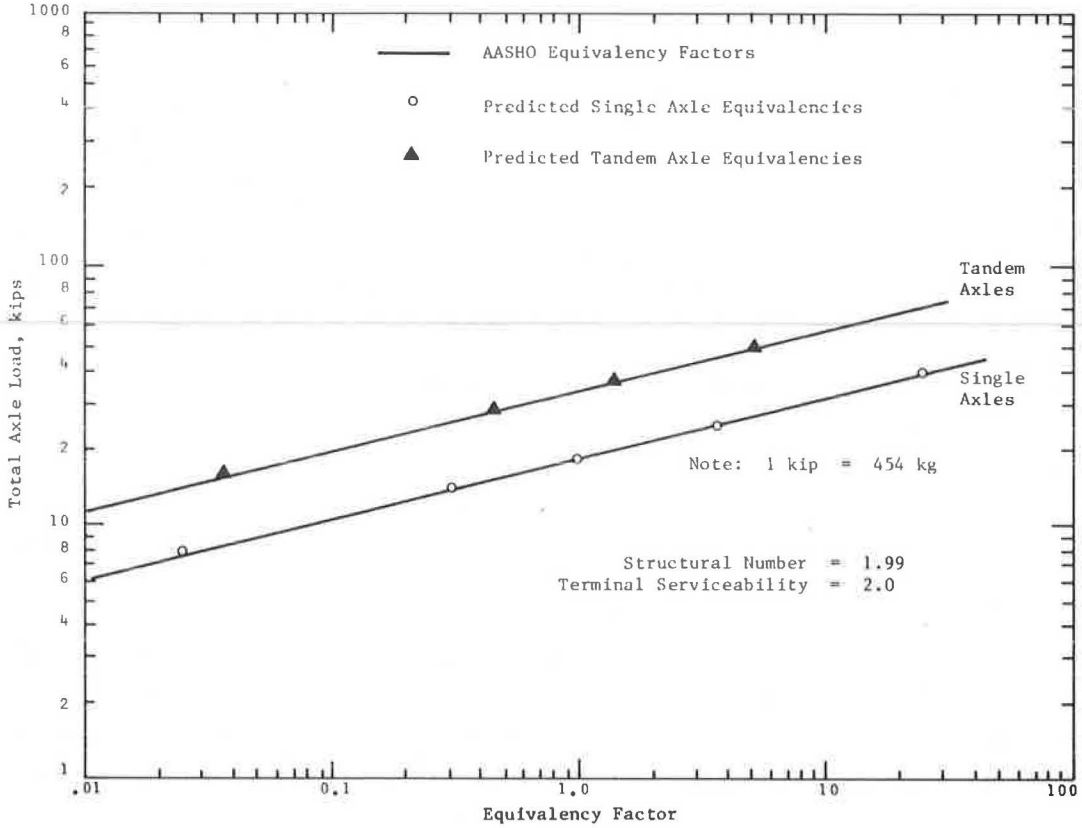

Figure 10. Development of AASHO equivalency factors based on subgrade compressive strain using the Curvature Method—SN = 1.99.

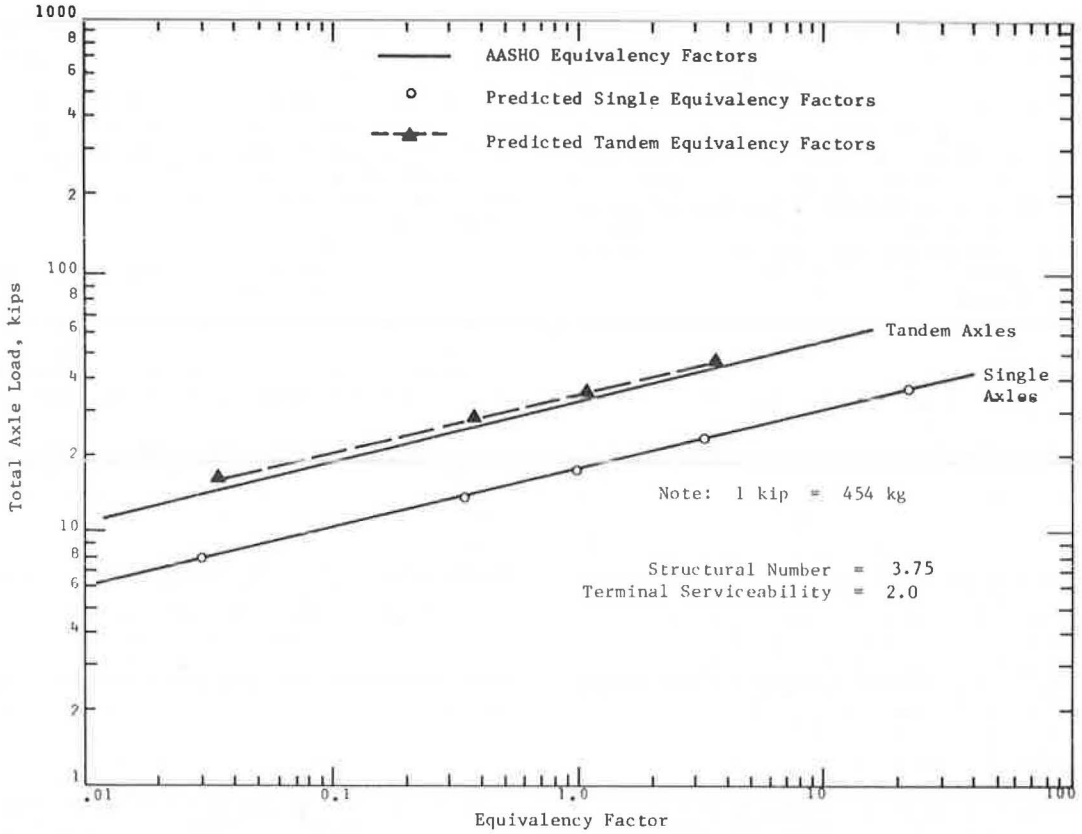

Figure 11. Development of AASHO equivalency factors based on compressive strain using the Curvature Method—SN = 3.75.

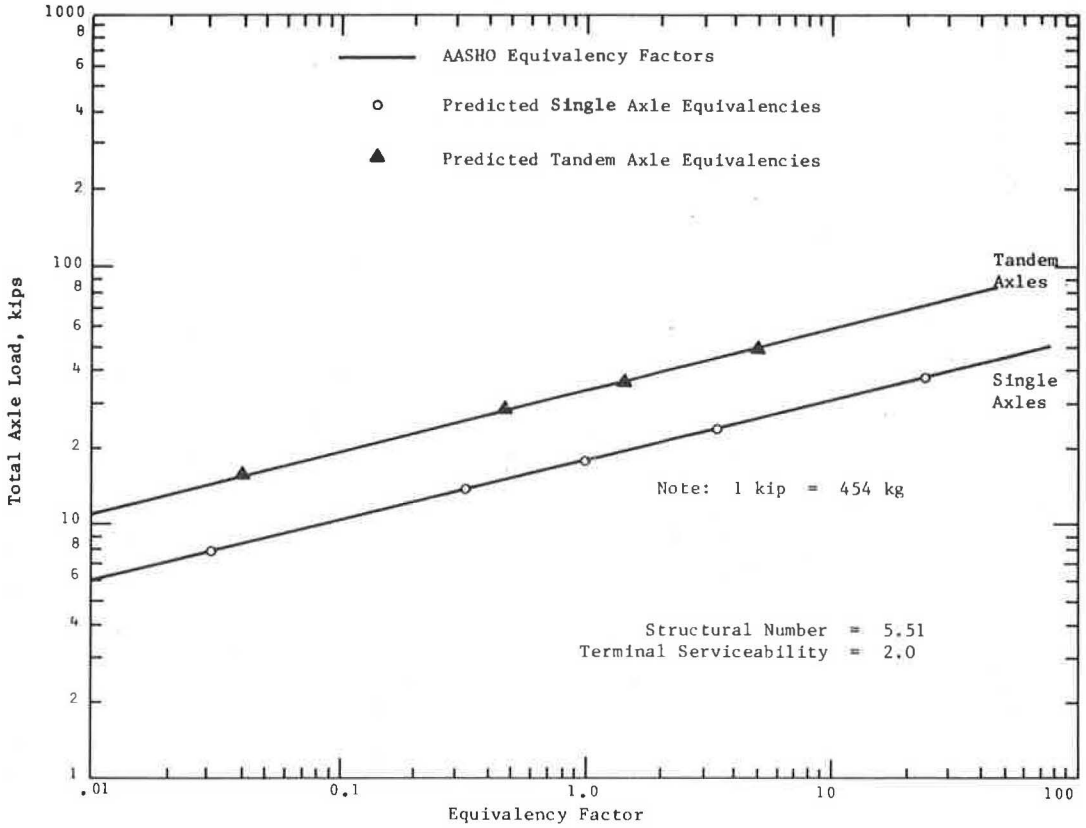

Figure 12. Development of AASHO equivalency factors based on subgrade compression strain using the Curvature Method—SN = 5.51.

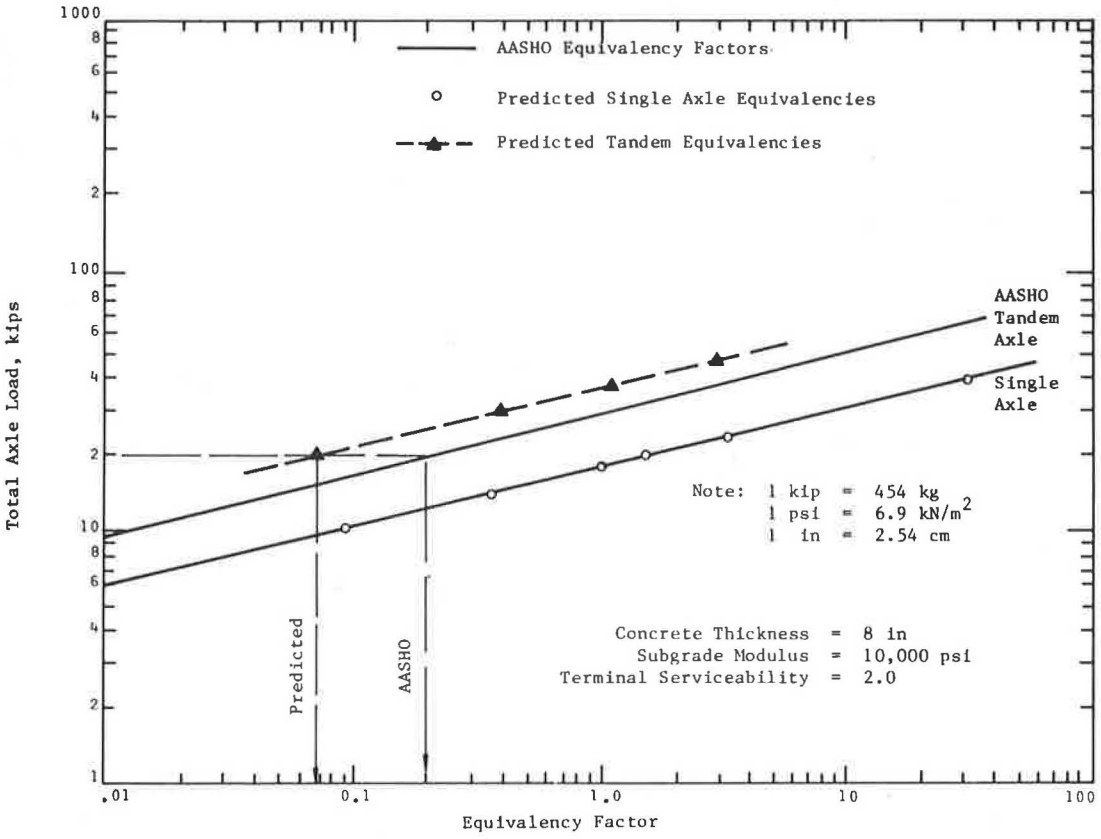

Figure 13. Development of AASHO equivalency factors based on a stress criterion using ELSYM 5 for the Curvature Method.

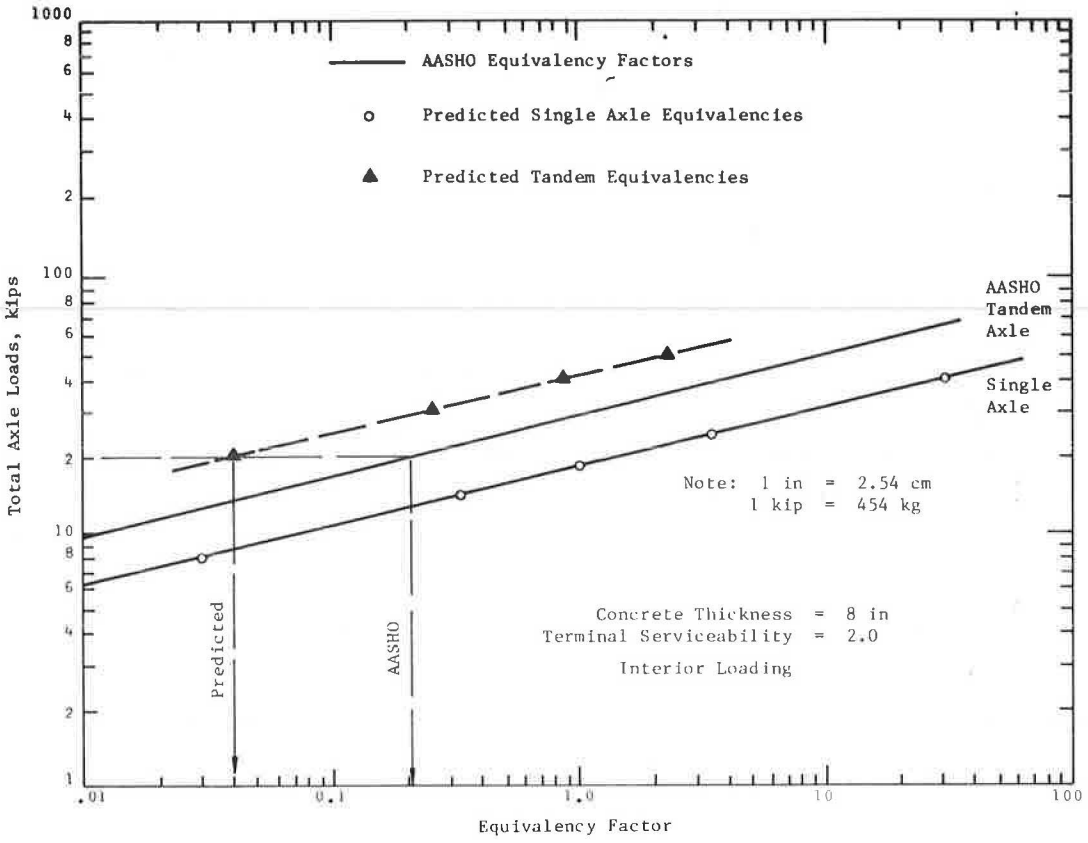

Figure 14. Development of AASHO equivalency factor based on a stress criterion using SLAB 49 for the Curvature Method—interior loading.

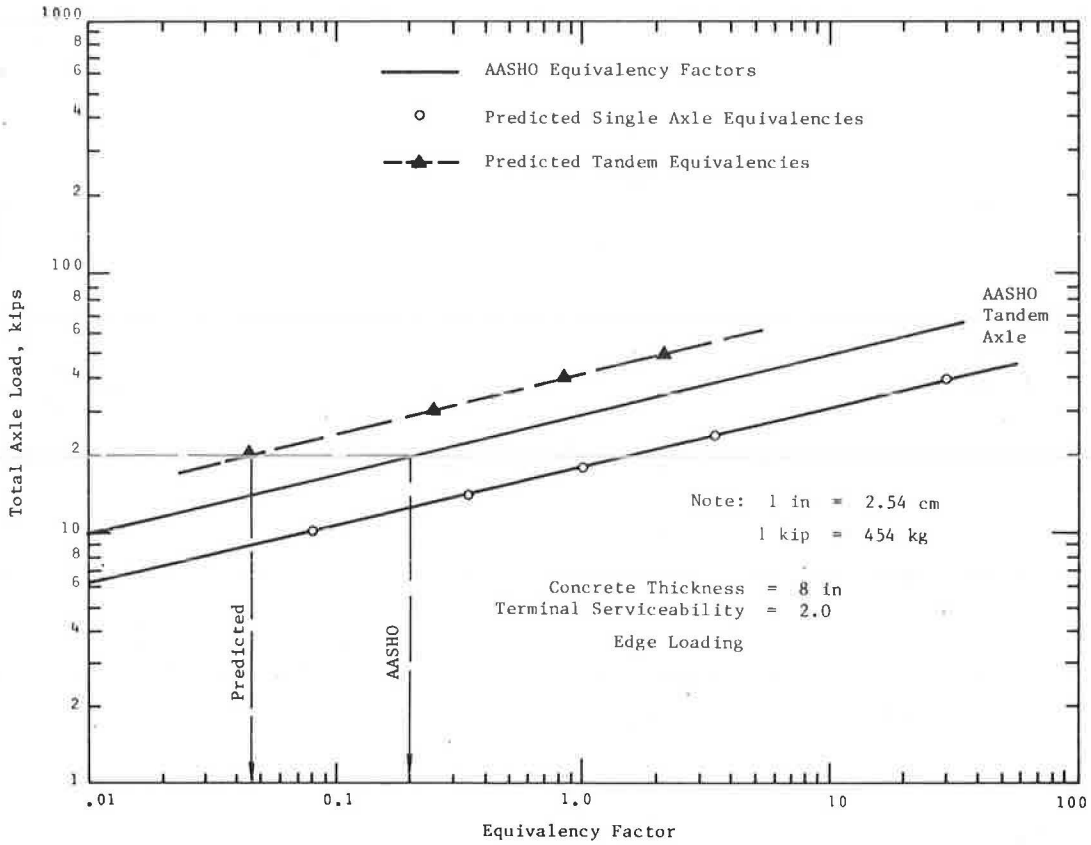

Figure 15. Development of AASHO equivalency factor based on a stress criterion using SLAB 49 for the Curvature Method—edge loading.

SUMMARY

Relationships between performance equivalency factors and asphalt tensile strain and subgrade vertical strain were developed for flexible pavements loaded with the AASHO axle configurations. Using this relationship, equivalency factors were generated for triple- and five-axle configurations. Because of the volume of those tables, the reader is referred to FHWA Report No. RD-79-73 (27), Appendix B and C. Because asphalt concrete strain correlates better with AASHO load equivalency factors under comparable loading conditions, Appendix C of FHWA Report No. RD-79-73 is recommended when triple- and five-axle configurations are expected. If the pavement structures under evaluation vary significantly from the AASHO material properties and thicknesses, the engineer should consider developing equivalency factors for site-specific situations. Care must be exercised in using load equivalency factors obtained from AASHO correlations if actual longitudinal spacing between axles or transverse spacing between dual tires change from those used at the AASHO Road Test.

The performance equivalency factors for other axle configurations were extended based on a structural number of approximately 3.75. The structural number becomes an important variable in determining equivalency factors for terminal serviceability greater than 2.5. Therefore, caution should be used in applying these developed values for terminal serviceabilities greater than 2.5.

In predicting equivalency factors based on asphalt tensile strain, only asphalt thicknesses greater than 3 in. (7.6 cm) should be used. The reason is that elastic layer theory (ELSYM 5) for certain conditions computes compressive strains in thin asphalt concrete layers. If less than 3 in. (7.6 cm) of asphaltic concrete exists, then subgrade vertical strain should be used to compute the equivalency factor as shown in Figures 10-12.

Equivalency factors were shown to be dependent on pavement type and loading condition. The rigid pavement equivalency factors were not predicted adequately by the mechanistic analysis (stress-strain analysis) procedures used in this study. Therefore, the AASHO equations must be relied on to generate equivalency factors for other than standard axle configurations. It is recommended that the dynamic effect of tandem loads on jointed concrete pavements as compared to single axles be reviewed and evaluated in further detail. This should determine whether the initial assumption is correct and illustrate why a 36-kip (160 kN) ESAL tandem axle load is approximately 2.45 times as damaging as an 18-kip (80 kN) ESAL single axle load for rigid pavements and only 1.38 times more damaging for flexible pavements.

REFERENCES

1. D.E. Peterson. Pavement Damage Due to Excessive Truck Overloads. Utah Department of Transportation.
2. Richard A. Graves, III. Special Interstate Truck Weight Study. Department of Transportation of Georgia, July 1972.
3. T.Y. Chu and R. Winfrey. Changes in Legal Vehicle Weights and Dimensions. NCHRP, Report 141, 1973.
4. E.J. Yoder and M.W. Witczak. Principles of Pavement Design, 2nd ed. Wiley, New York, 1975.
5. The Asphalt Institute. Documentation of the Asphalt Institute's Thickness Design Manual. Research Series No. 14, College Park, Md., Aug. 1964.
6. H.F. Southgate, R.C. Deen, J.H. Havens, and W.B. Drake, Jr. Kentucky Research: A Flexible Pavement Design and Management System. Proc., 4th International Conference on the Structural Design of Asphalt Pavements, Univ. of Mich., Ann Arbor, 1977.
7. J.A. Deacon. Load Equivalency in Flexible Pavements. Proc., Association of Asphalt Paving Technologists, Vol. 38, Univ. of Minn., Minneapolis, 1969.
8. J. A. Deacon. Equivalent Passages of Aircraft with Respect of Fatigue Distress of Flexible Airfield Pavements. Proc., Assn. of Asphalt Paving Technologists, Vol. 40, Univ. of Minn., Minneapolis, 1971.
9. M.W. Witczak. Full-Depth Asphalt Airfield Pavements. Research Report 72-2, The Asphalt Institute, College Park, Md., 1972.
10. R.L. Terrel and S. Rimscriting. Pavement Response and Equivalencies for Various Truck Axle--Tire Configurations. Washington Department of Highways and Federal Highway Administration, Nov. 1974.
11. R.D. Layton, R.G. Hicks, et al. The Energy, Economic and Environmental Consequences of Increased Vehicle Size and Weight. DOT-05-60142, U.S. Department of Transportation, 1977.
12. F.W. Jung and W.A. Phang. Elastic Layer Analysis Related to Performance in Flexible Pavement Design. Research Report 191, Ministry of Transportation and Communications, Ontario, Canada, Mar. 1974.
13. D.V. Ramsamooj, K. Majidzadeh, and E.M. Kauffmann. The Analysis and Design of the Flexibility of Pavement. Proc., International Conference on the Structural Design of Asphalt Pavements, Univ. of Mich., Ann Arbor, 1972, pp. 692-704.
14. F.C. Fredrickson, P.J. Diethelm, and Zwiers. Minnesota Department of Highways Flexible Pavement Design--1969. HRB, Highway Research Record 329, 1970.
15. R.I. Kingham. Development of the Asphalt Institute's Deflection Method for Designing Asphalt Concrete Overlays for Asphalt Pavements. Research Report 60-3, The Asphalt Institute, College Park, Md., June 1969.
16. R.I. Kingham. A Correlation of California and Canadian Benkelman Beam Deflection Procedures. Research Report 70-1, The Asphalt Institute, College Park, Md., Jan. 1970.
17. F.W. Jung, R.K. Kher, and W.A. Phang. Subsystem for Predicting Flexible Pavement Performance. TRB, Transportation Research Record 572, 1976.
18. W.R. Barker and N.B. William. Development of a Structural Design Procedure for Flexible Airport Pavements. Report No. FAA-RD-74-199, U.S. Army Engineer Waterways Experiment Station, Vicksburg, Miss., Sept. 1975.
19. J.B. Rauhut, J.C. O'Quinn, and W.R. Hudson. Sensitivity Analysis of FHWA Structural Model VESYS II, Vol. 1. Preparatory and Related Studies, Report FHWA-RD-76-23, Austin Research Engineers Inc., Mar. 1976.
20. A.S. Vesic and S.K. Saxena. Analysis of Structural Behavior of Road Test Rigid Pavements. NCHRP, Report 97, 1970.
21. Thickness Design for Concrete Pavements. Portland Cement Association, 1966.
22. H.J. Treybig, B.F. McCullough, P. Smith, and H. Von Quintus. Overlay Design and Reflection Cracking Analysis for Rigid Pavements, Vol. 1, Development of New Design Criteria. Final Report FHWA-RD-77-66, Jan. 1978.
23. D.J. Van Buren. The ESWL Concept and its Application to Abnormally Heavy Vehicles on Roads. Reprint from Civil Engineer in South Africa, Vol. 11, No. 8, Aug. 1969, pp. 191-203.

24. J.A. Deacon. Load Equivalency in Flexible Pavements. Proc., Assn. of Asphalt Paving Technologists, Vol. 38, Univ. of Minn., Minneapolis, 1969.
25. J.T. Christison, K.O. Anderson, and B.P. Shields. In Situ Measurements of Strains and Deflections in a Full-Depth Asphaltic Concrete Pavement. Proc., Assn. of Asphalt Paving Technologists, Vol. 47, Univ. of Minn., Minneapolis, Feb. 1978.
26. The AASHO Road Test: Report 5--Pavement Research. HRB, Special Report 61E, 1962.
27. R.F. Carmichael III., F.L. Roberts, P.R. Jordahl, H.J. Treybig, and F.N. Finn. Effect of Changes in Legal Load Limits on Pavement Costs. Report FHWA-RD-79-73, Austin Research Engineers Inc., July 1978.
28. A.P. Whittmore, J.R. Wiley, P.C. Schultz, and D. Pollock. Dynamic Pavement Loads of Heavy Highway Vehicles. NCHRP, Report 105, 1970.
29. H. Warren and W.L. Eieckmann. Numerical Computations of Stresses and Strains in a Multiple-Layer Asphalt Pavement System. Unpublished Internal Report, Chevron Research Corporation, Richmond, Calif., Sept. 1963.
30. W.R. Hudson and H. Matlock. Discontinuous Orthotropic Plates and Pavement Slabs. Research Report 56-6, Center for Highway Research, Univ. of Texas at Austin, May 1966.
31. AASHTO Interim Guide for Design of Pavement Structures. American Assn. of State Highway and Transportation Officials, 1972.
32. C.L. Monismith and Y.M. Salam. Distress Characteristics of Asphalt Concrete Mixes. Proc., Assn. of Asphalt Paving Technologists, Vol. 42, Univ. of Minn., Minneapolis, 1973, pp. 320-350.
33. F.N. Finn, W.J. Kenis, and H.A. Smith. Mechanistic Structural Subsystems for Asphalt Concrete Pavement Design and Management. TRB, Transportation Research Record 602, 1976, pp. 17-23.
34. H.J. Treybig et al. Asphalt Concrete Overlays of Flexible Pavements, Vol. 1, Development of New Design Criteria. Report FHWA-RD-75-76, Austin Research Engineers, Inc., June 1975.
35. A.I.M. Claessen, J.M. Edwards, P. Sommer, and P. Ug'e. Asphalt Pavement Design--The Shell Method. Proc., 4th International Conference on Structural Design of Asphalt Pavements, Vol. 1, Univ. of Mich., Ann Arbor, Aug. 1977.
36. C.E. Santucci. Thickness Design Procedure for Asphalt and Emulsified Asphalt Mixes. Proc., 4th International Conference on Structural Design of Asphalt Pavements, Univ. of Mich., Ann Arbor, Aug. 1977.

Mathematical Model for Predicting Pavement Performance

P. ULLIDTZ AND B.K. LARSEN

A computer program is developed for predicting the performance of a road as a function of loads, climate, and structural design. The fundamental principle is to divide the road into 0.3-meter lengthwise subsections. Parameter values are assigned to the subsections through a second order autoregressive process. For each subsection the dynamic load and the resulting fatigue and permanent deformations are calculated week by week over the desired period of time. The output as well as the input to the program is stochastic. This means that the deterioration as a function of time will be different for subsequent simulations of nominally identical pavements. The program computes the slope variance, the rut depth, and the amount of cracking, which is summarized into the Present Serviceability Index (PSI). The submodels are based on theoretical considerations and to some degree on adaptation of laboratory tests and field observations. To test the computer program, 180 sections of the AASHO Road Test were selected for simulation. The results of these simulations were encouraging. In addition to structural design of flexible pavements the program may be used to determine the most economical maintenance strategy, to study the effect of changes in legal axle loads, and to evaluate new pavement materials, such as waste materials. The program may also be used to transfer experience from the industrialized countries to the developing countries. Finally the program may, with some changes, be used for design of, and maintenance planning for, airfield pavements.

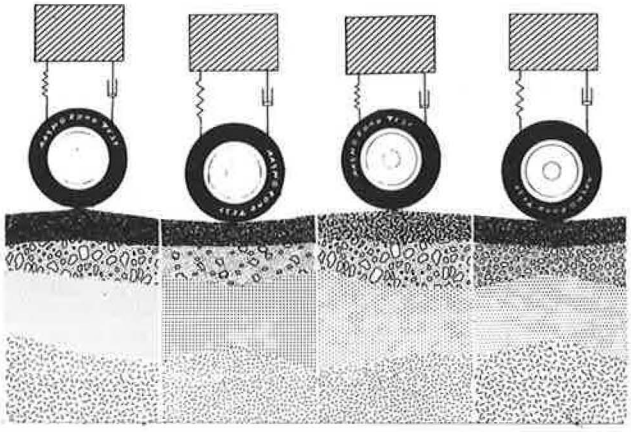

Figure 1. Illustration of the program.

In 1978 a computer program was developed for predicting flexible pavement performance (1). The program was developed on a microcomputer and is capable of predicting longitudinal roughness, rutting, and cracking of three-layer pavements, consisting of asphalt, gravel base, and subgrade. The program was presented at the annual meeting of the Association of Asphalt Paving Technologists in 1979 (2).

In 1980 a committee was formed by the National Road Directorate in Denmark to work out new design models for pavement structures. These new models were to be used to work out improved methods for pavement design. The committee therefore decided to select models that were as complete as possible. For flexible pavements the predictive design model mentioned above was selected. The computer program was rewritten for the National Road Directorate's Burroughs computer and has since undergone extensive testing and modification. The modified model is described in this paper.

OUTLINE OF THE MODEL

The structure of the model is the same as in the original version of the model and is illustrated in Figure 1. The main principle is to consider the road as consisting of a number of short sections, which again are divided into subsections 0.3 m long. Each section is considered separately, and the structural and functional condition are calculated week by week for the desired period of time. Variation of the permanent deformations of the subsections will result in longitudinal roughness, which is combined with the mean level of permanent deformation (rut depth) and structural deterioration (percentage of cracked subsections) into a Present Serviceability Index (PSI) value. Variations in permanent deformations and crack propagation for each subsection are caused by variations in materials parameters and in thicknesses of the layers as well as variations in the resulting dynamic force from subsection to subsection.

First the materials parameters are determined from the climatic conditions of the week considered (for example, temperature of asphalt and effects on unbound materials of frost melting). The loads are then applied through a system consisting of two sets of mass, spring and shock absorber (a quarter car model), simulating a heavy vehicle load. The resulting dynamic force is calculated at points spaced 0.3 m apart (one subsection apart). The force at each point will depend on the shape of the surface (the longitudinal roughness) and on the velocity of the vehicle. For each subsection the effects of the loading are calculated in terms of permanent deformation of each material and reduction of the remaining life of the asphalt layer caused by fatigue. The new PSI value is then calculated and the procedure is repeated for the following week, under a new climatic condition and with a different shape of the surface.

The program may also be used in connection with stage construction, where an overlay is applied either at a given point in time or when the pavement has reached a certain condition. In this version the program may also be used for maintenance purposes. First the previous performance of the pavement is simulated; and when this agrees with the known performance, the model may be used with some confidence for extrapolation to study the effect of applying overlays of different thicknesses. The model could also be modified for use with flexible airfield pavements, where the effects of pavement irregularities on pilot, passengers, and aircraft could be determined directly.

GENERATING PARAMETERS

The input to the program (and the output from it) is stochastic, i.e., parameters such as surface elevation, elevation of interfaces, bitumen content, and so forth, vary from point to point. To obtain a pattern of variation similar to the variations in real pavement structures, a second order autoregressive process is used to generate the parameters (3).

In a second order autoregressive process the value for X_t is determined from

$$X_t = \Phi_1 \cdot X_{t-1} + \Phi_2 \cdot X_{t-2} + a_t \quad (1)$$

where Φ_1 and Φ_2 are constants, and a_t is an independent random variable with mean value = 0 and a constant variance of ($E|a_t| = 0$, $\text{var}|a_t| = \sigma_a^2$).

The constants Φ_1 and Φ_2 are determined from

$$\Phi_1 = \left\{ [\rho_1(1-\rho_2)]/(1-\rho_1^2) \right\} \text{and } \Phi_2 = [(\rho_2-\rho_1^2)/(1-\rho_1^2)] \quad (2)$$

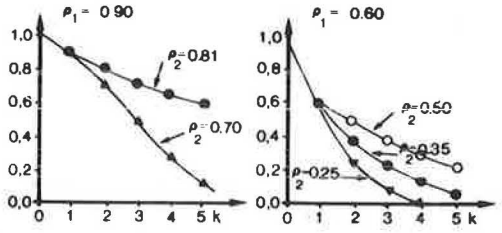

Figure 2. Autocorrelation coefficients.

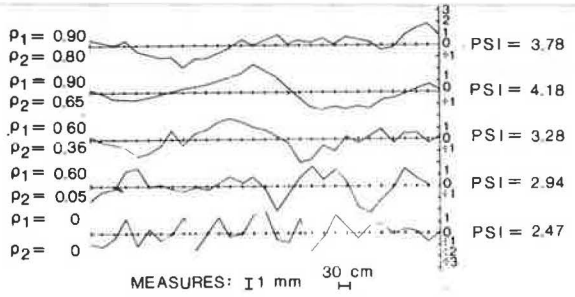

Figure 3. Road profiles as a function of ρ_1 and ρ_2.

where ρ_1 is the autoregression coefficient for a distance = Z (here Z = 0.3 m), and ρ_2 is the autoregression coefficient for a distance = 2 • Z (ρ_k is the autoregression coefficient for a distance = k • Z). The variance of a, σ_a^2, is calculated from

$$\sigma_a^2 = \sigma_x^2 \cdot (1 - \rho_1\Phi_1 - \rho_2\Phi_2) \quad (3)$$

where σ_x^2 is the variance of X.

By selecting different values of ρ_1 and ρ_2 it is possible to obtain different autocorrelation functions, and thus to approximate the actual autocorrelation function of the parameter considered. This is illustrated in Figure 2. The effect of selecting different values of ρ_1 and ρ_2 is also illustrated in Figure 3. In this figure the surface elevation is shown as a function of distance at points 0.3 m apart. Figure 3 shows the elevations for five different combinations of ρ_1 and ρ_2, but all with a standard deviation, σ_x, of 1 mm. The PSI values are calculated from the longitudinal profiles. Variations from 2.5 to 4.2 are possible. As the standard deviation is kept constant, the variation in PSI is solely due to the variations in ρ_1 and ρ_2.

In the program the distribution of X may be either normal or log normal. The input consists of the mean value, the standard deviation, ρ_1, ρ_2, and the type of distribution. The program then generates values at each point of the pavement, using a random number generator. Little information is available for evaluating ρ_1 and ρ_2. For the surface level the information is easily obtainable, however, and analysis of longitudinal profiles from a test pavement showed that $\rho_1 = 0.92$ and $\rho_2 = 0.75$ were reasonable values. For other parameters, values of 0.9 and 0.7 for ρ_1 and ρ_2, respectively, have been used when a large degree of autocorrelation was assumed. For low degrees of autocorrelation values of $\rho_1 = 0.6$ and $\rho_2 = 0.3$ were used.

ELASTIC PARAMETERS

The term elastic has been used to denote all recoverable (or resilient) deformations whether they are truly elastic (linear or nonlinear) or viscoelastic. Likewise E-value or E-modulus is used for the ratio between the dynamic stress and the elastic part of the strain (the secant modulus). Poisson's ratio is kept constant, and the same value (0.35) is used for all layers.

Asphalt

The E-modulus (or stiffness) of the asphalt may be calculated by two different methods; however the method to be used must be specified. One possibility is to use the method developed by Shell:

1. The volume concentration of aggregate, C_v, is calculated from

$$C_v = VA/(VA + VB) \quad (4)$$

where VA is the percentage volume of aggregate, and VB is the percentage volume of bitumen. The volume concentration is then corrected to allow for void contents larger than 3 percent (4).

$$C_v' = C_v / \left\{ (0.97 + 0.01) \cdot [100 - (VA + VB)] \right\} \quad (5)$$

If the void content is less than 3 percent this last step should be deleted.

2. Within certain limits the following relationship, which is derived from Van der Poel's nomograph (5), may be used for calculating the stiffness of the bitumen.

$$S_b = 1.157(10^{-7}) \cdot t_w^{-0.368} \cdot e^{-PI} \cdot (T_{RB}-T)^5 \quad (6)$$

where

S_b = bitumen stiffness in MPa,
t_w = loading time in seconds,
PI = penetration index (e is the base of the natural logarithm),
T_R = softening point ring and ball in degrees Celsius (or the temperature corresponding to a penetration of 800), and
T = temperature of the bitumen in degrees Celsius.

The relationship will give an approximate value of the bitumen stiffness within the following limits:

$0.01 \text{ sec} < t_w < 0.1 \text{ sec}$
$-1 < PI < +1$
$10°C < T_{RB}-T < 70°C$

Bitumen stiffnesses calculated from Equation 6 have been compared to values found from the PONOS computer program developed by Ullidtz and Peattie for Shell (6). The comparisons cover bitumens having initial penetrations ranging from 30 to 200 at temperatures from 0°C to 30°C and times of loading between 0.1 and 0.01 sec. The comparisons are shown in Figure 4.

3. The stiffness of the mix (E_1 MPa) is then calculated from (7).

$$E_1 = S_b \cdot \left\{ 1 + (2.5/n) \cdot [C_v'/(1-C_v)] \right\}^n \quad (7)$$

where

$$n = 0.83 \cdot \log_{10}[(4 \cdot 10^4)/S_b] \quad (8)$$

Moduli determined from this method are usually in good agreement with moduli found from bending tests. At high temperatures, however, bending tests tend to give moduli that are too low. When the temperature increases the modulus of an asphalt layer in a pavement will approach the modulus of the ag-

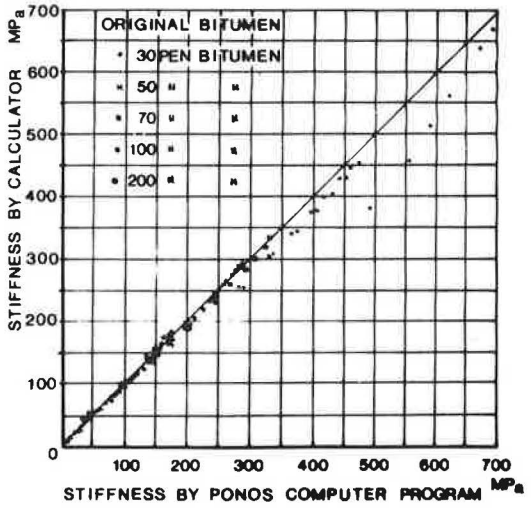

Figure 4. Comparison of bitumen stiffnesses obtained by Equation 6 and the PONOS computer program.

gregate, whereas the modulus of a beam used in a bending test will approach zero.

From the AASHO Road Test (8) a modulus-temperature relationship was found from back analysis of deflection data. Deflections corresponding to a vehicle velocity of 55 km/h at temperatures ranging from 0°C to 40°C were used. The following relationship was found.

$$E_1(t) = 15000 - 7900 \cdot \lg_{10} t°C, t > 1°C \quad (9)$$

where $E_1(t)$ is the asphalt modulus in MPa at t°C.

In Figure 5 this relationship is compared to moduli calculated from data on the asphalt mix using Shell's method. The difference at low temperatures could result from the strains in bending tests being lower than the in situ strains. The difference at low temperatures is not very important for the simulation, whereas the difference at high temperatures

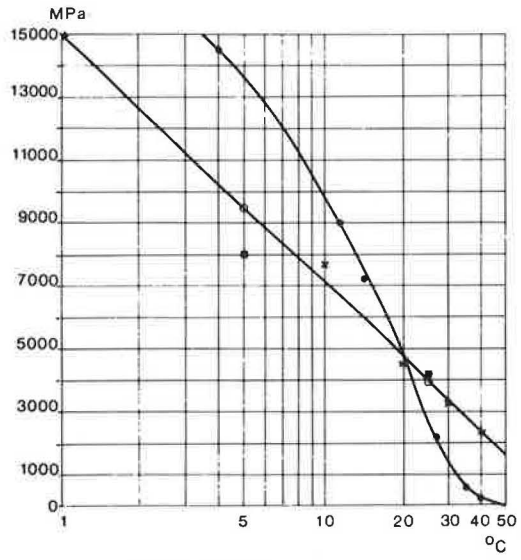

● THE SHELL METHOD
○ STRESS MEASUREMENTS FROM AARVE I (BUSCH 80)
× BACK CALCULATION OF DEFLECTION DATA
■ 16 Hz DEFLECTION MEASUREMENTS; AARVE I

Figure 5. Moduli of asphalt mix as a function of T.

is of vital importance. Using the values determined by Shell from sections of the AASHO Road Test results in severe deterioration during the summer period; such a deterioration was not observed during the tests.

For the input one may therefore choose between Shell's method and a relationship similar to that given by Equation 9. In the latter the two constants in the relationships should be input. No matter which method is selected for calculating the asphalt modulus, a lower limiting value that corresponds to the modulus of the aggregate should be used.

Unbound Materials

For the unbound materials it is also possible to use two different inputs for the elastic parameters. One method is to input the E-value for layer No. 2 (base course) and No. 4 (subgrade) and the ratio between the moduli of layers No. 3 and No. 4 (E_3/E_4). In this method the plastic parameters discussed in the following section will have to be input for each material.

The other method is a standard input developed in connection with the simulation of the AASHO Road Test. In this method the input consists of the CBR value of each of the unbound materials. The modulus of the subgrade E_4 is then calculated from

$$E_4 = 10 \cdot CBR \text{ MPa} \quad (10)$$

The accuracy of this equation, related to deformation and strength parameters, is disputed. Experiments carried out by the National Danish Road Laboratory (9) indicate that a better agreement is obtained with the relationship

$$E_4 = 10 \cdot CBR^{0.73} \text{ MPa} \quad (11)$$

Because Equation 10 is the most widely accepted relationship it is retained here.

The modulus of the subbase, E_3, is found from a relationship developed by Dorman and Metcalf (10)

$$E_3 = 0.2 \cdot h_3^{0.45} \cdot E_4 \quad (12)$$

where h_3 is the thickness of layer No. 3 in mm. This relationship was developed from deflection measurements and, therefore, corresponds to the horizontal direction. A factor 3 has been introduced to account for the anisotropy often found in granular materials. From analysis of stresses measured by Veverka (11), van Cauwelaert (12) found that the ratio between vertical and horizontal modulus, n, was 3 for a gravel and 5 for a sand. Theoretical considerations on compaction of granular materials leads to a minimum value of n = 2.25 for a material with an angle of internal friction θ = 30 degrees. Misra (13) suggests a value for shear sensitivity of 6, which leads to n = 3.8 (14). Gerard and Wardle (15) use n = 3. For stresses, strains, and deflections measured in the Danish Road Testing Machine (16), Ullidtz (14) has shown that an excellent agree- ment with calculated values is obtained when n = 3 is used.

Ideally the pavement response should be calculated using a theory incorporating anisotropy of the granular materials. In this instance, however, a modified version of the method of equivalent thicknesses is used. This method has been found to agree well with anisotropic theory as represented by the computer program CIRCLY (17,18). Finally the modulus of the base course, E_2, is calculated using the equation

$$E_2 = 0.2 \cdot h_2^{0.45} \cdot E_3 \quad (13)$$

where h_2 is the thickness of layer No. 2 (base course) in mm.

PLASTIC PARAMETERS

Plastic deformations include all nonrecoverable (irreversible or permanent) deformations and viscous deformation. An index p, is used to distinguish plastic from elastic parameters, e.g., E_p denotes the ratio of the dynamic stress to the plastic strain and is called the plastic modulus.

Asphalt

A simple method of evaluating the permanent deformations in the asphalt layer has been developed by Hill, Brian, and van de Loo for Shell (19), and a slightly modified version of this method has been used in the simulation program. In this approach the plastic strain in the asphalt is assumed to be purely viscous; i.e., the strain depends on the accumulated loading time only and is independent of the number of load applications.

To use this method a correlation between the plastic modulus of the mixture, $E_{1,p}$, and the plastic or viscous part of the bitumen stiffness, $S_{bit,p}$, must be established. This is most easily done by creep tests. In the vicinity of the total accumulated loading time the relationship may be expressed as

$$E_{1,p} = A_1 \cdot S_{bit,p}^{B1} \tag{14}$$

where A_1 and B_1 are constants. For most of the tests reported by Shell, A_1 was in the region of 70 to 90 and B_1 from 0.3 to 0.5 with moduli in MPa. Because of a certain nonlinearity of some bituminous mixtures (20), the relationship should preferably be determined at a realistic stress level. Tests carried out by Celard (21) and Francken (22) show that the strain is not purely viscous but depends on the number of load applications in addition to the accumulated loading time. It might, therefore, be more correct to use the same kind of relationship given in the section on unbound materials.

The viscous part of the bitumen stiffness may be calculated from

$$S_{bit,p} = 3\eta/t_a \tag{15}$$

where η is the viscosity of the bitumen, and t_a is the accumulated loading time, equal to the number of load repetitions, N, multiplied by the loading time, t_w, of each wheel passage. In the program an approximate value of η is found from

$$\eta = 1.3 \cdot 10^{[3+(T_{RB}-T/10)]} \text{Nsec/m}^2 \tag{16}$$

Unbound Materials

For unbound materials the stress level and the time of loading (or number of load applications) seem to be the most important factors. For constant volume unconfined compression tests Goldstein (23) found that the strain-time relationship could be described by the following general equation:

$$\dot{\epsilon} = K \cdot \sigma^n \cdot t^{-\alpha} \tag{17}$$

$\dot{\epsilon}$ being the axial strain velocity, σ the axial stress, t the time of loading and K, n, and α soil parameters (24). Assuming that the loading time of each wheel passage is constant and $\alpha = 1$ this relationship may be written as

$$\epsilon_p = A \cdot N^B \cdot (\sigma_1/\sigma')^C \tag{18}$$

where

N = number of load applications,
σ' = reference stress equal to 0.1 MPa, and
A,B,C = constants;

or as

$$E_p = 1/A \cdot N^{-B} \cdot (\sigma_1/\sigma')^{1-C} \cdot \sigma' \tag{19}$$

for combinations of N and σ_1 that do not approach failure.

Triaxial tests on granular materials reported by Barksdale (25) indicate that the constant C ranges from 1 to 2 (average 1.67), i.e., from a plastic modulus which is independent of the stress level to a modulus inversely proportional to the major principal stress. One of the tests shows a value of 0.13 for the constant B. Similar tests on cohesive soils (including the AASHO Road Test subgrade) carried out by Poulsen (26) give the same range for C (average 1.66) and a range of 0.07 to 0.15 for B (average 0.11). When the constants B and C are known, they may be input to the program; if they are not known, a standard input of B = 0.1 and C = 1.6 is recommended.

For stress levels approaching the short term strength or for large numbers of stress repetitions Equation 18 is no longer satisfactory. If a road structure is designed such that the limit of Equation 18 is never reached, then the rate of permanent deformations in the structure will be decreasing with the number of loadings as it did in the VESYS II M program (27). The permanent deformations developing shortly after opening of the road may, of course, be large, depending on the stress-plastic strain relationship; but after the first resurfacing or leveling of the roughness or rutting, only small plastic deformations will develop. To predict road failures due to progressive plastic deformations, a more adequate model capable of describing the material behavior at higher stress levels is needed.

According to Vyalow and Maksimyak (28) the deformation of a clay material as a function of time may be divided into three phases: phase 1, decreasing strain rate (corresponding to the above relationship); phase 2, constant strain rate; and phase 3, accelerated strain rate eventually leading to failure, see Figure 6. In the simulation program passing from phase 1 to phase 2 has been assumed to take place when the plastic strain has reached a critical level. The equations for the plastic strain thus become

$$\epsilon_p = A \cdot N^B \cdot (\sigma_1/\sigma')^C \quad \text{for } \epsilon_p < \epsilon_o \tag{20}$$

continuing along the tangent to this relationship:

$$\epsilon_p = \epsilon_o + (N - N_o) \cdot A^{1/B} \cdot B \cdot \epsilon^{1-1/B} \cdot (\sigma_1/\sigma')^{C/B} \tag{21}$$

for $\epsilon_p > \epsilon_o$

$$\text{where } N_o = \epsilon_o^{1/B} \cdot A^{-1/B} \cdot (\sigma_1/\sigma')^{-C/B} \tag{22}$$

A relationship for the third phase has not been included in the program. Using this model on tests carried out by Lashine and reported by Pell and Brown (29), the points marked o or x in Figure 7 are obtained for a limiting strain of 5 percent and 4.5 percent, respectively. Although the agreement with experimental results is quite satisfactory, limited evidence exists to support this model. One reason for using the model is that it is simple enough to be used in a simulation program where a very large number of calculations have to be carried out. For cohesive soils Poulsen (26) found that the stress level at which 10^5 load repetitions would result

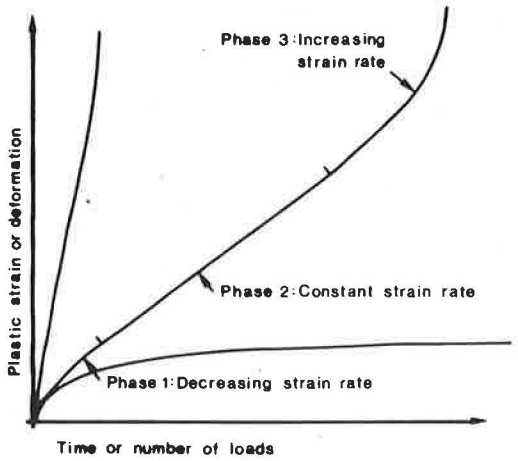

Figure 6. Three phases of deformation.

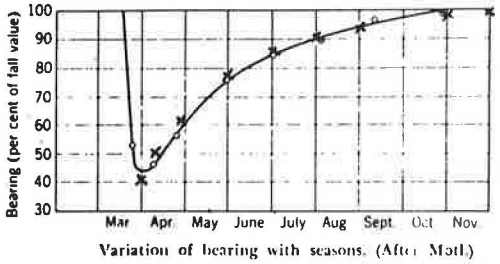

Variation of bearing with seasons. (After Motl.)

(Yoder & Witczak, 1975)

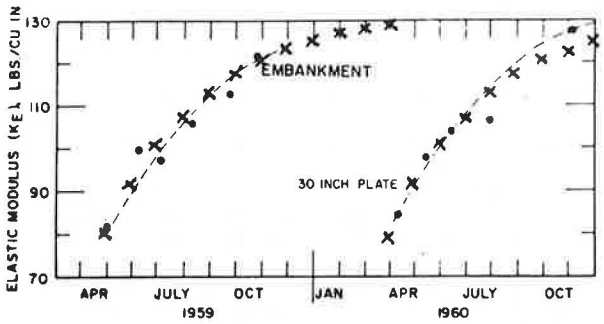

(The AASHO Road Test, 1962)

Figure 7. Measured strains compared to calculated strains.

in failure or a plastic strain of 2 percent was proportional to $(M_o/1\ MPa)^{1.16}$, where M_o is the elastic modulus at a stress level of 0.01 MPa. This relationship with the modulus agrees well with Kirk's relationship between permissible stress and modulus (30). Assuming this relationship to the elastic modulus to be correct, one obtains

$$A = \left\{ 1/[(E/E')^{1.16} \cdot C] \right\} \cdot A' \quad (23)$$

where

A,C = constants corresponding to Equation 20,
E = elastic modulus of the material, and
E' = reference modulus.

As described in the section on unbound materials two different types of input may be used for the elastic parameters. When using the first alternative, A in Equation 20 should be input for each unbound layer corresponding to the respective reference modulus (E'). With the second alternative A' is calculated from the CBR value

$$A' = 5/CBR \cdot 0.017 \quad (24)$$

The constant 0.017 was the mean A-value determined for the AASHO subgrade soil by Poulsen (26) and corresponds to a mean subgrade CBR of 5 percent.

The critical strain, ϵ_o, may be found from experiments such as those shown in Figure 7; or it may be estimated from a known relationship between number of loads and permissible stress or strain based on permanent deformations (7,26,31). The additional plastic strain caused by the loads from N_i to N_j at a constant stress level is calculated with the strain hardening procedure, see Figure 8 (32). To use the time hardening procedure would not be practical because of the excessive amount of computer storage required.

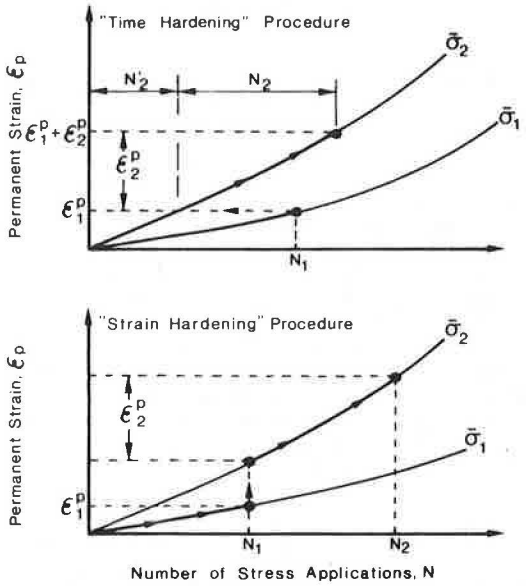

Figure 8. Procedures to predict cumulative loading from simple tests.

FATIGUE PARAMETERS

The general relationship for determining fatigue characteristics developed by Cooper and Pell (33) was used to predict the fatigue life of the asphalt layer:

$$\log \epsilon_r = [(14.39) \cdot (\log V_B + 24.2) \cdot (\log SP_i - 42.7 - \log N)] \div [(5.3) \cdot (\log V_B + 8.63) \cdot (\log SP_i - 15.8)] \quad (25)$$

where

ϵ_r = maximum allowable tensile strain, in microstrain, for N load applications,
V_B = percentage volume binder in the mix, and
SP_i = initial Ring and Ball softening point of the bitumen.

The logarithms are to base 10.

In Equation 25, N corresponds to the number of loads determined in laboratory tests. In the original equation given by Cooper and Pell the laboratory-determined fatigue life had been multiplied by a factor of 100 to allow for the influence of rest periods (factor of 5) and crack propagation (factor

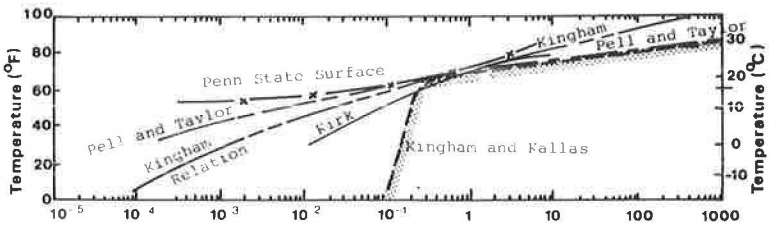

a. Plots of normalized values $K_1(T)$ versus temperature $K_1(T)/K_1(21°C)$

Figure 9. Temperature correction factor for asphalt fatigue life.

of 20). In the present version of the simulation program these two factors are input values.

In connection with the work on the simulation program there was an attempt to make a theoretical estimate of the crack propagation time in the relationship

$$CP = 10^{(N/N_o - f)} \cdot 100 \quad (26)$$

where CP is the crack propagation in percent of total thickness, and f is the factor for crack propagation.

To follow the crack propagation in the asphalt and thus make possible a gradual decrease of the modulus, the above relationship has been used in the simulation program. The crack propagation factor was found to increase with decreasing asphalt thickness. For the AASHO Road Test simulation, however, a constant factor of 2.7 has been used. A factor of 3 has been used for rest periods, giving a combined factor of only 8.1 between in situ and laboratory determined fatigue life. No factor has been included for the lateral distribution of the traffic loads. According to Verstraeten et al. (34) the fatigue life should be multiplied by a factor of 5 when the traffic is not canalized.

To allow for the influence of temperature on fatigue life, the revision suggested by Rauhut et al. (35) has been used. Of the temperature-fatigue life relationships shown in Figure 9 those resulting in the longest fatigue life have been selected and have been approximated by three straight lines, shown dotted in the figure. The correction factors are given below:

$$0.1 \cdot 10 \exp [(T+17.8)/98.7] \quad \text{for } T < 16°C \quad (27)$$

$$0.22 \cdot 10 \exp [(T-16)/7.6] \quad \text{for } 16°C < T < 21°C \quad (28)$$

$$1.0 \cdot 10 \exp [(T-21)/3] \quad \text{for } T > 21°C \quad (29)$$

CLIMATIC FACTORS

Climatic factors affect the performance of the pavement in two different ways. The frost and thaw cycles change the bearing capacity of the unbound layers and changes in temperature alter the elastic and plastic parameters of the asphalt layer.

Temperature of Asphalt Layer

As discussed in the previous chapter the temperature of the asphalt layer will influence the elastic modulus of the material, the plastic strains, and the fatigue life and is therefore important for the performance of the pavement. For known climatic conditions the temperature input could be the mean temperature of each week of the year, possibly supplemented by the standard deviations. To reduce the amount of input, however, an approximate relationship in the form of a cosine function has been chosen:

$$T = [(T_1 + T_2)/2] + [(T_1 - T_2)/2] \cdot \cos\{[(U - U_0)/26] \cdot \pi\} \quad (30)$$

where

T_1 = maximum temperature during the year, in degrees Celsius,
T_2 = minimum temperature in degrees Celsius,
U = week number (counted from New Year), and
U_0 = number of weeks from the beginning of the year to the week of maximum temperature.

The temperature found from the above relationship is the mean weekly air temperature; whereas the asphalt temperature during the daytime hours, when most of the loads are applied, is somewhat higher. According to Barker et al. (36), the asphalt temperature, T_{asp}, may be estimated from the air temperature, T_{air}, as

$$T_{asp} = 1.2 \cdot T_{air} + 3.2 \quad (31)$$

where temperatures are in degrees Celsius.

Effect of Frost Melting on Unbound Materials

If unbound materials are allowed to freeze, the pavement may be damaged by frost heave and/or by loss of bearing capacity during the frost melting period in the springtime. Of these two types of distress, the latter is usually by far the most important and is the only one accounted for in the program. This is done by multiplying the modulus of each of the unbound materials by a factor R, corresponding to the frost sensitivity of that material:

$$R = [1-(1-R_o)] \cdot [e^{A \cdot U_T}] \quad (32)$$

where

R_o = minimum factor corresponding to the week of thaw, the factor is a function of the soil type and the freezing index value;
U_T = number of weeks after the week of thaw; and
A = (negative) constant.

Variations in moduli found from Equation 32 have been compared to values reported by Yoder and Witczak (37) and to values from the AASHO Road Test (8) in Figure 10. For the subgrade the factor is applied only to the upper part of the subgrade that has been exposed to frost. The frost penetration is calculated from an approximate relationship developed from Schweizerische Normenvereinigung (38). Expressed in centimeters the frost penetration, D_f, is

$$D_f = 4.5 \cdot \sqrt{Ig} + 0.5 \cdot D_0 \quad (33)$$

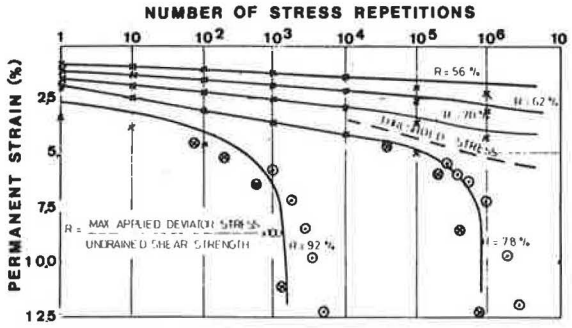

+ $\epsilon_p = 0.04125 \times N^{.0757} \times (\sigma_1/\sigma_B)^{2.8}, \epsilon_p < \epsilon_o$

⊗ Constant strain rate, $\epsilon_p > \epsilon_o$ = 4.5%

⊙ Constant strain rate, $\epsilon_p > \epsilon_o$ = 5.0%

Figure 10. Seasonal variation of subgrade modulus.

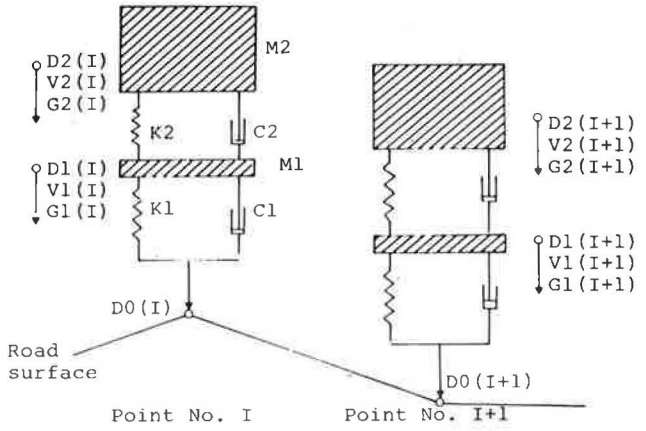

Figure 11. Mechanical analogue.

where Ig is the freezing index value (°C • days), and D_0 is the pavement thickness in centimeters. Equation 33 corresponds to silty or clay subgrades with a moisture content of 18 to 25 percent and a dry density of 1.6 t/m³. For materials that are less frost susceptible, correct determination of the frost penetration is less important.

LOADING

The performance of the pavement is affected by the number of vehicles, the size of the loads, and the speed of the vehicles. In addition to the static load, the vibrations of the vehicle will cause a dynamic load. The dynamic load will depend on the spring and shock absorber system of the vehicles as well as on the longitudinal profile of the pavement surface.

Mechanical Analogue

For loading of the structure a simple mechanical analogue consisting of two systems of mass, spring, and shock absorber as shown in Figure 11 has been chosen. The lower system (M1, K1, and C1) represents the mass of axle and wheel, the spring constant of the tire, and the tire damping; and the upper (M2, K2, and C2) the mass of vehicle body, and the load transferred to one wheel, and the spring constant of the suspension. All relationships are assumed to be linear, but it would not be complicated to introduce nonlinear relationships, e.g., as suggested by Osman (39) and used by Ullidtz (40).

To calculate the force exerted on the surface of the road, the wavelength of the vibration of the mechanical analogue at the reasonant frequencies must be long compared to the distance between two consecutive points in which the force is calculated. When this is the case the acceleration of the masses may be assumed to remain constant between two points. In the program a distance of 50 mm is used between the points. If the vehicle velocity is low, the masses small, and/or the spring constants large, the mechanical analogue may only be used if the distance between the points is decreased.

Loading Time

The influence of loading time on the performance of the asphalt layer is similar to the influence of temperature; i.e., elastic, plastic, and fatigue behavior are affected. For the unbound layers, on the other hand, the loading time has no influence according to the material models used in this program. The loading time corresponding to the middle of the asphalt layer is therefore used and is calculated on the assumption that the load at that depth ($h_1/2$, where h_1 is the thickness of the asphalt layer) is uniformly distributed over a circular area with radius a + $h_1/2$, where a is the radius of the contact area between the tire and the road surface:

$$t_w = (2a + h_1)/V \quad (34)$$

where t_w is the loading time, and V is the velocity of the vehicle. In calculating the loading time no reduction has been made for the influence of dual tires or for lateral distribution of the loads. The results, therefore, should be on the conservative side.

Summation of Loads

For the unbound materials the compaction during construction of the pavement is assumed to correspond to a certain number of wheel passes. This is an input parameter; but a value of 1,000, as used in the simulation of the AASHO Road Test, appears to give reasonable results.

For the permanent deformation of unbound materials, the summation of loads is restarted at the compaction number each time the material has been frozen, i.e., each spring. The large suction values during freezing followed by a redistribution of the moisture during melting causes a certain remolding of the unbound materials. To account for this effect it is necessary to restart the summation after each frost period. All loads are summed for the asphalt layer except loads occurring during periods when the unbound materials are frozen because the load-associated damage to frozen asphalt is negligible.

PAVEMENT PERFORMANCE

Calculating Stresses and Strains

Several programs have been developed during the last decade for calculating stresses in layered structures. Most programs are based on a generalization of Burmister's equations for a two-layered structure (41). The programs developed by Chevron and Shell are widely used and are capable of calculating the stresses, strains, and vertical deflections at an

arbitrary point of an n-layer, linear-elastic system loaded at the surface. Few road building materials, however, are linear elastic; practically all materials have nonlinear stress-strain relationships.

Finite-element methods (FE methods) can be used to handle this nonlinearity (42-45). Although the finite-element method is not exact, results close to the correct values may be obtained provided the number of elements is adequate. In addition to calculating stress and strain in nonlinear elastic structures, the finite-element methods may also be used to calculate plastic (or permanent) deformation (46).

Both exact elastic theory and finite-element methods require large digital computers. In deterministic design of road structures this is usually not a problem, because only a few structures will have to be evaluated; but a stochastic design based on a simulation with thousands of calculations would be prohibitively expensive. For the purposes considered in this study calculations must be based on simple equations, capable of providing approximately correct answers.

The elastic stresses and strains could be estimated using the methods developed by Westergaard (47) for calculating stresses in concrete pavements. This has two drawbacks: (a) the subgrade condition is unrealistic (a Winkler foundation), which is of more importance to a flexible structure than to a concrete pavement, and (b) the plastic strains cannot be computed.

Another approach--the one selected for this work--is to use a combination of Boussinesq's equations (48) and the method of equivalent thicknesses (49,50). This method may be modified to incorporate a nonlinear elastic subgrade (50) and may also be used to evaluate the plastic deformations. In the present version of the program the method of equivalent thicknesses is used to calculate the horizontal strain at the bottom of the asphalt layer and to determine the stress field in the pavement. That is, when the equivalent thicknesses are known, the stresses may be calculated at any point of the pavement. The stresses and strains are calculated as components of the loading of both wheels in a dual wheel assembly.

Calculating Permanent Deformation

To calculate the permanent deformations the separative method (51) is used. The stress field is determined by the equivalent thicknesses calculated from the elastic parameters. (The increase in permanent deformation, Δd, between the equivalent depths z_1 and z_2 and caused by the loads from N_1 to N_2 is then found by using the plastic strain-stress relationships given in Equations 20 and 21):

$$\Delta d = A \cdot (3P/2\pi\sigma')^C \cdot \left\{ [1/z_1^{(2C-1)}] - [1/z_2^{(2C-1)}] \right\} \times \{(N_2^B - N_1^B)/(2C-1)] \quad (35)$$

when z_1 is larger than that depth where the combination of stress level and number of repetitions (assuming the same stress level for all loads) would cause a permanent strain larger than the critical strain, ϵ_o. If the critical depth is larger than z_2, the increase in permanent deformation is found from:

$$\Delta d = A^{1/B} \cdot B \cdot \epsilon_o^{(1-1/B)} \cdot (3P/2\pi\sigma')^{C/B} \times \left\{ [1/z_1^{(2C/B-1)}] - [1/z_2^{(2C/B-)}] \right\} \cdot [(N_2-N_1)/(2C/B-1)] \quad (36)$$

VERIFICATION

The model has been verified by simulating the performance of the 180 four-layer flexible pavement sections in the AASHO Road Test. Details of these simulations are given by Ullidtz (52). A typical result of the simulation of one of the duplicate test sections is shown in Figure 12. The number of simulated and measured axle loads required to reduce PSI to 2.5 are compared in Figure 13. The same excellent agreement was found for all other loops and axle loads. Comparisons of predicted and actual number of loads to cause class 2 cracking are shown in Figure 14, and predicted and measured rutting are compared in Figure 15.

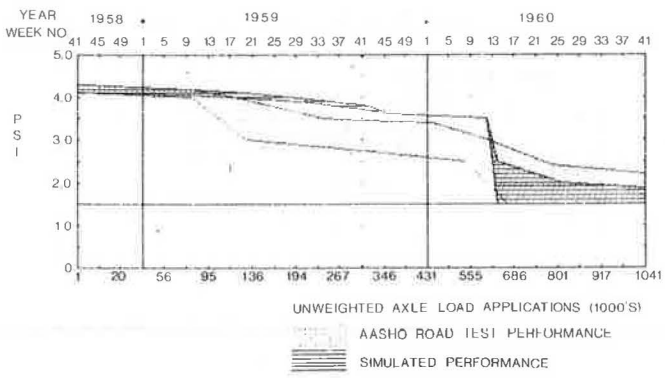

Figure 12. Loop 6, design 6-9-8, duplicated test section performance.

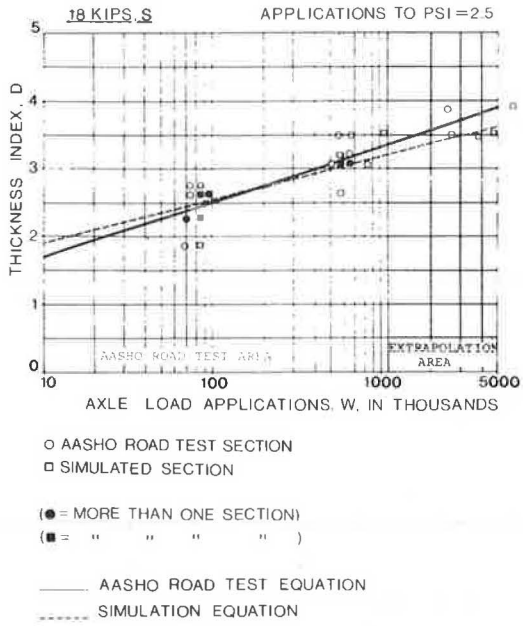

Figure 13. Relationship between design and axle application, loop 4, 18 kips, S.

The model was used to extend the traffic loading over a 20-year period, rather than the 2 years of the AASHO Road Test. The results indicate that by concentrating the traffic loading into 2 years, the AASHO Road Test overestimated the permissible number of loads by a factor of about two. (Illinois uses a regional factor of about 1.8.)

Finally the program was used to transfer the AASHO Road Test to Danish climatic conditions, where winters are somewhat milder and summers are cooler than in Illinois. This resulted in an increase in the permissible number of loads by a factor of about two.

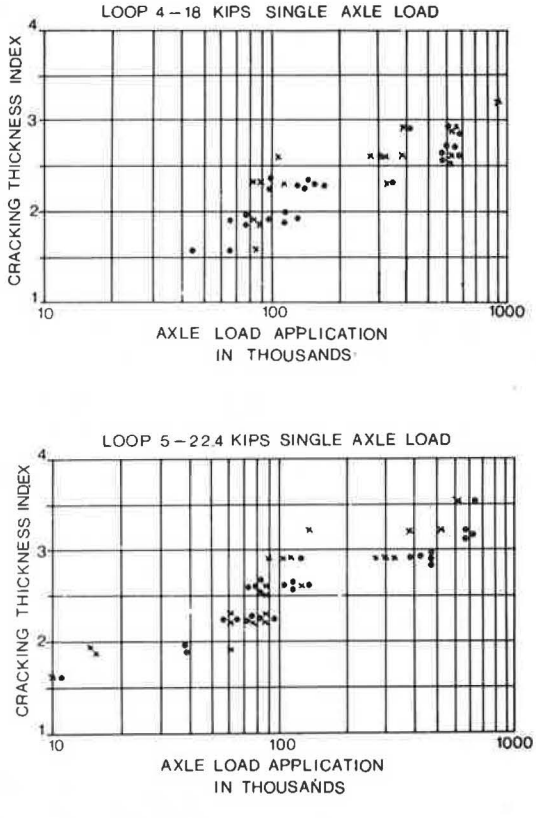

Figure 14. Axle applications to initiation of cracking.

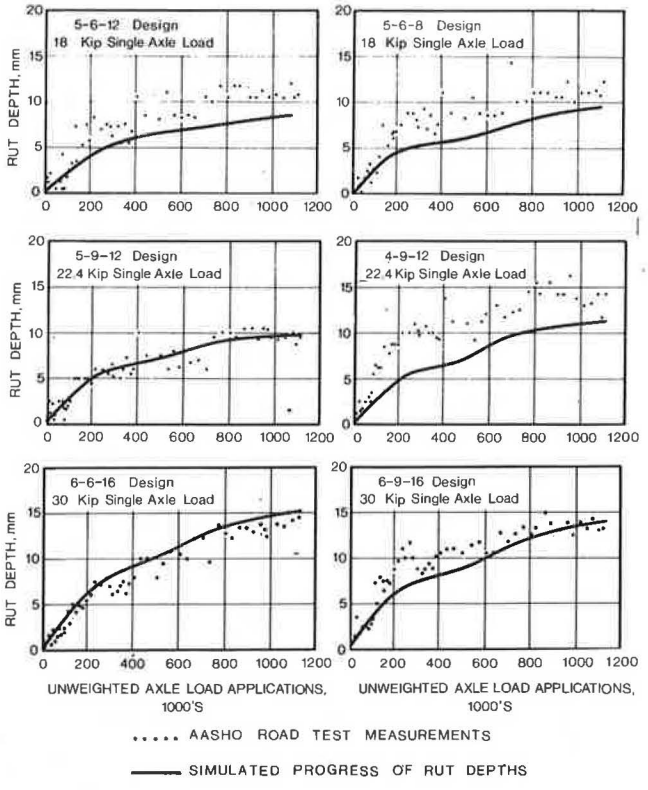

Figure 15. Measured and simulated rut depths.

CONCLUSIONS

The computer program described in this paper is capable of predicting the performance of flexible pavements, in terms of roughness, rutting, and cracking, as a function of climatic conditions and traffic loading. The input to the program consists of fundamental material parameters, which may be determined in the laboratory or through in situ testing, and the pattern of variation (autocorrelation coefficients) of the parameters along the length of the pavement. For each week of the design life of the pavement the dynamic traffic loads at points 0.3 m apart are calculated. Also the reduction of remaining life of asphalt and the permanent deformations of each layer are determined as a function of loading and of the seasonal conditions of the pavement materials.

The model has been verified by simulating the performance of the 180 four-layer flexible pavement sections in the AASHO Road Test. Situations where the model, with some modifications, may prove to be useful are

- Determining maintenance or rehabilitation requirements. Past performance of an existing pavement is simulated and the future performance, after different kinds of maintenance, is predicted. In the present program, overlays may be applied either as a function of time or as a function of pavement condition.
- Evaluating importance of supervision. The effects of variations in material parameters or layer thicknesses could be studied.
- Studying new materials. If the fundamental parameters of new materials, such as waste products, can be determined in the laboratory from dynamic triaxial testing, the model may be used to study the usefulness of these materials for pavement structures.
- Evaluating effects of different truck-wheel arrangements. Size of load, tire pressure, and suspension system may be evaluated for different pavement structures. With some modifications the effects of multiple interconnected axles may also be evaluated.
- Transferring experience. The model was used to transfer the AASHO Road Test to Danish conditions. Similarly the model may be used to transfer experience gained in the Northern hemisphere to the varied conditions of developing countries.

Finally it should be mentioned that the program could be modified to predict airfield performance and evaluate the effects of runway conditions on aircraft and passengers.

ACKNOWLEDGMENT

The Danish Road Directorate, Ministry of Transport, and The Technical University of Denmark sponsored the research which is the basis for this paper.

REFERENCES

1. P. Ullidtz. Computer Simulation of Pavement Performance. Report 18, Institute of Roads, Transport and Town Planning, The Technical University of Denmark, Copenhagen, 1978.
2. P. Ullidtz. A Fundamental Method for Prediction of Roughness. Assn. of Asphalt Paving Technologists, Univ. of Minnesota, Minneapolis, 1979.
3. G.E.P. Box and G.M. Jenkins. Time Series Analysis. Holden Day, New York, 1976.

4. W. Van Draat and P. Sommer. Ein Gerät zur Bestimmung der dynamischen Elasticitätsmoduln vor Asphalt. Strasse und Autobahn, Vol. 16, 1965.
5. C. Van der Poel. A General System Describing the Viscoelastic Properties of Bitumens and Its Relation to Routine Test Data. Journal of Applied Chemistry, Vol. 4, 1954.
6. P. Ullidtz and K.R. Peattie. Pavement Analysis by Programmable Calculators. ASCE, Transportation Engineering Journal, Sept. 1980.
7. W. Heukelom and A.J.G. Klomp. Road Design and Dynamic Loading. Proc., Assn. of Asphalt Paving Technologists, Vol. 33, Univ. of Minn., Minneapolis, 1964.
8. The AASHO Road Test. Report 5--Pavement Research. HRB, Special Report 61E, 1962.
9. A. Poulsen and R.N. Stubstad. Fastlaeggelse af E-modulen for underbundsmateriale ved målinger i marken. Interne Notater 108. The National Danish Road Laboratory, 1980.
10. E.M. Dormon and C.T. Metcalf. Design Curves for Flexible Pavements Based on Layered System Theory. HRB, Highway Research Record 71, 1965.
11. V. Veverka. Modules, Contraintes et Déformations des Massifs et Couches Granulaires. Centre de Recherches Routiéres, Bruxelles, Rapport de Recherche 162, vv, 1973.
12. F. van Cauwelaert. Contraintes et Deplacements dans un Massif Semi-infini Anisotrope a Plan Isotrope, Application au Compactage. (unpublished), 1979.
13. B. Misra. Stress Transmission in Granular Media. ASCE, Journal of the Geotechnical Engineering Division, Vol. 105, No. GT9, Sept. 1979.
14. P. Ullidtz. Prediction of Pavement Response Using Nonclassical Theories of Elasticity. Notat 81-1. Institute of Roads, Transport and Town Planning, The Technical University of Denmark, Copenhagen, 1981.
15. C.M. Gerrard and L.I. Wardle. Rational Design of Surface Pavement Layers. Australian Road Research, Vol. 10, No. 2, 1980.
16. C. Busch et al. AARVE I, sammenligning af en fulddybdeasfalt og en traditionel befaestelse, Report 29. Institute of Roads, Transport and Town Planning, The Technical University of Denmark, Copenhagen, 1980.
17. C.U. Jacobsen and C. Dahl. Vejbefaestelsers deformationer. M.Sc. thesis, Institute of Roads, Transport and Town Planning, The Technical University of Denmark, Copenhagen, 1981.
18. L.J. Wardle. Program CIRCLY--User's Manual. CSIRO, Division of Applied Geomechanics, 1977.
19. J.F. Hills, D. Brian, and P.J. van de Loo. The Correlation of Rutting and Creep Tests on Asphalt Mixes. Institute of Petroleum, Paper IP 74-001, 1974.
20. A.O. Bohn, R.N. Stubstad, A. Sørensen, and P. Simonsen. Rheological Properties of Road Materials and Their Effect on the Behavior of a Pavements Section Tested in a Climate Controlled, Linear Track Road Testing Machine. Assn. of Asphalt Paving Technologists, Univ. of Minnesota, Minneapolis, 1977.
21. B. Celard. General Problem of Rutting, Second Question--Flexible Roads. 15th World Road Congress, Mexico, 1975.
22. L. Francken. Permanent Deformation Law of Bituminous Road Mixes in Repeated Triaxial Compression. Proc., 4th International Conference on the Structural Design of Asphalt Pavements, Univ. of Michigan, Ann Arbor, 1977.
23. M. Goldstein. Proc., Brussels Conference 58 on Earth Pressure Problems, 1958.
24. L. Šuklje. Rheological Aspects of Soil Mechanics. Wiley-Interscience, New York, 1969.
25. R.D. Barksdale. Laboratory Evaluation of Rutting in Base Course Materials. Proc., 3rd International Conference on the Structural Design of Asphalt Pavements, Univ. of Michigan, Ann Arbor, 1972.
26. J. Poulsen. Laboratorieundersøgelser af underbundsmaterialer. Interne notater 61, The National Danish Road Laboratory, 1976.
27. J.M. Kenis. Predictive Design Procedures. Proc., 4th International Conference on the Structural Design of Asphalt Pavements, Univ. of Michigan, Ann Arbor, 1977.
28. S.S. Vyalov and R.V. Maksimyak. Etude du Méchanisme de Déformation et du Rupture des Sols Argileux. Bulletin de Liaison des Laboratoire des Ponts et Chausseés 86, 1976.
29. P.S. Pell and S.F. Brown. The Characteristics of Materials for the Design of Flexible Pavement Structures. Proc., 3rd International Conference on the Structural Design of Asphalt Pavements, Univ. of Michigan, Ann Arbor, 1972.
30. J.M. Kirk. Vurdering af befaestelsers baereevne. Dansk Vejtidsskrift, årg. 38, nr. 5, 1961.
31. M.W. Witczak. Design of Full-Depth Asphalt Airfield Pavements. Proc., 3rd International Conference on the Structural Design of Asphalt Pavements, Univ. of Michigan, Ann Arbor, 1972.
32. C.L. Monismith, N. Ogawa, and C.R. Freeme. Permanent Deformation Characteristics of Subgrade Soils due to Repeated Loading. TRB, Transportation Research Record 537, 1975.
33. K.E. Cooper and P.S. Pell. The Effect of Mix Variables on the Fatigue Strength of Bituminous Materials. Transport and Road Research Laboratory, Crowthorne, Berkshire, England, Report LR 663, 1974.
34. J. Verstraeten, J.E. Romain, and V. Veverka. The Belgian Road Research Centers Overall Approach to Asphalt Pavement Structural Design. Proc., 4th International Conference on the Structural Design of Asphalt Pavements, Univ. of Michigan, Ann Arbor, 1977.
35. J.B. Rauhut, W.J. Kenis, and W.R. Hudson. Improved Techniques for Prediction of Fatigue Life for Asphalt Concrete Pavements. TRB, Transportation Research Record 602, 1976.
36. W.R. Barker, W.N. Brabston, and Y.T. Chou. A General System for the Structural Design of Flexible Pavements. Proc., 4th International Conference on the Structural Design of Asphalt Pavements, Univ. of Michigan, Ann Arbor, 1977.
37. E.J. Yoder and M.W. Witczak. Principles of Pavement Design. 2nd ed., Wiley, New York, 1975.
38. Schweiserische Normenvereinigung, Frost, Frosttiefe. 1972.
39. M. Osman. Incidence sur le Comfort et la Sécurité des Petits Mouvements Verticaux du Vehicule et de l'uni de la Chausseé. Bulletin de Liaison des Laboratoire des Ponts et Chausseés 89, 1977.
40. P. Ullidtz. Effects of Surface Irregularities Simulated on a Micro Computer. 9th IRF World Meeting, Stockholm, 1981.
41. D.M. Burmister. The Theory of Stresses and Displacements in Layered Systems and Applications to the Design of Airport Runways. Proc., Highway Research Board, Vol. 23, 1943.
42. R.W. Clough and Y. Rashid. Finite Element Analysis of Axi-symmetric Solids. Journal of the Engineering Mechanics Division, Proc., ASCE, 1965.
43. A. Waterhouse. Stresses in Layered System Under Static and Dynamic Loading. Proc., 2nd International Conference on the Structural Design of Asphalt Pavements, Univ. of Michigan, Ann Arbor, 1967.

44. E.M. Duncan, C.L. Monismith, and E.L. Wilson. Finite Element Analysis of Pavements. HRB, Highway Research Record 228, 1968.
45. K.L. Taylor. Finite Element Analysis of Layered Road Pavements. Univ. of Nottingham, U.K., 1971.
46. R.W. Kirwan, M.S. Snaith, and T.E. Glynn. A Computer Based Subsystem for the Prediction of Pavement Deformation. Proc., 4th International Conference on the Structural Design of Asphalt Pavements, Univ. of Michigan, Ann Arbor, 1977.
47. H.M.S. Westergaard. Stresses in Concrete Pavements Computed by Theoretical Analysis. Proc., Highway Research Board, Vol. 5, Part 1, 1925.
48. I. Boussinesq. Application des Potentiels á l'étude de l'équilibre et du Mouvement des Solides Elastique, 1885.
49. N. Odemark. Undersökning av elasticitetsegenskaperna hos olika jordarter samt teori för beräkning av belägningar enligt elasticitetsteorin. Statens Vğinstitut, Meddelande 77, 1949.
50. P. Ullidtz. Overlay and Stage by Stage Design. Proc., 4th International Conference on the Structural Design of Asphalt Pavements, Univ., of Michigan, Ann Arbor, 1977.
51. E.N. Thrower. Methods of Predicting Deformation in Road Pavements. Proc., 4th International Conference on the Structural Design of Asphalt Pavements, Univ. of Michigan, Ann Arbor, 1977.
52. P. Ullidtz and B. Larsen. Predictive Design of Flexible Pavements--Verified Through Computer Simulation of the AASHO Road Test. Report 35, Institute of Roads, Transport and Town Planning, The Technical University of Denmark, Copenhagen, 1982.

Geogrid Reinforcement of Asphalt Pavements and Verification of Elastic Theory

A.O. ABDEL HALIM, RALPH HAAS, AND WILLIAM A. PHANG

The idea of reinforcing flexible pavements has existed for some years, and a few attempts have been made to use metallic and other materials. These have not been effective. Recently, however, a new, high-strength plastic geogrid material known as Tensar has become available; and pavement reinforcement has been suggested as one of its possible civil engineering applications. Consequently, the first phase of a research program initiated in early 1981 examined the potential of a variety of materials for pavement reinforcement, including geogrids. The conclusion was that these materials did indeed offer potential and should be further evaluated. A comprehensive experimental program of tests of reinforced and unreinforced pavements was carried out in the latter half of 1981 and early 1982. Descriptions are presented of the experimental and analytical program and the comparative results. The results of the unreinforced test sections were used to verify the basic elastic layer theory. The analysis shows that the theory provides a reliable tool to predict flexible pavement responses under the design load. A calibration factor that includes the effect of the dependence of elastic moduli on stress level was suggested; the result is a better agreement between predicted and measured values. The results show that the plastic geogrid used was effective as a reinforcement, in terms of carrying double the number of load repetitions or implying a substantial saving in asphalt thickness and minimizing fatigue cracking.

Many existing roads are becoming inadequate because of rapid growth in traffic volume and axle loading. The escalating cost of materials and energy and a lack of resources provide an incentive for exploring alternatives in building new roads and rehabilitating existing ones. Flexible pavement reinforcement is one such alternative. If it could reduce the thickness of paving materials or extend pavement life and be both cost and performance effective, it would be a viable alternative.

Nonmetallic materials, such as fabrics, have been used to a significant degree in some areas of North America and claims have been made that these materials have reinforcement properties. The low strength, high extensibility, and low modulus of these materials make this doubtful. Moreover, there is little if any documented evidence to demonstrate that any fabric reinforces a pavement or extends its life except in warmer climates, where some fabrics may be effective in crack reflection and waterproofing. In view of new technological developments in nonmetallic reinforcing materials, however, reinforcing flexible asphalt pavements may now be worthwhile. The reinforced flexible pavement concept described in this paper includes the initial design analysis, the experimental program carried out to verify the concept, and the analysis and verification of the elastic layer theory.

REINFORCED PAVEMENT CONCEPT

Feasibility Study

In late 1980 a comprehensive research program was initiated to evaluate existing metallic and nonmetallic reinforcing materials, including geotextiles (1). It included the design and implementation of an experimental program as a cooperative effort between Royal Military College (RMC) at Kingston, the Ontario Ministry of Transportation and Communications, Gulf Canada Ltd., and the University of Waterloo.

The primary candidate arising from the evaluation was a new high-strength, plastic mesh or geogrid material known as Tensar. This material is made from polypropylene and is biaxially oriented to give strengths on the order of mild steel in both directions.

Program Objectives

The experimental program was carried out at RMC in Kingston. The design involved varying thicknesses of reinforced and unreinforced full-depth asphalt

with varying strengths of subgrade in a 2.4 m x 4 m test pit. For each test series, half the pavement was reinforced with the plastic mesh; and the other half was not. The main goal of the experimental program was to thoroughly investigate, under a variety of controlled conditions, the mechanical behavior and load-carrying capabilities of flexible pavements that had been reinforced with the plastic mesh. When compared with unreinforced (control) sections, the structural benefits of the reinforcement could be evaluated. Also, the results of the program were to be used to verify or modify the basic elastic layer theory and develop initial design procedures for reinforced asphalt pavements.

Review of Reinforced Pavement

Many construction techniques use reinforcement elements strong in tension or bending to enhance the strength and stability of other materials; for example, steel bars are used to reinforce concrete when it is to be subjected to high tensile stresses or strains. Pavement reinforcement has usually been associated with portland cement concrete (PCC) pavements. Here steel reinforcement holds cracks together thereby reducing maintenance and extending life. Also, reinforcement elements have been used in concrete overlays to prevent reflection cracking (2-5).

There has been limited use of reinforcement elements to provide an adequate tensile strength to the asphalt layer (6-8). In most of these investigations analysts constructed models and conducted field trials to assess the effect of using steel or fabric materials to improve the tensile properties of the asphalt layer (9,10). A better approach would be to assess and analyze the behavior of a reinforced pavement and use the results as a basis for design. The types of results expected from these experiments would be

1. Properties of the reinforcement,
2. Mechanical behavior of the pavement under various conditions of traffic and environmental stresses, and
3. An understanding of the basic mechanisms that operate when reinforcement is incorporated in the pavement.

Basis for the Experimental Program

One of the first steps in this investigation was to study the effect of the major variables (1). This analytical phase involved the following steps: (a) evaluate available structural theories, select the most appropriate one, and modify if necessary; (b) apply the selected theory to a range of possible design situations for reinforced pavement structures; (c) identify critical stresses and strains and best location(s) for the reinforcement; and (d) assess the compatibility of the reinforcement material with asphalt concrete.

The results were used to plan an experimental program. This program was intended to verify the basic hypothesis (i.e., that flexible pavements could be reinforced effectively), to provide feedback for updating or modifying the analysis, and to provide a basis for planning and carrying out full-scale field trials. The following sections present details of the experimental part of the investigation.

EXPERIMENTAL INVESTIGATION

Test Facility

Experimental pavement sections were constructed in a test pit at the Royal Military College (RMC) in Kingston. A brief description of the facility follows.

Test Pit

Asphalt pavement sections, reinforced and unreinforced (control), were constructed within a 4 m by 2.4 m by 2 m deep concrete pit. The test pit includes a sump and water distribution system at the bottom that allowed the pit to be flooded to any desired depth.

MTS Loading System

The loading system at the RMC Structural Engineering Laboratory includes three independent closed-loop electrohydraulic actuators and ancillary equipment designed and packaged by Material Testing Systems, Co. Ltd. (MTS). For this investigation a hydraulic actuator rated at 50 kN (11.25 kips) was used.

Controlled Variables

Test Loops

The experimental program was divided into five series of tests, called loops. The test pit was set up for each series (or loop); half of the pit was reinforced and the other half was left as a control section. For each loop the asphalt thickness and the subgrade condition (either dry or saturated) were the controlled variables. Between four and nine tests were performed for each loop, and each test was performed on a different section of the test pit. The five loops are described in Table 1.

Table 1. Test loops and controlled variables.

Loop No.	Test No.	Asphalt Thickness (mm)	Subgrade Condition	Description
1	1	150	Dry	Control
	2	150	Dry	Reinforced
	3	150	Saturated	Reinforced
	4	150	Saturated	Control
2	1	165	Dry	Control
	2	165	Dry	Reinforced
	3	165	Dry	Reinforced
	4	165	Dry	Control
3	1	250	Saturated	Control
	2	150	Saturated	Reinforced
	3	150	Saturated	Reinforced
	4	200	Saturated	Control
	5	250	Saturated	Control
	6	150	Saturated	Reinforced
4	1	200	Dry	Reinforced
	2	200	Dry	Reinforced
	3	250	Dry	Control
	4	250	Dry	Control
	5	250	Saturated	Control
	6	250	Saturated	Control
	7	200	Saturated	Reinforced
	8	200	Saturated	Reinforced
	9	200	Saturated	Reinforced
5	1	115	Dry	Control
	2	115	Dry	Control
	3	115	Dry	Reinforced
	4	115	Dry	Reinforced

Objectives of Test Loops and Testing Sequence

The main objective of the experimental program was to determine and compare the reinforcing effects of the geogrid in the asphalt pavement. The design of these test loops was conducted in a logical manner to assess predetermined parameters related to reinforcement evaluation. For example, the first loop was designed to compare the behavior and performance of the reinforced section with an unreinforced section of the same thickness (150 mm) on a weak subgrade. Permanent deformation and vertical deflections were monitored throughout the test until complete failure occurred on the unreinforced section.

In loop 2, strain carriers were installed at the bottom of the asphalt layer to compare tensile strain in the critical zone between reinforced and unreinforced sections of the same thickness (165 mm) on a stronger subgrade. Results of these two loops were of major importance because they compare the reinforced sections with unreinforced sections under identical geometric, loading, and environmental conditions.

When the first objective was achieved (basic comparisons between reinforced and unreinforced), the second objective was to find the equivalent thickness of the reinforced layer. Loops 3 and 4 were designed to establish a relationship between the thicknesses of the reinforced and unreinforced sections. In loop 3 two unreinforced sections (200 mm and 250 mm) were tested against a thinner reinforced section of 150 mm on weak subgrade. The results of this loop showed that a value of (50 to 100 mm) equivalent thickness might represent the reinforcement effect.

Based on this finding loop 4 tests were performed with an unreinforced section of 250 mm and a reinforced section of 200 mm to confirm the minimum saving value (50 mm). Loop 5 was designed to compare the vertical stresses on the subgrade (strong subgrade) for reinforced and unreinforced asphalt sections of the same thickness (115 mm). Results of the five loops are presented later in the discussion.

Dynamic and Static Loading Patterns

Reinforced and unreinforced pavement sections were loaded through a 300-mm (12-in.) diameter, rigid circular plate placed on the pavement surface. The loading pulse was sinusoidal with a peak load of 40 kN for each cycle and a frequency of 10 Hz. The loading program was designed to represent typical traffic loadings on pavements under operating conditions. The cyclic loading was continued until preselected criteria for failure was reached.

After certain numbers of selected cycles, dynamic loading was discontinued and a static loading sequence (5 to 10 static cycles) was applied as a time lengthened, stepwise approximation of one cycle of loading. In addition to obtaining static load response per se, this static loading sequence was necessary for monitoring the array of displacement gauges, strain gauges, and strain carriers in each section. During static loading 10 kN increments of load were applied, to a maximum of 40 kN, followed by smaller decrements to 0 kN. For loops 4 and 5 this was changed into a single increment and single decrement (0-40-0 kN). Dynamic loading was then resumed.

Test Materials and Preparation of Test

Subgrade Preparation

The subgrade for each loop consisted of a 1.2 m depth of medium to coarse sand. The sand was initially placed in 150 mm lifts and compacted at an optimum moisture content of 11.5 percent using a plate tamper. Before each loop (or series of tests), the original subgrade condition was duplicated by removing the top 150 mm of sand, turning over the next 150 mm and recompacting in two lifts at optimum moisture content. A Troxler nuclear densitometer was used to monitor moisture content and compaction. For selected tests the subgrade was flooded from below to fully saturate the sand up to the sand-asphalt interface.

Asphalt Layer Construction

For the first 4 loops a local MTC grade HL4 hot-mix asphalt was used. A 25 mm lift of hot mix (125°C) was first placed on the subgrade for all tests. The mesh was then placed on half the pit, and the other half was left unreinforced as the control section. Next the reinforced and unreinforced halves were covered with one additional 50 mm of asphalt and compacted using four passes of a plate tamper. Additional uniform 25 mm to 75 mm lifts were placed and compacted to bring the pavement structure to the desired thickness. The density of the pavement was monitored using a Troxler densitometer to ensure uniform asphalt consistency between reinforced and unreinforced test sections. Samples of the asphalt mix were taken from each loop and analyzed at the Gulf Canada Research Centre.

Tensar Geogrid

The geogrid material is a 50 mm by 50 mm mesh made by stretching both lengthwise and crosswise a sheet of polypropylene plastic with holes punched through it (Figure 1). The resultant mesh has strands that are about 1 mm thick by 3 mm wide at their narrowest and nodes at the junction of strands that are about 10 mm square and about 2 mm thick. The material weighs about 0.210 kg/m^2, is supplied in 3 m by 50 m rolls, and is estimated to cost about \$2/m^2. Lighter weights and smaller mesh geogrids are available. It has been termed as a geogrid to differentiate it from the conventional geotextile fabrics. Geogrid describes the open mesh structure that allows interlocking with surrounding materials thereby mobilizing its high tensile strength.

The type of geogrid used in this research is designated as AR-1 by the manufacturer; it has been developed to have the following general properties:

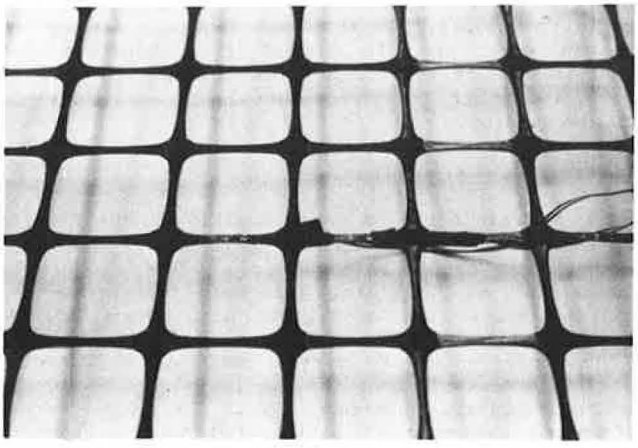

Figure 1. Plastic mesh with strain gauges before placing it in asphalt.

1. High tensile strength,
2. High modulus,
3. Low elongation,
4. Biaxial structure (i.e., strength in both directions), and
5. A grid with desired openings (i.e., 50 mm) for pavement purposes.

Strain gauges were bonded to the top and bottom of the mesh strands in loops 1, 2, 3, and 5. The gauges were attached to a wide area of mesh under the loading plate to monitor the strains induced in the mesh by the loads.

Instrumentation and Data Acquisition

The general arrangement of instrumentation used to monitor the pavement sections during testing is shown in Figure 2. The instrumentation and recording devices are summarized in the following subsections.

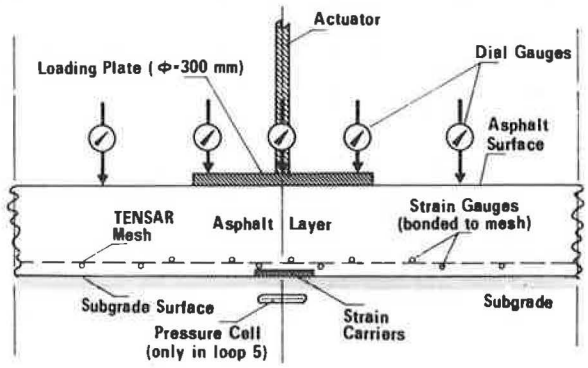

Figure 2. General arrangement of the instrumentation.

Actuator Load Cell and LVDT

The actuator load cell and linear variable displacement transducer (LVDT) are part of the closed-loop, electrohydraulic control system for the MTS actuator. During static load cycles both divices were accessed through the PDP 11/34 computer at pre-programmed intervals to record plate load and displacement (11).

Strain Gauges

Foil-type (120 ohm) strain gauges (SHOWA Y11-FA-S-120) were bonded to the top and bottom of the mesh at locations directly below the loading plate and at radial distances from the load center. The strain gauges were used to record the magnitude and distribution of elastic and plastic tensile strains generated in the reinforcement elements as a result of the loading.

Strain Carriers

Mastic strain carriers were supplied by the Alberta Research Council. Each unit consists of two (120 ohm) strain gauges embedded in a 150-mm square by 12-mm thick mastic plate. The mechanical properties of the mastic are compatible with those of the asphalt concrete. For each test setup of the last four loops, a strain carrier was placed directly under the centerline of the loading plate and at the subgrade-asphalt interface. This location corresponds to the zone of anticipated maximum tensile strains in the asphalt layer.

Dial Gauges

Dial gauges were placed on the rigid loading plate and at radial distances from the plate. The dial gauges were read during static load cycles and were used to determine the elastic and plastic surface deflection profile for a given number of load cycles.

Pressure Cells

For loop 5 a circular plate pressure cell was embedded in the subgrade directly below the center of loading and was used for each test. It was buried about 50 mm below the sand-asphalt interface. Each pressure cell consists of two cylindrical aluminum plates, 133 mm in diameter, fastened back-to-back to give a total thickness of 13 mm. The plates are in the form of a recessed disc made of a 6.5-mm thick annulus surrounding a pressure sensitive diaphragm 2 mm thick. A four-arm strain gauge configuration (Wheatstone Bridge) is bonded to each top and bottom diaphragm of the pressure cells.

The pressure cells were placed in the subgrade to investigate relative vertical stress gradients generated below the loaded areas for reinforced and unreinforced test sections. The pressure cells were calibrated in situ before and after the final test loop by placing the rigid loading plate at the surface of the sand subgrade directly above the pressure cell. The pressure cells were monitored during static load cycles by using a multichannel data acquisition system.

Failure Criteria

Certain failure criteria were established as a means to compare objectively the performance of the reinforced and control sections. Failure was said to have occurred if

1. A permanent deformation of 30 mm was measured,
2. Extensive cracks developed,
3. A steady increase occurred in the measured values of stresses on the subgrade,
4. Surface deflection increased as much as 20 percent, or
5. Horizontal strain at the interface increased by 30 percent.

The values were applied to both control and reinforced sections in all loops to determine the number of load cycles at which failure actually occurred. It was clear from the observations and the test results that a number of factors affected the mode of failure for each loop. Among these factors are the age of the asphalt when the test begins, the temperature, and the subgrade (dry or saturated).

It is noteworthy that the failure of the mesh did not have to be considered in the criteria because the strains on the mesh on all loops did not exceed 30 percent of its yield strain of 15 percent.

RESULTS AND ANALYSIS

The large amount of information collected and analysis conducted makes it impossible to report all results and analysis for all loops. The following presents some typical results.

Results of the First Loop

Results of the first loop showed that permanent deformation resistance of the reinforced pavement was improved, also, the number of cycles to failure were significantly higher. It is important to note

that the unreinforced section had failed completely at the end of the test (punched through) whereas the reinforced section remained together. This latter observation suggests that lower levels of tensile strain and vertical stress result from using the reinforcement layer. This observation was to be confirmed in the next test loop.

Results of the Second Loop

Similar to loop 1, loop 2 tests were carried out to compare the performance of control and reinforced sections for the same pavement thickness on a strong subgrade. The results are shown in Figures 3, 4, and 5 and are as follows:

1. The total permanent deformation (i.e., penetration of the loaded plate) for the control section was higher at the end of the test compared with the deformation of the reinforced section at the same number of loading cycles. This confirms the results of loop 1.
2. The total number of repetitions of the 40 kN load to a limiting deformation of 30 mm more than doubled for the reinforced sections (350,000 versus 150,000).
3. No significant plastic tensile strain was measured at the bottom of the reinforced sections compared with the control section (see Figure 5). This result confirmed the explanation given for loop 1 of the low levels of stress and strain induced in the reinforced sections.
4. The value of the elastic tensile strain measured at the bottom of the reinforced layer was less by more than 30 percent than that for the control section.
5. A highly significant observation was the development of tension (fatigue) cracks on the surface of the control sections (initiated at the bottom of the asphalt layer). Clearly, the reinforcement reduces the number and severity of such cracks. This observation also confirmed the reasoning of the failure mode that occurred in the control section in loop 1.

Results of the Third Loop

As the results of loops 1 and 2 indicate, the life of pavement sections, in terms of number of loads carried, can be doubled for the same thickness of asphalt if reinforcement is used. Loop 3 was designed to investigate the equivalent thickness of asphalt that may be saved by using reinforcement. The results shown in Figures 6, 7, and 8 suggest the following:

1. Reinforcement may provide a significant saving of asphalt thicknesses (between 50 and 100 mm) for the conditions of this experiment (Figure 6).
2. No significant plastic strains were monitored in the case of the thinner (150 mm) reinforced sections, but they were significant on the unreinforced sections (Figure 7).
3. The measured vertical elastic rebound for the thinner reinforced section was smaller than the thicker (200 mm) control section and slightly larger than that of the (250 mm) control section (Figure 8). This is another indicator that additional

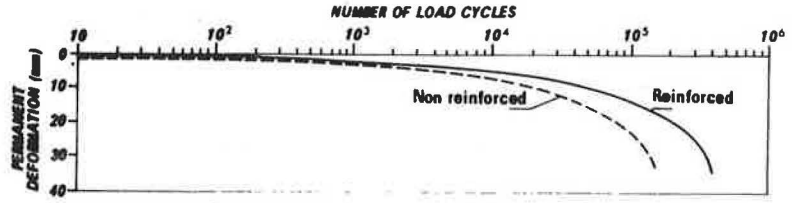

Figure 3. Permanent deformation for loop 2—strong subgrade.

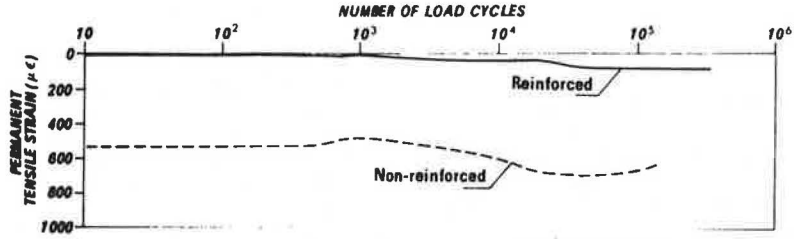

Figure 4. Permanent tensile strain in the asphalt at bottom of layer for loop 2.

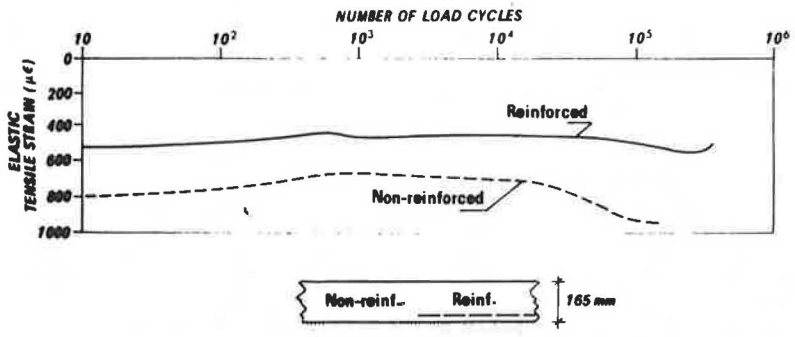

Figure 5. Elastic tensile strain in the asphalt at bottom of layer for loop 2—40 kN load.

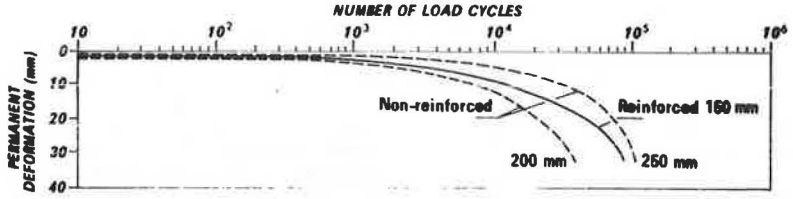

Figure 6. Permanent deformation for loop 3—weak subgrade.

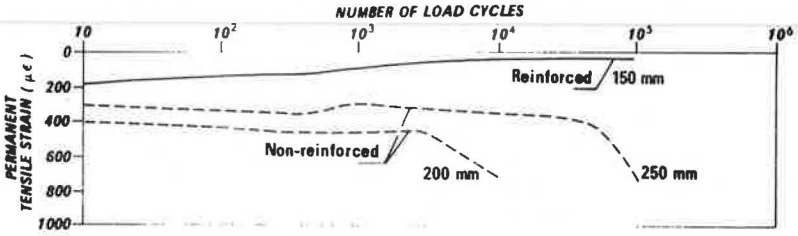

Figure 7. Permanent tensile strain in the asphalt at bottom of layer for loop 3.

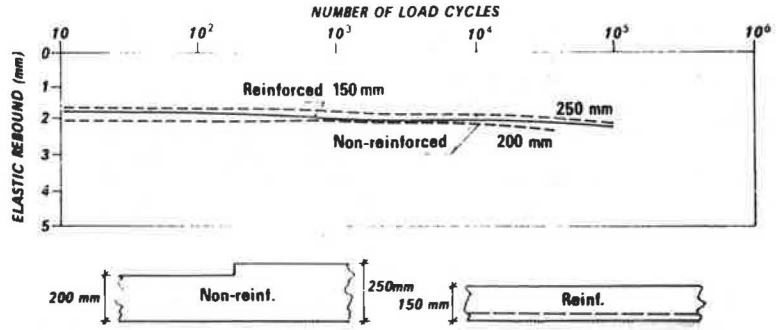

Figure 8. Elastic rebound for loop 3.

structural strength is added to the thinner section by using reinforcement.

The results of this test loop suggest that a minimum saving of asphalt thickness of 50 mm is possible. Of course this remains to be verified for actual field conditions.

Results of the Fourth Loop

The results of this loop (200 mm and 250 mm reinforced sections with dry and saturated subgrade and 250 mm unreinforced sections with dry and saturated subgrade) confirmed the hypothesis of loop 3 that a minimum of 50 mm of asphalt could be saved by using reinforcement. Also, as can be seen in Figure 9, loop 4 strongly confirmed that the elastic tensile strains caused by the 40 kN load in the thinner reinforced section are less than the strains on the thicker (by 50 mm) control section.

Furthermore, Figure 9 shows two other significant differences between the tensile strains measured on the reinforced and unreinforced pavements. First, the unreinforced pavement showed a higher value of residual strain or creep (ε_p in Figure 9-b) which explains the cause of the higher values for permanent tensile strain on this section. Second, the compressive strain on the unloaded adjacent reinforced section was higher than that measured on the unloaded adjacent control section under similar conditions (almost double). This difference is probably caused by the interaction between the asphalt layer and the geogrid reinforcement. Of course this adds to the structural strength of the reinforced pavement.

Results of the Fifth Loop

The last loop featured pressure cells under each test section to monitor the vertical stresses 50 mm under the subgrade interface. The presence of these cells (155-mm diameter aluminum plates) affects the values of the permanent deformation because they act as additional reinforcement for the subgrade layer. However, the major objective of this loop was to monitor the vertical stresses under the loaded sections and to use the data in subsequent analyses.

Figure 10 shows the relationship between the ratio of the measured stress for the control section to the reinforced section versus number of cycles. It clearly shows that the subgrade stress is 30 to 40 percent higher under the control (unreinforced) section.

Comparison of Results

The results of the experimental program have clearly demonstrated significant differences in the performance of the reinforced and unreinforced sections. Results of loops 1 and 2 indicate that reinforced sections of the same thicknesses would carry more than double the number of load cycles to failure compared to the unreinforced sections. The reinforcement reduces the elastic tensile strain at the bottom of the asphalt layer by about 30 percent.

Cracks were observed early on the unreinforced sections and progressed into severe cracks on the surface. On the other hand, very few (hairline) cracks were observed on the reinforced sections at the end of the loading cycles. Two unreinforced sections, one in each loop, were punched through,

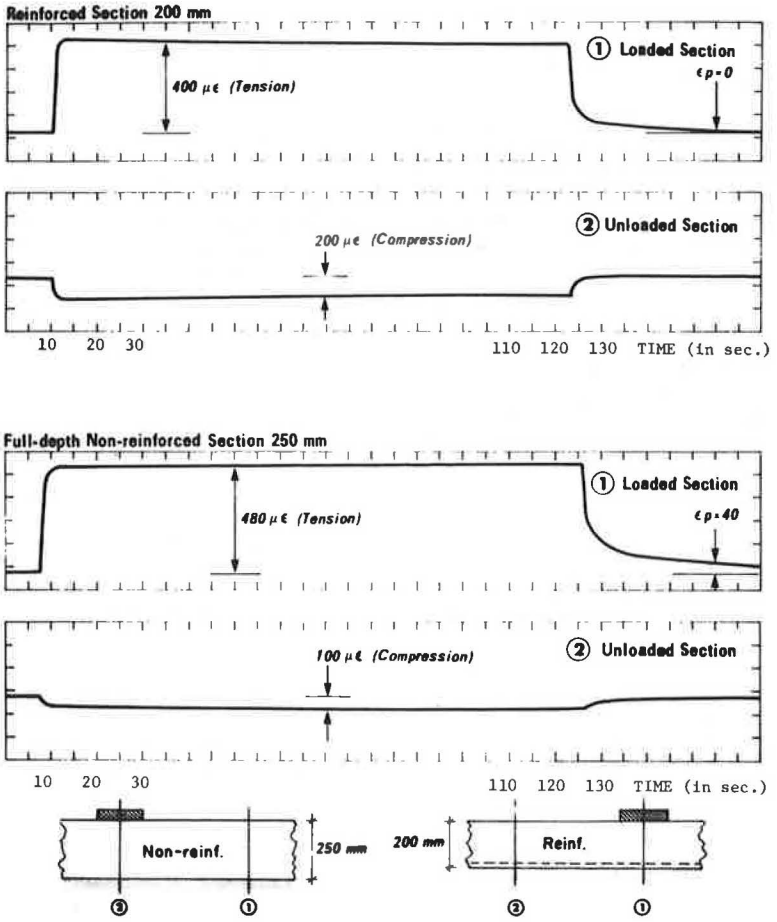

Figure 9. Tensile strain pulses for loop 4—weak subgrade.

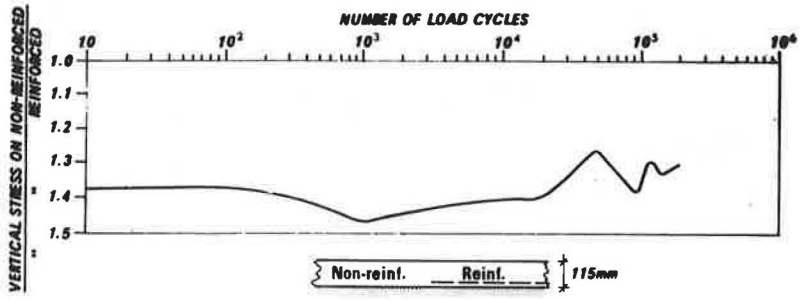

Figure 10. Stress ratio of the unreinforced section to the reinforced section for loop 5—strong subgrade.

whereas the reinforced sections held together even after higher numbers of load cycles.

Results of loops 3 and 4 suggest that a possible saving of between 50 to 100 mm of asphalt material can be obtained by reinforcing the thinner sections. In loop 3, a comparison between the 150 mm reinforced and 200 mm unreinforced sections shows that the thinner reinforced section is significantly stronger than the unreinforced section. The results of this loop suggest that a reinforced section can be 50 mm thinner than an unreinforced section and still show less permanent deformation and less permanent tensile strain under a higher number of load cycles than was applied to the thicker unreinforced section. Furthermore, the presence of the mesh in the thinner sections of loops 3 and 4 resulted in reducing the elastic tensile strain by about 20 percent compared with the strains under the thicker unreinforced layer.

A comparison of the 150-mm reinforced section with the 250-mm unreinforced section of loop 3 shows that the maximum possible saving of asphalt material under the circumstances is about 100 mm. Although the elastic rebound of the 250-mm unreinforced section was less than the elastic rebound of the 150-mm reinforced section, the reinforced section performed better as far as the permanent tensile strain and fatigue cracks were concerned.

The results of loop 5 help to explain the findings of the previous loops. As shown in Figure 10, the ratio between the vertical stresses on the subgrade under the unreinforced sections were 30 to 40 percent higher than the stresses under the reinforced sections. This difference is explained by

the effect of the reinforcing mesh. The vertical stresses will be distributed on a larger area under the reinforced section, resulting in less pressure on the subgrade. This difference can be further explained by Figure 11 where deflection bowls at different load cycles are shown for the reinforced and unreinforced section in loop 2. The following differences are apparent:

1. The spread of the deflection bowl for the reinforced section is larger than for the unreinforced.
2. The slope of deflection bowl for the unreinforced is steeper than the slope of the deflection bowl for the reinforced section suggesting higher values for shear and vertical stresses.
3. Fatigue cracks developed on the unreinforced section resulted in a smaller area of stress distribution and higher stress values (10^5 cycles).

Table 2 summarizes some selected results of the five loops.

VERIFICATION OF THE ELASTIC LAYER THEORY

The experimental program also provided the opportunity to examine the validity of the elastic layer theory under simulated field conditions, similar to those assumed in the theory itself. Furthermore, it provided sufficient data to verify asphalt pavement responses (elastic deflections, horizontal tensile strains, and vertical stresses) when subjected to a wide range of variables. Therefore, the results of this program were used to verify the application of a selected elastic layer model to predict responses of the unreinforced pavements.

A multilayer elastic model, BISAR, (12) was used in the analysis to predict surface deflections, horizontal strains, and vertical stresses for the tested sections. The predicted values under the maximum load (40 kN) compared well with the measured values. However, there was experimental evidence to suggest that elastic moduli of pavement layers depend on the level of stress imposed on the layers. Calibration factors were established to modify the moduli so that better agreement is reached between the predicted and measured data.

An iterative technique was used for the analysis. For example, the analysis started with using an average value for the elastic modulus of the subgrade (based on test measurements). With this value and the measured surface deflection for the section

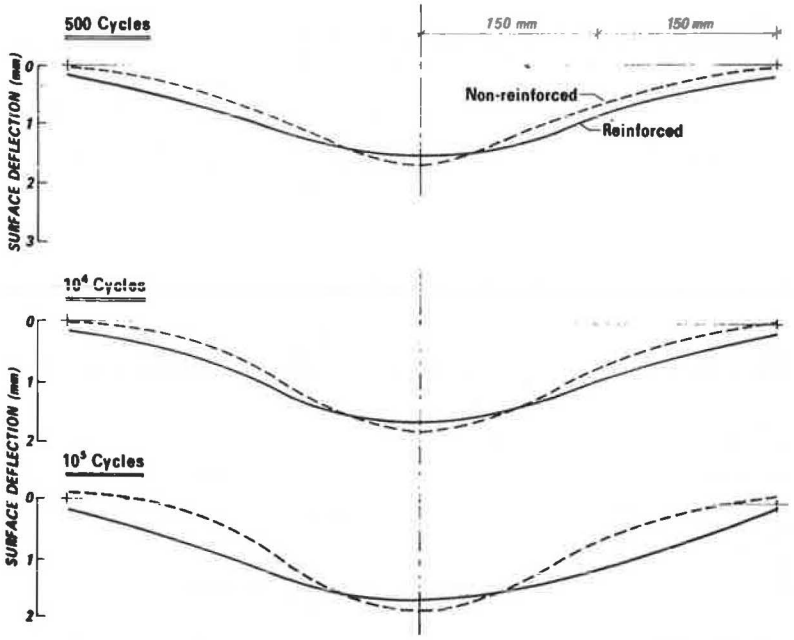

Figure 11. Surface deflection bowls of unreinforced and reinforced sections for loop 2.

Table 2. Summary of selected results.

Loop No.	Section	Thickness (mm)	Total No. of Cycles	Total Penetration (mm)	Permanent Tensile Strain ($\mu\epsilon$)
1	Control	150	100,000	53.0[a]	
	Reinforced	150	100,000	37.0	
			200,000	76.0	
2	Control	165	150,000	30.0	760
	Reinforced	165	350,000	27.1	140
3	Control	255	113,500	31.8	735
	Control	200	37,500	29.3	700
	Reinforced	150	90,000	29.7	0
4	Control	255	135,000	15.0	710
	Reinforced	200	135,000	13.0	180
5	Control	115	300,000	10.2	880
	Reinforced	115	300,000	6.8	80

[a]This section punched through at 100,000 cycles.

considered, an initial value for the elastic modulus of the asphalt layer can be obtained as shown in Figure 12. The relationships shown in the figure were obtained using the elastic layer program; BISAR, for different thicknesses and elastic moduli. Using these initial values of the moduli as input into the program (along with the other elastic constants, thicknesses, number of layers, and load value), the stresses, strains, and deflections in each layer were computed. The iterative process was carried out, by choosing new values of the moduli for both subgrade and asphalt, until the difference between the predicted and measured values of surface deflections and horizontal strains were less than an acceptable value. The highest number of iterations found necessary was seven. The results of this analysis are discussed below.

Comparison of Deflections and Strains Under Maximum Load (40 kN)

This comparison is important because most flexible pavement design methods adopt surface deflections and horizontal tensile strain as criteria for design. As can be seen in Table 3, the predicted values of maximum surface deflection and horizontal strain at the bottom of the asphalt layer are very close to the measured values.

Comparison of Deflections and Strains Under Different Load Values

The results of calculated deflection and strains that assumed constant values of elastic moduli were found to differ from the measured values under different loads. The discrepancy was more pronounced on the thinner sections than on the thicker ones. Perhaps this can be explained by the fact that under the small-load value (10 kN), the effect of the dead weights of the loading system and the asphalt layer (which were ignored in the analysis) represent a significant portion of the actual loading at this small-load value. Obviously this weight would have more effect on the thinner and weaker sections than on the thicker and stronger sections. This explanation is supported by results of the tests shown in Table 4. (The difference is higher for the 165 mm and 200 mm compared to the 250 mm section--26 percent, 32 percent, and 10 percent, respectively.) However, the problem was minimized by introducing calibration factors derived from the measured data. This was done first by using the following model to derive the appropriate moduli:

$$E_p = E_o\ [1 + \sin (C + 2.06P)] \ldots 1 \quad (1)$$

where

- E_p is the elastic modulus of the asphalt or subgrade layer under load P (kN) in MPa,
- E_o is initial value of elastic modulus of the layer in MPa,
- C is constant and was found to be equal to 28, and
- P is the applied load in kN.

The value of E_o was calculated using the values of E_p for p = 40 kN found in Table 4. The plot in Figure 13 shows the relationship given by the model in Equation 1. Because the values of P in the experimental program were fixed at 10, 20, 30, and 40 kN,

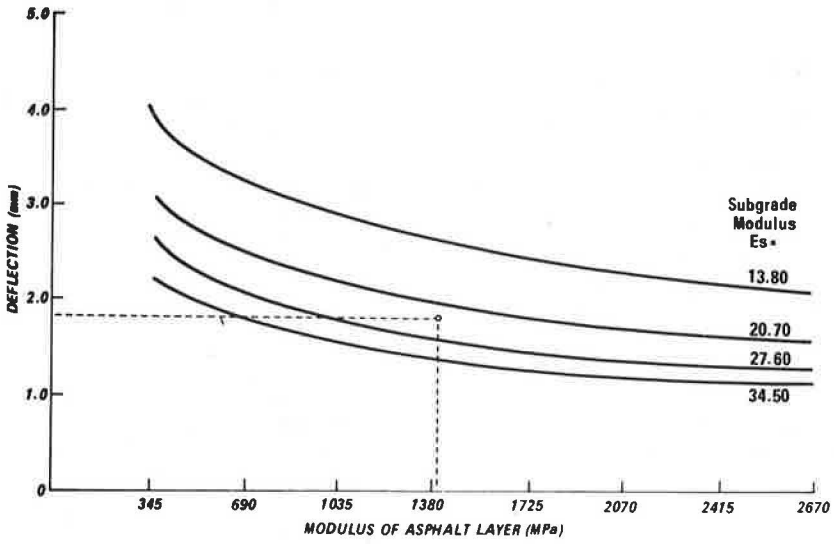

Figure 12. Computed relationships between deflection and elastic moduli for asphalt thickness of 165 mm.

Table 3. Comparison of measured and predicted deflections and strains under maximum load (40 kN).

Thickness (mm)	Asphalt Modulus (MPa)	Subgrade Modulus (MPa)	Measured Deflection (mm)	Measured Tensile Strain (mm)	Predicted Deflection (mm)	Predicted Tensile Strain (mm)	Error (%) Deflection	Error (%) Strain
115	2,997	33.3	1.57	605	1.54	589	2.0	3.0
165	1,399	23.3	1.81	680	1.80	715	1.0	5.0
200	965	17.6	1.98	805	2.05	765	4.0	5.0
250	1,233	15.2	1.69	440	1.70	452	1.0	3.0

Table 4. Comparison of deflections and strains under different load values

Load (kN)	Calibration Factor, F_p	Asphalt Modulus, $E_p=F_p \times E_{40}$	Subgrade Modulus, $E_p=F_p \times E_{40}$	Thickness (mm)	Measured		Predicted E_{40}		Predicted E_p		Error E_{40} (%)		Error E_p (%)	
					Deflection	Strain	Deflection	Strain	Deflection	Strain	Deflection	Strain	Deflection	Strain
10	0.905	1,266	21.1	165	0.54	243	0.45	179	0.50	200	17.0	26.0	7.0	17.0
20	1.000	1,399	23.3		0.97	358	0.90	358	0.91	358	7.0	0.0	7.0	0.0
30	1.034	1,447	24.4		1.34	475	1.35	536	1.30	518	1.0	13.0	3.0	9.0
40	1.000	1,399	23.3		1.81	680	1.80	715	1.80	715	1.0	5.0	1.0	5.0
10	0.905	873	15.9	200	0.61	282	0.51	191	0.58	215	16.0	32.0	5.0	24.0
20	1.000	965	17.6		1.08	475	1.03	382	1.03	382	5.0	19.0	5.0	19.0
30	1.034	998	18.2		1.51	622	1.54	573	1.49	555	2.0	8.0	2.0	10.0
40	1.000	965	17.6		1.98	805	2.05	765	2.05	765	4.0	5.0	4.0	5.0
10	0.905	1,116	13.8	250	0.51	122	0.42	110	0.47	125	17.0	10.0	7.0	2.0
20	1.000	1,233	15.2		0.93	217	0.85	226	0.85	226	9.0	4.0	9.0	4.0
30	1.034	1,275	15.7		1.31	315	1.27	330	1.23	328	3.0	5.0	6.0	4.0
40	1.000	1,233	15.2		1.69	440	1.70	452	1.70	452	1.0	3.0	1.0	3.0

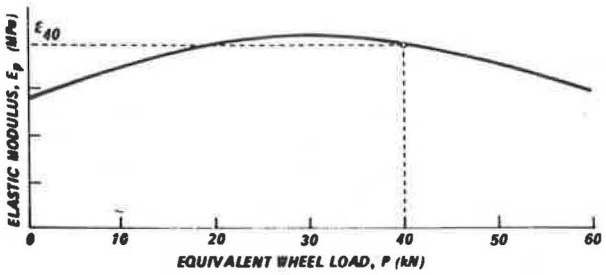

Figure 13. Relationship between elastic modulus of asphalt or subgrade (E_p) and the load (P).

it was easy to derive the following formula from the suggested model,

$$F_p = E_p/E_{40} \quad (2)$$

where

F_p is the calibration factor obtained from the model and equal to 0.905, 1.000, 1.034, and 1.000 for 10, 20, 30, and 40 kN, respectively;
E_p as defined before; and
E_{40} is the elastic modulus used in the analysis for 40 kN.

The analysis assumed that the modular ratio of the two layer system at any load is the same as the ratio used in the analysis at 40 kN. The results of the analysis that considered variation in the elastic moduli were compared with the measured values and with the results of the analysis that assumed fixed elastic moduli (E_{40}). As can be seen from the comparison given in Table 4, the use of the calibration factors significantly improved the predictions of the model in most cases.

Significance of the Analysis

The analysis indicates that elastic layer theory is an acceptable tool to predict and analyze flexible pavement behavior. It also shows that adopting simple modifications, such as calibration factors to establish stress dependency for the elastic analysis, is more efficient and less time consuming than using other more sophisticated models. An interesting observation is that this variation of the theory was found to occur for the lower level of loading which in most cases is not of major concern in flexble pavement design methods. Finally, the most important finding of the study is that if the elastic constants of pavement layers can be determined accurately enough, the elastic layer theory could predict reliably pavement deflections and horizontal strains.

CONCLUSIONS

This paper presents a new, effective method of reinforcing asphalt pavements by using a new, nonmetallic high-tensile-strength geogrid. It also presents a methodology for testing, comparing, and analyzing the behavior of both reinforced and nonreinforced flexible pavements. In addition, important answers are provided to the question of the validity of the elastic theory and its use in flexible pavement design methods.

In view of the worldwide emphasis on energy conservation of resources, reinforced flexible pavements offer a promising alternative to conventional designs. The potential of this new technique can be summarized as follows:

1. Substantial thickness savings of asphalt material, or
2. Up to double the number of load repetitions, and
3 Prevention or minimization of fatigue cracks in the asphalt layer.

This potential of reinforced flexible pavements suggests that developing a construction technology for field installation and full-scale field trials to verify the findings of the experimental program would be worthwhile.

ACKNOWLEDGMENT

Invaluable advice and assistance to the research program was provided by RMC, MTC, Gulf Canada, and the University of Waterloo. Particular acknowledgment and appreciation is given to Peter Jarrett, Associate Professor of Civil Engineering at RMC, who is director of the test facility and played a leading role in the planning and execution of the experimental program; Nabil Kamel, Research Engineer with Gulf Canada Ltd; Laverne Miller, head of their Asphalt Research Group, who provided materials, testing, and other assistance; Louise Steele, formerly at the University of Waterloo and now with the PMS Group, who assisted the experimental program; Kelly McGillivray, undergraduate research assistant at Waterloo, who assisted with the analytical portions of the research; and Jamie Walls, formerly with RMC and now with Pavement Management Systems Ltd., who provided assistance in the experimental program.

REFERENCES

1. A.O. Abdelhalim and R. Haas. Flexible Pave-

ment Reinforcement: Assessment of Available Materials and Models and a Research Plan. Interim Rept. for Project No. 21130, Ontario Joint Transportation and Communications Research Program, Mar. 31, 1981.
2. J.R. Nowak. The Full Scale Reinforced Concrete Experiment on the Grantham By-Pass Performance During the First Six Years. Road Research Laboratory, Ministry of Transport, TRRL Report LR 345, Crowthorne, Berkshire, U.K., 1970.
3. J.M. Gregory, A.G. Burks, and V.A. Pink. Continuously Reinforced Concrete Pavements. Report of the Study Group, Road Research Laboratory, Ministry of Transport, TRRL Report 612, Crowthorne, Berkshire, U.K., 1974.
4. J.W. Galloway and J.M. Gregory. Trial of a Wire-Fibre-Reinforced Concrete Overlay on a Motorway. TRRL Report 764, Road Research Laboratory, Ministry of Transport, Crowthorne, Berkshire, U.K., 1974.
5. J.L. Vicelja. Methods to Eliminate Reflection Cracking in Asphalt Concrete Over Portland Cement Concrete Pavements. Proc. of the Assn. of Asphalt Paving Technologists, Vol. 32, 1963, pp. 200-227.
6. Egons, Tons, and E.M. Kroksky. A Study of Welded Wire Fabric Strip Reinforcement in Bituminous Concrete Resurfacing. Proc. of the Assn. of Asphalt Paving Technologists, Vol. 29, 1960, pp. 43-80.
7. G.A. Bicher, R. Harris, and V.J. Roggenveen. A Laboratory Study of Welded Wire Fabric Reinforcement in Bituminous Concrete Resurfacing. Proc. of the Assn. of Asphalt Paving Technologists, Vol. 26, 1957, pp. 468-485.
8. H.W. Busching and J.D. Antrim. Fiber Reinforcement of Bituminous Mixtures. Proc. of the Assn. of Asphalt Paving Technologists, Vol. 37, 1968, pp. 629-659.
9. H.W. Busching, E.H. Elliott, and Reyneveld. A State-of-the-Art Survey of Reinforced Asphalt Paving. Proc. of the Assn. of Asphalt Paving Technologists, Vol. 39, 1970, pp. 766-798.
10. J.H. Keitzman. Effect of Short Asbestos Fibers on Basic Physical Properties of Asphalt Paving Mixes. HRB, Bull. 270, 1960, pp. 1-19.
11. R.J. Bathurst, J. Walls, and P.M. Jarrett. Summary of Large-Scale Model Testing of Tensar-Reinforced Asphalt Pavement. Interim Rept. for Project No. 21130, Ontario Joint Transportation and Communications Research Program, Mar. 1982.
12. D.L. DeJong, M.G.F. Peutz, and A.R. Korswagen. Computer Program BISAR, Layered Systems under Normal and Tangential Surface Loads. External Report Shell, Laboratrium, Amsterdam, Jan. 1973.